SLOPE STABILITY ANALYSIS ALONG THE SELECTED ROAD SECTION FROM MORKA-GIRCHA-CHENCHA ROAD, GAMO ZONE, SOUTHERN ETHIOPIA

Hayat Abdela Jemal

A Thesis Submitted to the Department of Applied Geology

School of Applied Natural Science

Office of Graduate Studies

Adama Science and Technology University

Feburary, 2024

Adama,Ethiopia

Slope StabilityAnalysis along the selected road section from Morka-Gircha-Chencha Road, Gamo Zone, Southern Ethiopia.

Hayat Abdela Jemal

Advisor: Dr. Bayissa Regassa.

Co-Advisor: Mr. Tola Garo (MSc.)

A Thesis Submitted to the department of Geology
School of Applied Natural Science

Office of Graduate Studies
Adama Science and Technology University

February, 2024
Adama, Ethiopia

Declaration

I hereby declare that this Master Thesis entitled is "**Slope Stability Analysis along the Selected Sections of Morka-Gircha to Chencha Road, Gamo Zone, Southren Ethiopia"** my original work. That is, it has not been submitted for the award of any academic degree, diploma, or certificate in any other university. All sources of materials that are used for this thesis have been duly acknowledged through citation

Name of the Student	Signature	Date

Recommendation

We, the advisors of this thesis, hereby certify that we have read the revised version of the thesis entitled "**Slope Stability Analysis Along the Selected Sections of Morka-Gircha to Chencha Road,Gamo Zone, Southern Ethiopia**" was prepared under our guidance by **Hayat Abdela Jemal** and submitted in partial fulfillment of the requirements for the degree of Masters of Science in **Engineering Geology**. Therefore, we recommend the submission of a revised version of the thesis to the department following the applicable procedures.

______________________	______________________	______________________
Major Advisor	Signature	Date
______________________	______________________	______________________
Co-advisor	Signature	Date

Approval Page

We, the advisors of the thesis entitled "**Slope Stability Analysis along the Selected Sections of Morka Gircha to Chencha Road, Gamo Zone, Southern Ethiopia**" and developed by hayat abdela; hereby certify that the recommendation and suggestions made by the board of examiners are appropriately incorporated into the final version of the thesis.

Major Advisor	Signature	Date
Co-Advisor	Signature	Date

We, the undersigned, members of the Board of Examiners of the thesis by **Hayat Abdela** have read and evaluated the thesis entitled "Slope Stability Analysis Along the Selected Road Sections of Morka Gircha Chencha Road, Gamo Zone Southern Ethiopia" and examined the candidate during the open defense. This is, therefore, to certify that the thesis is accepted for partial fulfillment of the requirement of the degree of Master of Science in **Engineering geology**.

Chairperson	Signature	Date
Internal Examiner	Signature	Date
External Examiner	Signature	Date

Final approval and acceptance of the thesis is contingent upon the submission of its final copy to the Office of Postgraduate Studies (OPGS) through the Department Graduate Council (DGC) and School Graduate Committee (SGC).

Department Head	Signature	Date
School Dean	Signature	Date
Office of Postgraduate Studies, Dean	Signature	Date

ACKNOWLEDGEMENT

First of all I would like to express my profound gratitude and praises to the Almighty ALLAH for all good graces and mercies he granted me in my life and throughout my thesis work successful. Next,This work would not have been possible without the financial support and laboratory facilities of Adama Science and Technology University. I would like to express my special gratitude to my advisor Dr. Bayessa Regassa as well as to my co-advisor Mr. Tola Garo who made this work possible. Their guidance and advice helped me through all stages of writing this thesis. I am grateful to the staff in the civil and geotechnical engineering department of Addis Ababa Science and Technology University, who permitted me to use the necessary tools in the lab. Last but not least I would like to thank my friend and families for helping me through this project.

Table of Contents

LIST OF FIGURES

LIST OF TABLES

LIST OF ACRONYMS AND ABBREVIATIONS

ASTU…..…… Adama Science and Technology University.

AASHTO…. America Association of State Highway and Transportation Officials

ASTM……. American Society for Testing and Materials

ECDSWC…… Ethiopia Construction Design and Supervision Works Corporation

FEM……..…. Finite Element Method

FOS………...Factor of Safety

GIS……..…. Geographic Information System

LEM……..…Limit Equilibrium method

SNNP……...South Nation, Nationality and Peoples ‘Region

SRF……… Strength Reduction Factor

UCS………Unconfined Compressive Strength

USCS………Unified Soil Classification System

VES……..…Vertical Electrical Sounding

ABSTRACT

Slope failures are among the most common geo-environmental natural hazards in the world's steep and mountainous terrain, causing human life to be lost and civil engineering infrastructure to be destroyed. In southern Ethiopia, the road connecting Morka, Gircha, and Chencha traverses through highly harsh terrain with steep hill sides and deep valleys. The current study was carried out to identify and assess the slope stability along chosen road sections, as well as to suggest some remedial solutions based on field investigation and analysis results. A discontinuity survey, in situ rock testing, soil and rock sampling for laboratory analysis, slope geometry, and orientation measurements are all part of the extensive field survey research for this project.The field manifestations also revealed that four key rock slope sections, as well as two essential soil slope sections, were identified for stability research. Planar types of rock slope failure were observed during kinematic analyses using the Dips software at slope sections RSS2 and RSS4. Furthermore, deterministic approaches are employed to calculate the factor of safety by employing Rocplane and planar failures. The stability analysis was performed utilizing limit equilibrium and finite element methods for static dry, static saturated, dynamic dry, and dynamic saturated loading situations. According to the analysis of selected critical slope portions, the slope is stable for FOS larger than one and unstable for FOS less than one. Furthermore, soil laboratory examination found that soils are classed as silty soil and clayey silt (high plasticity), with a liquid limit range of 55.3 to 49.3%, a plasticity index range of 24.3 to 17.2%, and a moisture content range of 35.5 to 30.83%. The finite element results show that crucial soil slope sections three are unstable in static dry and dynamic dry conditions, but it is unstable in static saturated and dynamic saturated situations, and soil six is unstable in all condition. Changes in slope angle, slope height, result in increased slope stability, according to performance study of geometric profiles. Furthermore, the research suggests the placement of rock bolts, anchors, retaining walls, and drainage controls to avoid crucial slope portions from failing.

Keywords: Slope stability analysis, Factor of safety, Kinematic analyze Limit Equilibrium and Finite element method

CHAPTER 1

1. INTRODUCTION

1.1. Background of the study

The safety and long-term viability of mining, civil engineering, and environmental engineering projects around the world depend on slope stability assessment. When building roads, natural slopes are excavated to improve communication and the movement of people, commodities, and services. According to Mievi and Vlastelica (2014), these designed slopes are subject to weathering, which over time changes the geotechnical properties of slope materials and causes many slopes to fail even though they initially showed superior stability conditions. Every year, deaths, injuries, and significant property damage are caused by slope failures, a naturally occurring phenomenon that frequently occurs along the cut slopes of road corridors built in hilly regions of the world. (Aleotti & Chowdhury, 1999). One of the most frequent natural disasters that can cause large financial losses and endanger human lives is characterized as slope instability. It is a geodynamic process that alters the geomorphology of the earth's surface. The formation of weak zones, weathering, lithological disturbance, slope geometry, slope material strength, geohydrological conditions, structural discontinuity, and excessive rainfall are some of the common causes of slope failure. (Singh & Singh, 1992) Most part of the north, south, and western regions of the Ethiopian plateau face a record of slope instability both in superficial materials and at bedrocks due to the cutting of hills and road sides (Ayalew, 1999) .Numerous scholars (Bekele & Meten, 2022) have utilized a variety of analytical techniques, including limit equilibrium, kinematic, and finite element methods, to study slope stability. To examine the factor of safety, slope stability evaluations using the limit equilibrium method or the finite element method employing the shear strength reduction (SSR) technique can be carried out. The Kinematic method is the first step to evaluate but the kinematic method did not determine the causative factor and degree of the slope stability failure mode of the rock slope.

The complete equilibrium criterion seemed true because Morgenstern and Price (1965) created a rigorous approach that satisfied any form slip surface (Zhang et al., 2012). They were used in this investigation. In contrast to the limit equilibrium method, FEM can be utilized to solve complex problems utilizing stress and movement data. Furthermore,(Griffiths & Lane, 1999) demonstrating how the FEM-SRF provides the FOS for the critical slip surface automatically and without making any assumptions while simulating a slope.

The study region included also a portion of the plateau in southwest Ethiopia, where slope instability is a significant issue. The main cause of instability, which is mostly connected to the soil shear strengths, slope face inclination (topography), and water-saturated slope materials that may occur during the slope cut, may cause the slopes along the road cut to fail. Most of the roads that have been built cross across terrain that has been cut and filled, including hills, valleys, and hilly terrain.

This study was conducted on the slope stability analysis of rock slopes along Morka Gircha Chencha Road. To describe the engineering characteristics of materials along the road sections, different approaches and methods were used, such as extensive field surveys, discontinuity measurements, in situ tests, and laboratory experiments. The present study aims to identify and analyze the stability slope by using kinematic, limit equilibrium, and finite element methods and provide some remedial measures based on the analysis results.

Therefore, using the minimum of the two methods can determine the stability of the slope precisely. The present study area is found in the southwest part of Ethiopia, where slope instability is a critical issue.

1.2.Description of the study area

1.2.1. Location and Accessibility

The project area is located in South Nations, Nationalities, and People’s Regional State in Gamo Gofa Zone. The road project connects four administrative Woredas namely Kucha, Daramalo, Dita and Chencha. The project starting point is Morka town which is located at 82 km from Wolita Sodo City on the main Sodo-Sawla road and ends at Chencha town, the capital of Chencha Woreda. the road project of critical section is situated within UTM (WGS84) geographic coordinates of 321181.7634mE 328319.8087mE and 696307.3502mN-693988.4834mN. Morka-Chencha is a gravel road that is under construction to upgrade to the asphalt concrete road.This area can be accessible via Addis Ababa to wolita sodo 330 km asphalt road from sodo to morka 85km asphalt road. then to wacha all weathered road.

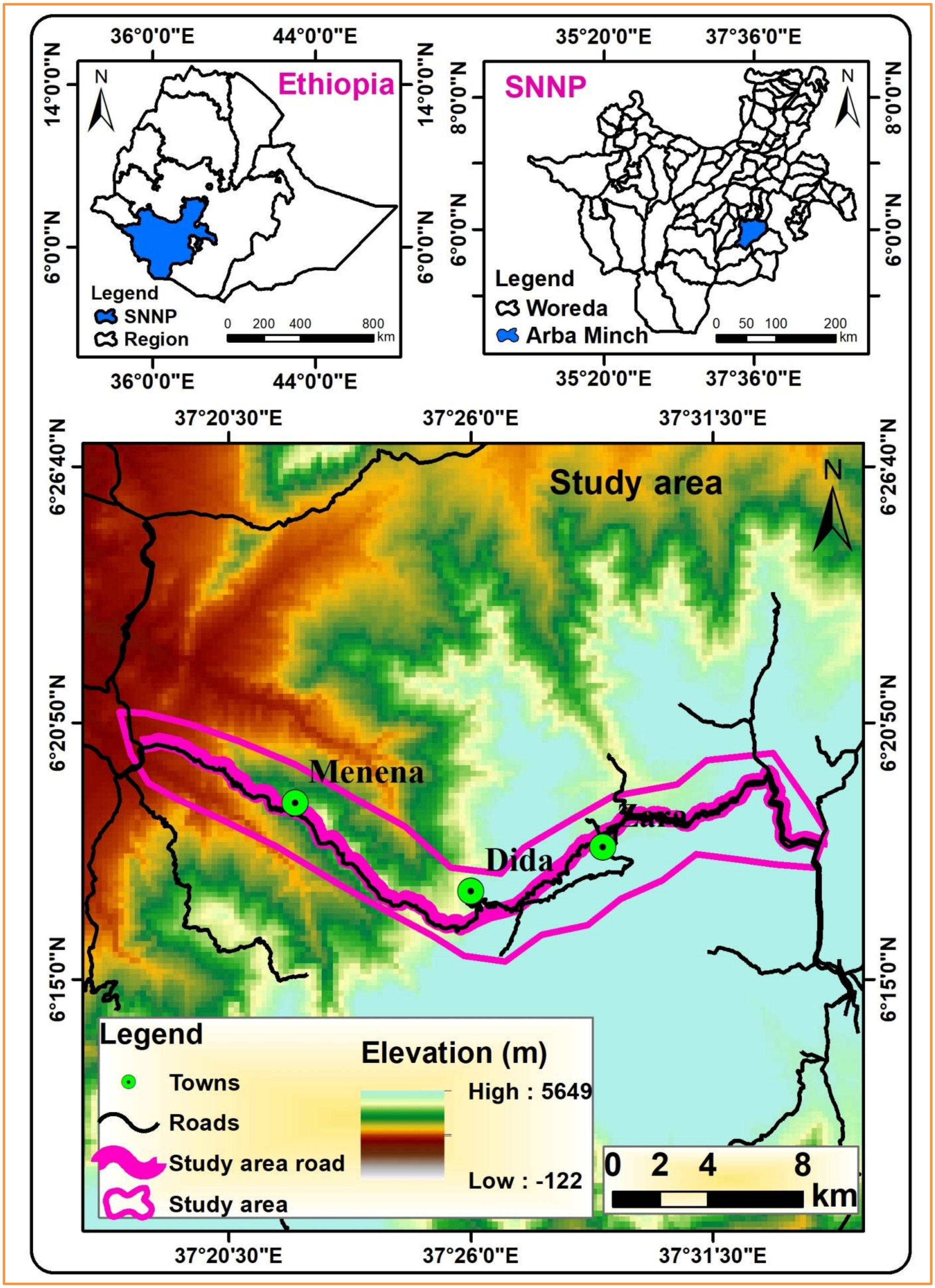

Figure 1.1 location map of the study area

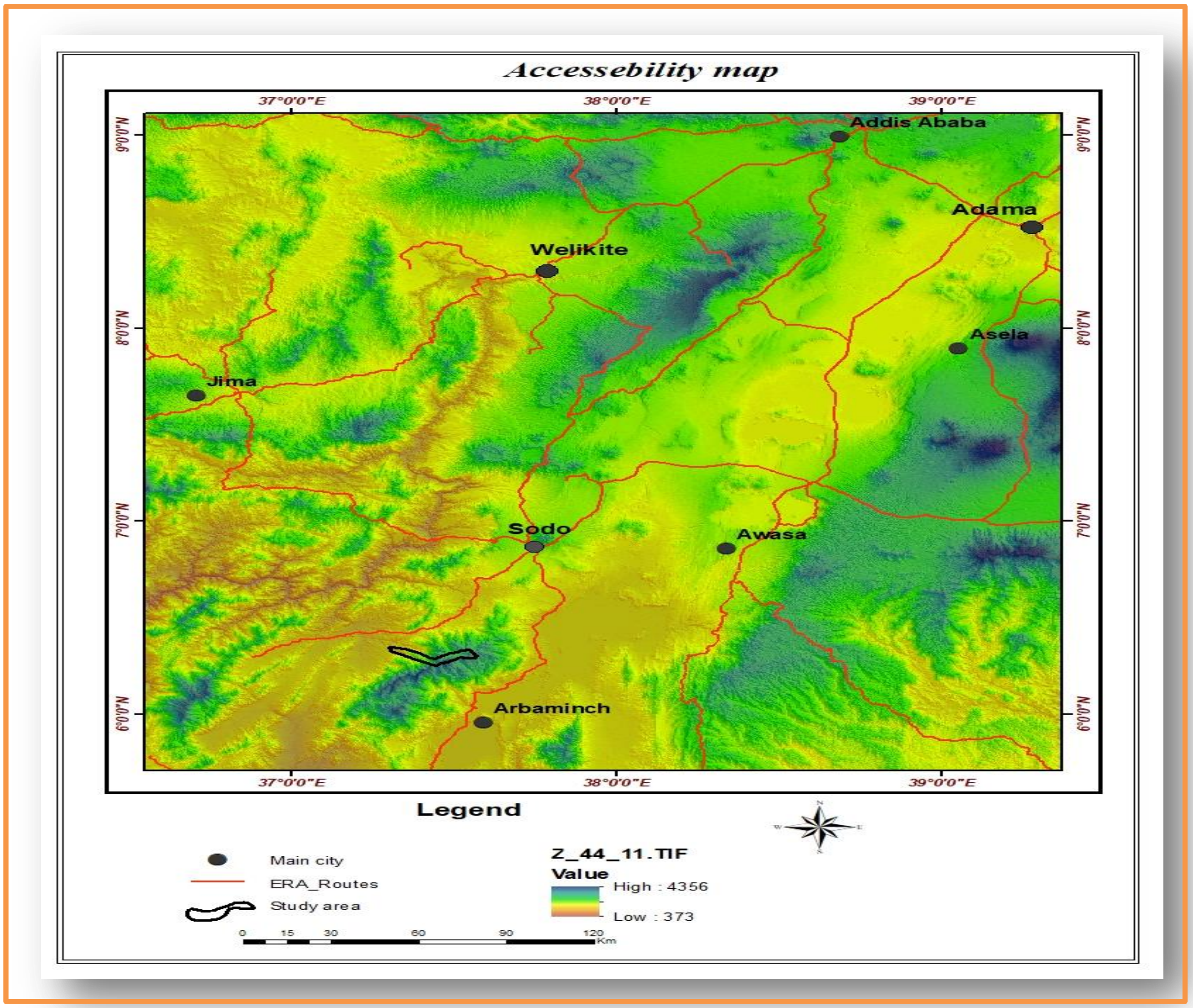

Figure 1.2 Accessibility map of the study area.

1.2.2. Physiography of the Study Area

The Main Ethiopian Rift (MER) and the southern plateau both include the route corridor. Its geomorphologic environment is primarily governed by internal (tectonic and volcanic forces) and external forces of activity that occurred one geological event at a time in the past. The volcanic activity in the area was the primary factor in the formation of the valleys, mountains, and distinct hills in the area surrounding the route corridor. Tectonic activity is linked to the formation of the Ethiopian rift valley. Furthermore, the formation of the Gorge system was influenced by outside factors. Consequently, the relief along the route corridor is made up of two types of landforms:the mountainous and gorge landforms, which constitute most of the terrain flat to rolling, and the escarpment landforms, which occur more or less at the end of the route corridor. The area varies in elevation from 2000 to 3300 m.s.l. Based on the basis of morphology and terrain, the road project can be grouped into four classes: dissected valleys, escarpments, and plateaus.

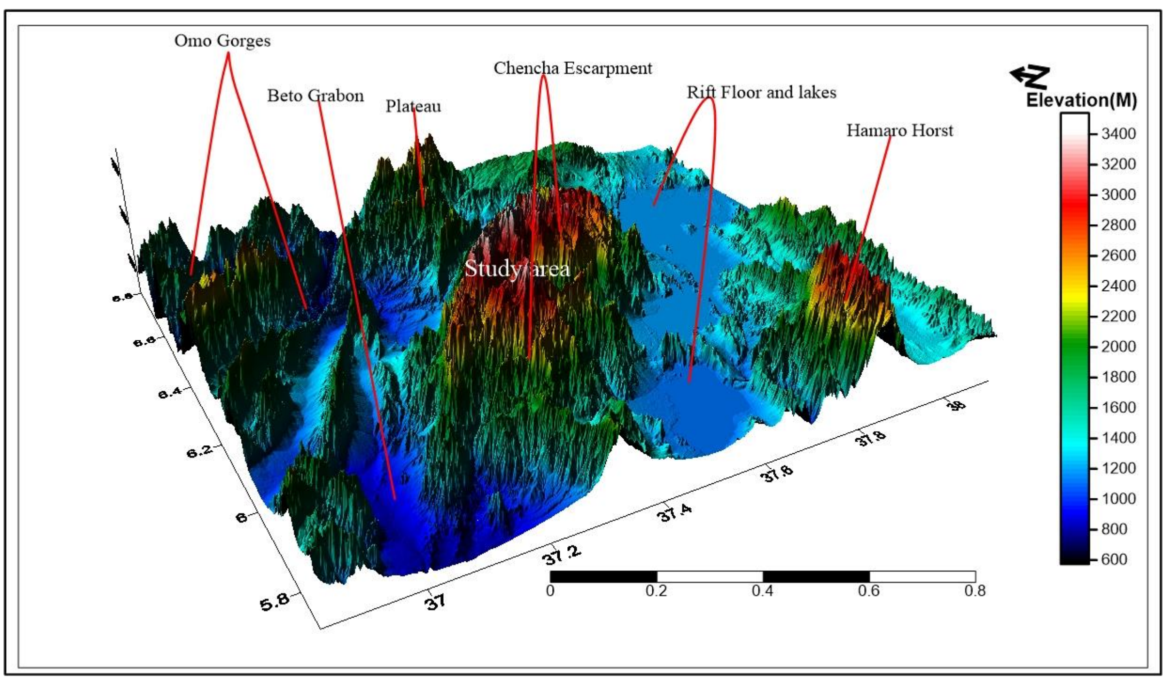

Figure 1.3 3D view Physiographic map of the area interpreted from digital elevation model (from Shuttle Radar Topography Mission SRTM– data, 30 m resolution).

1.2.3. Seismicity of the study area

1.2.3.1. **Regional Seismic Hazards**

One of the causes of slope instability, particularly in seismically active areas, is seismic activity (Hoek & Bray, 1981). A geohazard, such as an earthquake, can cause instability and harm to any infrastructure. The main Ethiopian Rift (MER) in Ethiopia is primarily linked to the earthquake probability. Afar Depression to the southwest, MER is a long, fault-bounded succession of depressions. As a consequence, the rift is causing a high level of seismic activity in the tectonic province, which is an appropriate geographic scale for assessing earthquake probability zonation depending on the proximity to the center of the rift. The tectonic margin's recent earthquake activity is abundant, indicating active zones that are constantly expanding. Ethiopia's proximity to the active zone limits of the rifting is indicated on the seismic hazard map of the country. the study area along the Morka-Gircha-Chencha road project belongs to a ground acceleration of 0.5.

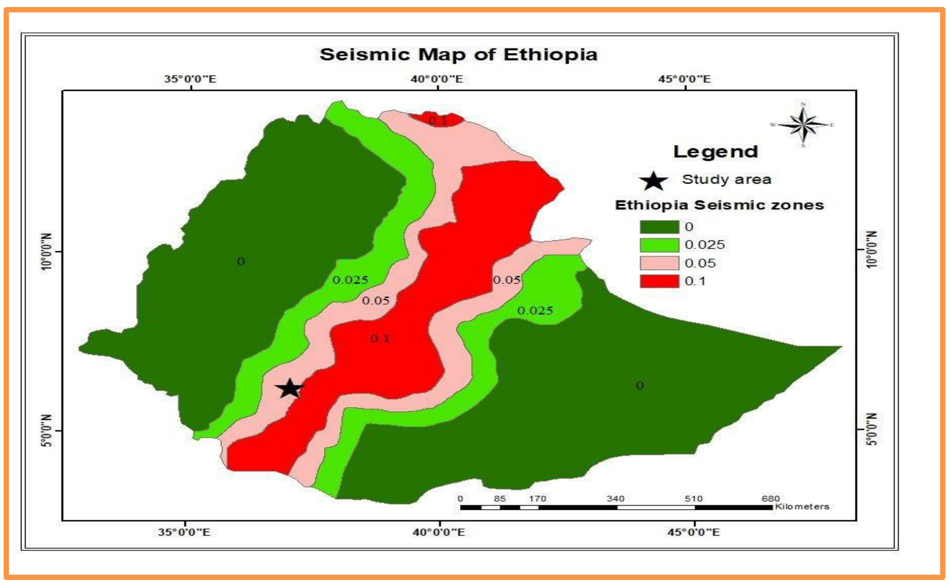

Figure 1.4 Seismic map of the study area(Dulbal,2020)

1.2.4. The climate condition of the study area

According to the map shown in the ERA Drainage Design Manual 2013, the project area is located in B2 Rainfall Regions, which receive high annual rainfall. It lies in one of the wettest zones of Ethiopia, and the mean annual rainfall of these regions is between 1600 and 1999 mm per year. Generally, the project road traverses through Kola, Woyna-dega, and Dega climatic areas. The higher altitude section of the corridor receives a large amount of annual precipitation for a longer period, mainly concentrated in the eight-month-long rainy period from March to October.

1.2.4.1. **Temperature**

The maximum and minimum mean annual temperature data for the study area were taken from the National Meteorological Agency of Ethiopia for chencha stations.

The maximum and minimum average annual temperatures of chencha in the study area are 28.07 ºC to 8.1 ºC and 25.45 ºC to 10.39 ºC, respectively.

The weather conditions for some of the period under review have been unfavorable for road construction, and significant rain has been recorded on the days shown below. The maximum and minimum average annual temperatures of chencha in the study area range from 20.59 ºC to 9.73 ºC.

	Jan	Feb	Mar	Apr	May	Jun	Jul	Aug	Sep	Oct	Nov	Dec
Chencha TMPMAX	20.36	20.59	20.51	20.53	20.43	20.24	20.41	20.67	20.48	20.57	20.61	20.53
Chencha TMPMIN	10.25	10.22	10.25	10.06	10.06	9.95	10.02	9.73	9.99	10.02	9.99	9.97

Figure1.5 Mean average temperature of the study area (2012-2019).

(Sources: National Meteorological Agency of Ethiopia).

1.2.4.2. Rainfall Of The Study Area

According to Abebe et al. (2010), slope failures are typically caused by intense rainfall. During periods of intense rainfall, the distribution of pore water pressures in the soil varies greatly depending on the hydraulic conductivity, terrain, level of weathering, and type of soil. The current study region experiences a range of tropical and subtropical meteorological conditions. Additionally, the research location experiences slope instability during the wet season. The National Meteorological Agency of Ethiopia provided the research area with rainfall data for chencha stations. The greatest and minimum monthly rainfall amounts at Chencha station were 153mm and 12.08mm, respectively (Fig. 1.6).According to field observations, slope instability in the study area occurs more frequently during months of may and October where heavy rainfalls.

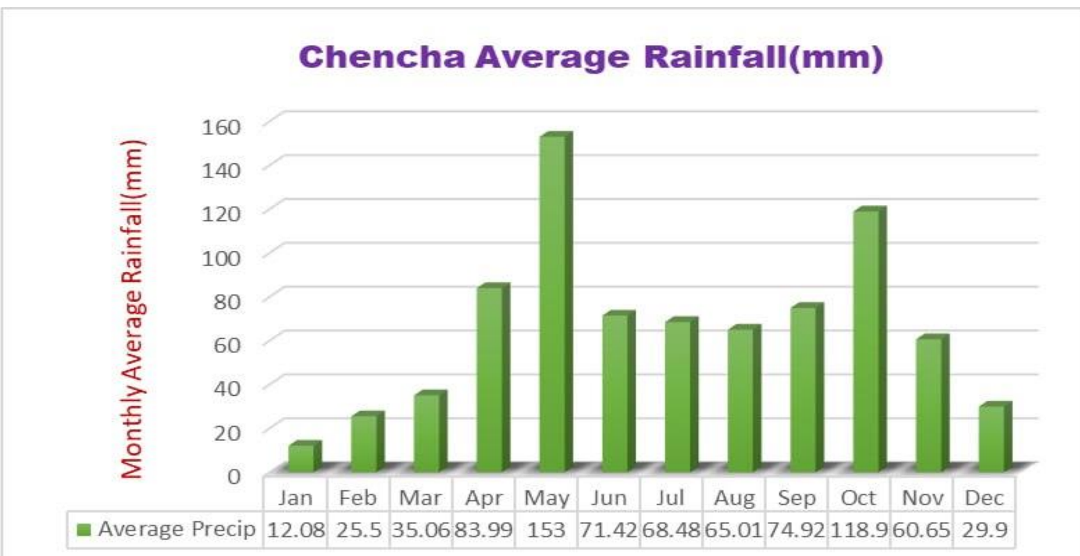

Figure 1.6 Monthly Rainfall data of the study area (2012-2019)

1.3.Statement of the Problem

Slope instability is one of the most hazardous processes in the world and is caused by the failure of soil, rock, or a combination of soil and rock along the road (Cheng and Lau, 2008). Similarly, most of the north, south, and western regions of the Ethiopian plateau face a record of slope instability both in superficial materials and at bedrock due to the cutting of hills along road sides (Ayalew, 1999).

Slope failures are very likely to occur on the main route that connects Morka, Gircha, and Chencha. Problems with slope instability are most prevalent during the rainy season. The project road features difficult, inclining terrain. The area is vulnerable to issues with slope stability because of its steep slope. The study area is covered by loose colluvium deposits, thick residual clay soil, and highly weathered and fractured rocks that were caused by intense and prolonged rainfall. As a result, these features have low shear strength, which may cause a landslide or slope failure. Additionally, some of the rocks were impacted by earth flows, debris flows. Therefore, this study is intended to carry out a slope stability analysis on slope sections along the road and provide some remedial measures based on the field investigation, laboratory tests, and stability analysis results. Therefore, the purpose of this study is to perform a slope stability analysis on slope portions along the road and to offer some corrective solutions based on the findings of the field investigation, the results of the laboratory tests, and the results of the stability analysis.

1.4. Objective of the Study

1.4.1. General Objective

The main objective of this study is to identify and analyze slope instability problems along the road that connects Morka, Gircha, Chinch, Gamo Gofa Zone, and southern Ethiopia.

1.4.2. Specific Objective

- To locate critical slope instabilities along a selected road section
- To determine the factor of safety of critical slope sections.
- To forward effective remedial measures for identified problems.

1.5. Significance of the study

The result of the study will be essential to providing detailed information about the slope stability of the road. The current investigations will be used as input data for designing slope instability countermeasures for future road upgrades and maintenance works. It also recommends corrective actions that could reduce the dangers posed by slope instability issues. Slope stability evaluations are concerned with identifying critical geological materials and environmental and economic parameters that will affect the road. Understanding the causative and triggering factors responsible for slope instability may provide insight into the possible mechanism of landslides in the area, which may help in the development of potential remedial measures. It may also be a source of information for subsequent researchers who wish to work on the same subject in different study areas.

1.6. Limitations and scope of the study

Most soil slope failures were found along the road segments in the current study area. However, because of time, resource, and financial constraints, the investigations were limited to only a subsection of the slopes that showed high potential instability. This study is limited to the use of the empirical method due to a lack of primary data and, in addition, lack of sufficient secondary data.

Organization of the paper/study

Chapter 1: describes background of the study, problem of the statement, objectives.

Chapter 2: deals with literature review in which previous works related to the current study has been reviewed. In addition, factors which contribute to slope instability was discussed. Later, conceptual frame work and general methodology was developed.

Chapter 3: Concern with the methodology followed to analyses the stability of the slope in the study area. It discusses each and every procedure followed to analyses the stability of the slope for the present study.

Chapter 4: Deals with the geological set up which includes type of lithology and geological structure of the study area has been summarized. In addition, local geology of the study area was also discussed.

Chapter 5: Deals with result and discussion of slope stability analyses in which the result of stability analyses was illustrated and interpreted. Later, prices discussion on the analyzed result was undertaken.

Chapter 6: Deals about conclusion and recommendations. Conclusions were made from stability analyses result. Finally, recommendation on the possible remedial measure was forwarded based on the analyses result.

CHAPTER 2

2. LITERATURE REVIEW

2.1. INTRODUCTION

The resistance of an inclined surface to failure by sliding or collapsing may be referred to as slope stability (Kliche, 1999). Finding at-risk areas, looking into potential failure mechanisms, figuring out how sensitive a slope is to various triggering mechanisms, designing the best slopes in terms of safety, dependability, and cost, and designing potential corrective measures are the primary goals of slope stability analysis, according to (Eberhardt et al., 2003).

In Ethiopia, built infrastructure including roads, buildings, and dams are all damaged by a variety of natural geological fluctuations and ground slope instability, rock slope instability, surface floods, and soil erosion. Road construction is one of the most significant investments in Ethiopia. However, the pass country mountainous region also experienced a significant amount of slope instability along its highways. External variables like heavy rain and earthquakes, which result in significant economic damage and human casualties worldwide, frequently induce slope failure and landslides (Eberhardt et al., 2003).

2.2. **Slope stability studies in Ethiopia.**

(Beyene & Assefa, 2022) investigated the assessment of slope stability for a few portions of the Gohatsion-Dejen road of the Blue Nile Gorge, Central Ethiopia. They used probabilistic and deterministic methodologies. Four carefully chosen critical slope sections two from failing colluvium sections and two from rock slopes were tested for stability. With the aid of the SLIDE software and for rock slopes with a planar mode of failure, the stability study of colluvium slopes was done for the worst possible conditions, both present and future. by the deterministic and probabilistic method-supporting ROCPLANE software.

(MISGANA, 2018) used slope stability probability classification, stereographic projection, limit equilibrium, and probabilistic analysis methods to examine the stability of the slope along the Mana Begna to Lemlem Bereha route. According to the analysis's findings, the crucial rock and soil slopes were both unstable, especially under dynamic saturation circumstances.

In order to zone and mitigate areas at risk of high and extremely high landslides, (Woldegiorgis, 2008) carried a regional research on the Blue Nile basin. By employing remote sensing and a GIS technique to divide the area into separate danger zones and using geology, groundwater quality, drainage, slope, structures, aspect, and land cover as causative elements, Ayele (2009) evaluated the landslide hazard in the Abay Gorge of Central Ethiopia.

In Ethiopia, there have been over 700 reported landslide sites, the majority of which harm rural populations, infrastructure, farmland, dwellings, and about 54 sites along road sections(Woldearegay, 2013). Landslides are the most prevalent and widely dispersed types of geohazard in Ethiopia. Rock falls, colluvial material failure by rotation, and debris slides are frequent occurrences along the road segment due to slope instability issues. The majority of the time, slope instability is caused by the presence of loose, unconsolidated materials (colluvial materials), highly worn rock, steep natural slopes, inadequate drainage conditions, and the occurrence of heavy seasonal rains (Woldearegay, 2013).

The slope stability of the road from Gutane Migiru to Finca'a Sugar Factory was investigated by Lamessa & Meten in 2021. From a kinematic analysis perspective, this study indicated wedge and planar failure as the primary types of rock failure. Using the software Rocplane and Swedge, for planar and wedge mechanisms of rock failure, respectively, the factors of safety and probability of failure were computed. Similar to this, slide software was used to analyze the stability of soil slopes. Critical rock and soil slopes were both shown to be unstable in dynamic saturated conditions as opposed to slopes in dry conditions by the deterministic and probabilistic stability calculations (Lamessa & Meten, 2021)

2.3. **Slope Stability Governing Factors**

The stability of the slope is governed by a number of variables; some of these elements operate as driving forces, while the other factor acts as a resistive force. The geometry of the slope and potential failure planes, surface drainage, groundwater conditions, the mineral composition, and the shear strength parameters of the materials that make up the slope are examples of internal factors, while seismicity, rainfall, and human activity are examples of external factors (Raghuvanshi, 2019).

2.3.1. **Rainfall**

The influence of rainfall, one of the external and triggering causes of slope instability, is frequently the primary cause of slope failure occurrence(Ayalew et al., 2004).Rainfall that seeps into the slope will make the possible failure plane more unstable by weakening its shear structure (Pantelidis, 2009). Rainfall has several effects, one of which is to raise the elevation of groundwater levels (Wyllie & Mah, 2004).

2.3.2. **Human activities**

The slope may become unstable as a result of human activities, such as inappropriate slope changes and excavations. The most common human actions that might cause a slope to fail include unexpected slope cutting, a steepening of the gradient, inappropriate excavation at the slope's toe, and adding an additional load. 2017 (Hamza & Raghuvanshi, 2017).

2.3.3. **Seismicity**

Another element that affects slope stability is seismic activity, particularly in seismically active areas (Hoek & Bray, 1981).According to (Pantelidis, 2009), an earthquake must have a minimum magnitude of 4-5MM in order to cause slope failure. For crucial constructions like steep slopes, it is advised from a safety standpoint to take seismicity into account. (Dehls et al., 2012).Under seismic loading circumstances, planar rock slope failures will be easily destabilized because horizontal seismic acceleration increases the driving force along the failure plane.

2.3.4. Geometry of the slope

The failure plane's dip and dip direction, slope height, upper slope angle, and tension crack are all factors that are taken into consideration while determining the geometry of a slope, particularly for rock slopes. The stability of the slope is influenced by each of the factors either separately or collectively. The slope is typically unstable on steeper slopes (Raghuvanshi, 2019). Potential failure planes are one of the factors that determine the stability of the rock and soil slope. In rock slope failure, the persistence of discontinuities such as joints, faults, and shear planes acts as failure planes along which the slope will fail. Surface water that infiltrates into the slope, mainly through tension cracks, will produce water force and lubricate the failure plane, which later enhances slope instability. Similar to this, failure planes are created in soil slopes by weak soil layers that occasionally rest on hard strata. The prospective failure plane's dip should be smaller than the slope face's dip but more than the friction angle along the failure plane for a particular form of rock slope failure to occur (Hoek & Bray, 1981).

2.3.5. Surface Water Drainage and Groundwater Conditions

Due to decreased effective stress within discontinuities and decreased shear strength along discontinuities, groundwater on a rock slope primarily affects stability (Zare & Jimenez, 2015). The presence of water reduces shear strength and increases pore water pressure close to the probable failure surface, which may facilitate sliding (Hack, 2002).According to (Ermias et al., 2017) increasing groundwater in a soil slope causes the creation of pore water pressure, which lowers the shear strength of the soil mass.

2.4. Types of slope failure.

The typical slope failures that are expected to occur in soil slopes are translational, planar, or wedge, circular, non-circular, and combinations of both circular and non-circular(Abramson et al., 2001). Planar slope failure occurs in a soil layer or relict joint with relatively low strength, which influences the failure surface, while translational type failure occurs where shallow soil contains overly strong material(Chowdhury & Flentje, 2011). According to (Abramson et al., 2001), the circular mode of failure also occurs on slopes with homogeneous materials, primarily soil slopes. The majority of non-circular failure modes are seen in slopes with a diverse composition.

- Rotational failure
- Translational failure
- Compound failure
- Wedge failure

Rotational failure

When anything fails by rotating along a slip surface, it is said to have failed by rotation, and the shape that results on the slip surface is curved. It travels lower and outward as it fails. The form is circular in homogeneous soils and non-circular in heterogeneous soils. There are three possible methods for rotational failure to happen:

1. Face failure or slope failure
2. Toe failure
3. Base failure

- When there is a weak layer in the soil above the toe, face failure ensues. The failure plane in this instance crosses the incline above the toe.
- The most frequent failure occurs at the toe of the slope and is referred to as a toe failure.
- On finite slopes, such as earthen dams, embankments, man-made slopes, etc., rotational failure can be observed.

Translational failure

- In the case of infinite slopes, translation failure occurs, and the failure surface is parallel to the slope surface.
- When a slope has no clearly defined borders and the soil under the free surface has the same characteristics up to the same depths along the slope, the slope is said to be endless.
- As previously stated, if the soil beneath this layer is a strong or hard stratum and the soil along the slope has similar attributes up to a certain depth, the weak topsoil will produce a parallel slip surface when it fails.
- This kind of failure can be seen in naturally occurring slope formations as well as slopes made of layered materials.

Compound failure

Combining rotational and translational sliding failures is referred to as a compound failure. Failure happens when the slip surface curves at both ends but has a level or flat middle point, as the combination suggests. When a hard soil level develops at a sufficient depth from the toe, the slip surface may become flat.

Planar Failure

According to(Raghuvanshi, 2019) planar failure occurs when the discontinuity plane's strike is almost parallel to the slope's strike and its daylights on the slope face. According to(Pantelidis, 2009), planar failure describes the sliding of a rock block along one or more parallel failure planes that are oriented adversely to the slope face. Typically, structural discontinuities like bedding planes, fractures, joints, or the contact between bedrock and an upper layer of weathered material serve as failure surfaces. Generally, planar failure happens:

- when the sliding plane and the slope face's impacts are 20-degrees apart from one another.
- The failure plane is sunlit on the slope face, and the dip of the discontinuity is smaller than the dip of the slope.
- The angle of friction on the surface is smaller than the dip of the planar discontinuity.

Wedge Failure

When two structural discontinuity planes collide obliquely and their lines of intersection are pointed in the direction of the slope face, the wedge mode of failure results. On these two intersecting planes, the rock mass will slide in the downward direction of the line of intersection (Pantelidis, 2009). When two weak planes connect to form a wedge, a rock slope fails due to wedge failure. Both discontinuity's lines of intersection roughly parallel the slope strike and dip in the direction of the slope plane.

if any of the following apply, wedge failure is more likely to occur:

- The slope's dip is steeper than the dip of the line connecting the two discontinuities.
- The line of intersection must daylight on the slope face, and the dip must be greater than the angle of friction of the surface.

- The line of intersection must also daylight in the slope because the plunge must be less than the inclination of the slope face.

Toppling Failure

According to (Goodman, 1989)the fall of the rock slope is caused by the overturning of rock strata or discontinuities that are sinking sharply into the slope face. Additionally, (Alejano et al., 2010) defined toppling failure as the overturning of a rock block through an axis point that is below its center of gravity. A series of fractures that strike parallel to the slope face and steeply drop into the rock mass cause this form of failure to occur most frequently in rock masses that have been separated into a number of columns(Norrish & Wyllie, 1996). A tightly spaced jointed rock mass and a sharply dipping discontinuity that sets that dip away from the slope surface are necessary for toppling failure. When rock columns or blocks rotate around a fixed base, topping failure occurs. The two types of toppling are flexural and block toppling. Flexural toppling happens when a line of beds is sharply sloped away from a rock face. The weighted centroid may fall outside the base of the column due to the presence of multiple close joints in the rock mass, which can also result in block toppling.

2.5. Stabilization Methods of Rock and Soil Slopes

For slopes made of rock and soil, stabilization techniques provide slope stability. According to (Abramson et al., 2001). the slope stabilization approach increases resistive force by building retaining structures or supports, decreasing driving force by extracting material from the unstable ground, and decreasing driving force by employing chemical treatments to improve the soil. Numerous construction projects, including roads, railroads, tunnels, dams, mines, residential areas, and industries, require stable slopes and the prevention of rock falls in rocky terrain. When the causes of slope stability are discovered, the best slope correction method is selected based on feasibility, stability, and cost (Kazmi et al., 2017). These remedial techniques can help lower the probability of slope failures by addressing their causes(Kazmi et al., 2017). An unstable rock slope can be stabilized using a variety of techniques, A rock slope can be stabilized using a number of techniques, some of which are discussed here (Abramson et al., 2001).

Drainage Method: When surface and subsurface drains are correctly maintained, the drainage method can be used (Chen et al., 2001) In order to prevent hydrostatic pressure from building up at rock mass discontinuities, drainage is required (Abramson et al., 2002). The two main causes of slope instability are the saturation of the subsoil and the accumulation of pore water pressure. With correct surface and subsurface drainage system design, the likelihood of pore water pressure and subsoil saturation building up can be reduced, boosting slope stability (Kazmi et al., 2017).

Ditches: Surface drainage systems like ditches, which are typically lined with concrete, can direct surface runoff away from slopes.

Trenches: These types of surface drainage, which are typically lined with geosynthetic fiber, are also capable of intercepting significant amounts of water before they fill the slope.

Horizontal and vertical drain pipes: Drain pipes that run horizontally and vertically: This type of subsurface drainage system is set up to catch water-containing beds or discontinuities.

Re-sloping and unloading: is a technique for removing overburden, such as soil or rock material, from the upper portion of a slope in order to reduce the slope's angle below the angle of the underlying rock component (Hoek & Bray, 1981).

Scaling: using shovels, scaling bars, and chainsaws, scaling is the process of removing loose rock, dirt, and plants off the slope's face.

Rock Reinforcement Supports: According to(Cheng & Lau, 2014), a rock reinforcement support entails the use of external components such rock bolts, anchors, and shotcrete to strengthen the rock and prevent failure.

Rock bolts and Anchors: According to (Hoek & Bray, 1981) rock bolts and anchors are the most helpful supports because they stop rock blocks from slipping away from discontinuity planes. For slopes with fractured rock, concrete walls are combined with rock bolts and anchors to cover the broken rock areas.

Shotcrete: Mortar and fine aggregates make up the majority of shotcrete. Zones or beds of closely fragmented rock can be protected by applying a layer of shotcrete to the rock face. Additionally, shotcrete prevents falling small rock chunks. According to (Wyllie & Mah, 2004), shotcrete improves the tensile and shear strength of slopes, reducing the likelihood that they would fail (Wyllie & Mah, 2004).

Retaining Structures: Examples of gravity retaining walls, gabion walls, and reinforced earth retaining structures with strip metallic reinforcement elements include retention nets for rock slope faces, rockfall attenuation or stopping systems (rock trap ditches, benches, fences, and walls), and protective rock or concrete blocks against erosion.

2.6.Rock Mass Failure Criteria

2.6.1. **Mohr-Coulomb Failure Criterion**

Mohr-Coulomb criterion is used in soil mechanics, or the criterion proposed by Barton 1970. According to (Hammah et al., 2004), the Mohr-Coulomb failure or strength criterion has been extensively used in geotechnical applications. To calculate the shear strength of soil and rock materials, a typical stress-dependent strength envelope is frequently utilized. The following is one approach to express the Mohr-Coulomb criterion:

$$\tau = c + \partial n \tan\varphi \qquad \text{Eq 2.1}$$

where, τ = is the shear stress, σ= is the normal stress, c= is the cohesion of the material, and+φ is the material angle of friction.

2.6.2. **Barton-Bandis Failure Criterion**

(Wyllie & Mah, 2004) The shear strength of discontinuities can be calculated using an empirical law of fundamental friction angle, which was previously put forth by Barton in 1973. According to (Wyllie & Mah, 2004)), the combined influences of surface roughness, rock strength at the surface, applied normal stress, and shear displacement determine the shear strength of discontinuity surfaces in rock slopes. Failure of Barton-Bandis Barton (1973) suggests the following formulation for the criteria:

$$\tau = \partial n * \tan \{\text{JRC} * \log 10\ (jcs\ \sigma n) + \phi r\} \qquad \text{Eq (2.2)}$$

where: τ = Peak shear strength, ∂n = Effective normal stress, JRC = Joint roughness coefficient, JCS = Joint wall compressive strength, ϕr= Residual friction angle, Joint wall compressive strength (JCS) is the strength of a layer of rock adjacent to a joint and it controls the strength and deformation properties of the rock mass(Barton, 1973). According to(Barton & Choubey, 1977) the joint roughness coefficient (JRC) is the coefficient of joint surface roughness with a value ranging from 0- 20 (smoothest to roughest). A basic friction angle is an angle with a flat, planar, and un-weathered rock surface in which its value ranges from 25-35.

2.6.3. **Hoek-Brown Failure Criterion**

Hoek and Brown (1980) established a relationship between the maximum and minimum primary stresses to forecast the failure of complete and fragmented rocks. Relationships between the criterion and rock mass rating elements were introduced to characterise the qualities of the rock mass. Hoek and Brown (2019) proposed the Geological Strength Index (GSI), a generalised Hoek-Brown criterion. Use the following equation in the 2002 edition of the Hoek-Brown criterion:

$$\partial 1 = \partial 3 + \partial ci\ (mb\ \partial 3\ \partial ci + s)\ a \qquad \text{Eq (2.3)}$$

Where σ1 is the maximum and σ3 is the minimum effective principal stresses at failure respectively, mb, s, and α are the values of Hoek-Brown constants for the rock mass, and ∂ci is the uniaxial compressive strength of the intact rock.

2.6.4. **Rock mass classification system.**

The rock mass classification technique is intended to categorise rock masses based on qualitative variables such as strength, discontinuity condition, weathering condition, and structural orientation. These qualitative parameters will be converted into rated parameters, providing measurable data for support estimation, a foundation for estimating deformability and strength properties, and a platform for communication among researchers, designers, engineers, and contractors (Bieniawski, 1989). further believes that classification of rock masses is useful for measuring the effectiveness of rock-cut slopes by utilising the most important intrinsic and structural characteristics (Pantelidis, 2009).

2.6.5. **Rock Mass Rating (RMR)**

(Bieniawski, 1979) released the specifics of a rock mass classification system known as the Geomechanics Classification or the Rock Mass Rating (RMR) system, which was established by Bieniawski in 1973. One of the geomechanical classifications for slopes now in use is the Rock Mass Rating (RMR) (Bieniawski, 1979)A modified rating comprised of five categorization characteristics and one rating adjustment was also created by Bieniawski in 1989. The uniaxial compressive strength intact material, the rock quality designation (RQD), the space between discontinuities, the condition of the discontinuities, and the state of the groundwater are all factors in the rating adjustment in the direction of discontinuities. The five parameters described above are the RMR basic parameters, and they may be used to estimate discontinuity spacing, discontinuity condition, and groundwater condition in the field using visual observation and tools like a tape meter (Bieniawski, 1973).

Table 2.1 rock mass parameter and range of values,(De Mulder et al,2012

1.	Strength of intact rock material	Point load strength index (MPa)	> 10	4 – 10	2 – 4	1 – 2			
		Uniaxial compressive strength (MPa)	> 250	100 – 250	50 – 100	25 – 50	5 – 25	1 – 5	< 1
	Rating		*15*	*12*	*7*	*4*	*2*	*1*	*0*
2.	RQD (%)		90 – 100	75 – 90	50 – 75	25 – 50		< 25	
	Rating		*20*	*17*	*13*	*8*		*3*	
3.	Joint spacing (m)		> 2	0.6 – 2	0.2 – 0.6	0.06 – 0.2		< 0.06	
	Rating		*20*	*15*	*10*	*8*		*5*	
4.	Condition of joints		not continuous, very rough surfaces, unweathered, no separation	slightly rough surfaces, slightly weathered, separation <1 mm	slightly rough surfaces, highly weathered, separation <1 mm	continuous, slickensided surfaces, or gouge <5 mm thick, or separation 1–5 mm		continuous joints, soft gouge >5 mm thick, or separation >5 mm	
	Rating		*30*	*25*	*20*	*10*		*0*	
5.	Ground-water	inflow per 10 m tunnel length (l /min), or	none	< 10	10 – 25	25 – 125	> 125		
		joint water pressure/major in situ stress, or	0	0 – 0.1	0.1 – 0.2	0.2 – 0.5	> 0.5		
		general conditions at excavation surface	completely dry	damp	wet	dripping	flowing		
	Rating		*15*	*10*	*7*	*4*	*0*		

2.6.6. **Rock Quality Designation index (RQD)**

The classification of rock quality is an important criteria for characterising the rock mass.(Deere & Deere, 1989) created the Rock Quality Designation (RQD) index.Several characteristics influence the RQD index, including joint orientation, joint spacing, fracture frequency, and joint roughness (Azimian, 2016). The percentage of unbroken drill core pieces longer than 10cm recovered during a single core run is defined as RQD(Abzalov, 2016). The symbol represents the general equation.

$RQD = \sum$ Core pieces>10cm/Total length of core run × 100%

The volumetric joint count (Jv) is a jointing degree or inter-block size measurement that can be used to define rock mass jointing (Palmstrom, 2005).As defined by the Jv, joint spacing (S) is the distance between two successive discontinuities measured along a line on the rock surface. The Jv count is the number of joints that intersect a 1-m3 volume. According to (Palmstrom, 1974) the correlation between RQD and volumetric discontinuity joints Jv can also be used to determine the RQD, as shown in eq. 2.4.

$$RQD = 115 - 3.3Jv \qquad \text{Eq (2.4)}$$

Where Jv is the sum of the number of discontinuities per unit length for all discontinuity sets, which may be derived from the discontinuity set spacings inside a volume of the rock mass (Palmstrom, 1982), as follows: eq. 2.5

$$JV = 1/S1 + 1/S2 + 1/S3 + \cdots + 1/sn \qquad \text{Eq (2.5)}$$

Where s1, s2, and s3 are the mean discontinuity set spacings (Palmstrom, 2002). suggests that r=6 m be assumed. As a result, the volumetric discontinuity frequency Jv can be generalized as eq.2.7

$$Jv = 1/S1 + 1/S2 + 1/S3 + \cdots + Nr/6 \qquad \text{Eq (2.6)}$$

where Nr is the number of random discontinuities.

2.6.7. **Point Load Strength Index**

In the point load test, core specimens or irregular rock bits are placed between the conical platens and the applied force (P) and distance (D) between them are measured at failure. ASTM D5731 (1995) Furthermore, because of the convenience of testing straight, cut blocks, or irregular lumps, the point load test is one of the cheapest and most practical processes for evaluating the strengths of rocks. ASTM (2008). Many tests have been carried out to investigate the relationship between uniaxial compressive strength (UCS) and point load index (Is) for different rock types. According to (Broch & Franklin, 1972), the connection between uniaxial compressive strength and the point load strength index is as follows:

$$UCS = 24 * Is\ (50) \qquad \text{Eq 2.7}$$

Where Is (50) is the size corrected point load strength.

2.6.8. **Geological Strength Index (GSI)**

The geological strength index (GSI) is a field-based method for determining the strength of rock masses in order to build tunnels, caves, and other underground structures including geological data about rock mass, inputs from qualified and experienced field geologists/engineers about the visual impression of the rock structure, such as block and surface condition of discontinuities represented by joint characteristics (roughness and alteration), and reliable data in the form of rock mass strength properties that are used as input parameters for numerical analysis (Zhang et al., 2019). The GSI grouping method is frequently used as an empirical technique for measuring the strength and deformation properties of heavily joined rock masses (Hoek and Brown, 2019). Based on field observations of the rock mass structure, which ranges from blocky to fragmented, the GSI approach categorises the rock mass environment into five categories, ranging from very good to very bad (Hoek et al., 1988; Hoek and Brown, 1997). Marinos and Hoek (2000) proposed a quantitative GSI chart for estimating GSI.

2.6.9. **Uniaxial Compressive Strength (UCS) of Intact Rock**

In rock engineering profession, uniaxial compressive strength is regarded as one of the most essential characteristics in the characterization of rock material (Çobanoğlu & Çelik, 2008). The uniaxial compressive strength of intact rock material can be determined using rock cores in a laboratory test. The UCS can be calculated using the empirical formula (Broch & Franklin, 1972) from the point load strength index Is (50), as well as Schmidt hammer rebound hardness value (R) data in the laboratory and in situ experiments. Schmidt hammer hardness values (N-values) are used in rock mechanics to evaluate the uniaxial compressive strength (UCS) and modulus of elasticity (E) of undamaged rock in laboratory and in situ testing (Rahim et al., 2022).

Miller (1965) presented a link with the rebound number for estimating UCS from the Schmidt hammer rebound value for use in rock quality. Furthermore, (Barton & Choubey, 1977) computed the rock's uniaxial compressive strength (UCS) by multiplying the rebound number by the dry density of the rock using the equation below.

$$\log10\ (UCS) = 0.00088\gamma R + 1.01 \qquad \text{Eq 2.8}$$

Where, UCS is the uniaxial compressive strength in Mpa, γ is the dry rock densities in KN/m3 and R is the average Schmidt rebound value.

2.7. Shear strength parameter of the material composing the slope

The key criteria that define the resistive force operating normal to the failure plane are the shear strength parameters of the material that composes the slope (Raghuvanshi, 2019). Accordingly,the parameters are affected by discontinuity conditions such as roughness, continuity, aperture, and filling. Barton-Bandis (1990) determined the first non-linear shear strength along the failure plane or natural joints using (Barton, 1973) empirical law of basic friction angle, which is stated as follows:

$$\tau=\sigma n \tan[JRC \log 10(JCS/\sigma n)+\phi b] \qquad \text{Eq 2.9}$$

where τ= is peak shear strength (kPa), σn =is effective normal stress (kPa), JRC= is joint roughness coefficient, JCS =is joint wall compressive strength (kPa) and ϕb= is basic friction angle. Definitions of each parameter were given below.

2.7.1. Joint roughness coefficient (JRC):

It is the calculated coefficient of roughness of the joint surface, which spans from 0 to 20 (smoothest to roughest). This can be determined by comparing the discontinuity surface roughness to the joint roughness profile developed by (Barton & Choubey, 1977), which was later adopted by ISRM (1978), or by examining the relationship between the profiles' length and maximum amplitude. Back analysis of tilt tests of rock joints can also be used to determine it (Barton & Choubey, 1977).

2.7.2. joint wall compressive strength (JCS):

Joint wall compressive strength (JCS): It is the strength of the layer of rock adjacent to the joint, and it controls the strength and deformation properties of the rock mass (Barton, 1973). If the joint is unweathered, joint wall compressive strength (JCS) is equal to the unconfined compressive strength (c) of unweathered rock (Addis et al., 1990).The appropriate value of uniaxial compressive strength (c) determined from Schmidt rebound value (R) applied on an unweathered rock surface with unit weight will represent the joint wall compressive strength of the rock (JCS). However, for weathered rock surfaces or in the absence of Schmidt hammer reading, JCS will become a fraction of the uniaxial compressive strength of the rock, approximately (1/4 c) (Barton, 1976).

2.7.3. **Basic friction angle (ϕb):**

is an angle with a flat, planar, and unweathered rock surface that has a value ranging from 21º to 40º for the majority of the rock (Goodman, 1980). According to Barton (1973), its value ranges from 25° to 35° for most smooth, flat, and unweathered rock surfaces.A tilt test on smooth, flat, and unweathered joints cut from rock surfaces with a saw or the basic friction angle determined by Barton and Choubey (1977) can be used to estimate it. According to (Barton & Choubey, 1977), fundamental friction angle can be associated with residual friction angle (r) for differentially worn joints.

$$\phi r=(\phi b-20)+20(r/R)$$

where r represents the Schmidt rebound number on wet and weathered fracture surfaces and R represents the Schmidt rebound number on dry, unweathered sawn surfaces. Rocdata software (Rocdata 3.0, Rocscience, 2004) can calculate cohesion and friction angle along the failure plane using Equation 2.9, which is already included, as well as a joint roughness coefficient profile, a joint wall compressive strength range, and a basic friction angle table (Barton & Choubey, 1977). Furthermore, the rock's slope height and unit weight were input into the Rocdata software. Finally, using Rocdata software, cohesion and friction angles along failure planes or discontinuities will be calculated. Finally, using Rocdata software, cohesion and friction angles along failure planes or discontinuities will be calculated. Similarly, rock masses' cohesion and friction angle can be calculated using either back analysis of failed or failing slope failures (Hoek-Brown, 1980; Sharma et al., 1999). Furthermore, shear strength parameters can be calculated empirically based on rock mass classification (Bieniawski, 1989).

2.8. **Slope Stability Analyses Approaches**

2.8.1. Limit equilibrium method

Because of its simplicity and accuracy, LE analysis is now used in the majority of slope stability evaluations. These methods entail slicing the slope into small slices and applying relevant equilibrium equations (force and/or moment equilibrium). Many alternatives, such as the Bishop and Fellenius approaches, were proposed based on the assumptions made about the efforts between the slices and the equilibrium equations evaluated. In most circumstances, they produce identical effects. Modern limit equilibrium software allows for the handling of ever-increasing complexity inside an investigation. Complex stratigraphy, highly irregular pore-water pressure conditions, numerous linear and nonlinear shear strength models, practically any slip surface shape, dispersed or concentrated loads, and structural reinforcement are now all feasible. Limit equilibrium formulations based on the slice method are also increasingly being used to analyse the stability of structures such as tie-back walls, nail or fabric-reinforced slopes, and even the sliding stability of structures subjected to high horizontal loading caused by ice flows.

Ordinary method of slices

This method ignores all interslice forces and fails to achieve force equilibrium for both the slide mass and individual slices. However, this is one of the most basic processes based on the slice approach (Fellenius, 1936).This method, also known as the Swedish Method of Slices or the Fellenius Method, presupposes a circular slip surface.

Simplified Bishop

The simplified Bishop approach implies that there is no vertical interslice shear force and that the resulting interslice force is horizontal (Bishop, 1955). It satisfies the moment equilibrium but not the force equilibrium. The horizontal force equilibrium equation is used in this method to calculate the factor of safety. It excludes interslice pressures from the analysis but accounts for their impact with a correction factor. (Janbu et al., 1956) found that the correction factor is related to cohesion, the angle of internal friction, and the geometry of the failure surface.

Spencer Method

This is a very accurate approach that fulfils both force and moment equilibrium, and it works for any form of slip surface. The fundamental assumption in this method is that the inclinations of the side forces are constant throughout all slices.

Morgenstern and Price

Morgenstern and Price developed an approach similar to Spencer's, except that the inclination of the interslice resultant force is believed to fluctuate as a "portion" of an arbitrary function. This approach enables the specification of many forms of interslice force functions (Morgenstern & Price, 1965).

2.8.2. Finite element analysis

The use of FE in geotechnical analysis has grown in popularity as computer performance has improved. These approaches have several advantages: they can model slopes with a high degree of realism (complex geometry, loading sequences, presence of reinforcement material, water action, laws for complicated soil behaviour), and they can better visualise soil deformations in place. However, because of the greater number of variables available to the engineer, understanding the analytic output is crucial. Cases of extreme failure, such as the Nicoll Highway in Singapore, illustrate the necessity of knowing the numerical approach employed and the failure criteria. The strength reduction method is used to analyse slopes. This strategy is based on lowering the soil's cohesion (c) and tangent of the friction angle (tan). The parameters are gradually decreased until the soil mass fails. The relatively stable condition of the slopes in the field may be owing to the low magnitude of the shear strain, which prevents it from propagating towards the more stressed toe part and causing failure. In engineering sciences, the finite element method is a sophisticated computer approach. This method is by far the most commonly utilised for analysing geotechnical problems. In contrast to the limit equilibrium approach, the finite element method takes into account the soil's linear and nonlinear stress-strain behaviour when estimating shear stress for analysis. Slope failure arises in a finite element method through zones that are unable to withstand the shear loads imposed. As a result, the results of this analysis are thought to be more realistic than the limit equilibrium method (Griffiths & Lane, 1999).

As computer performance has improved, the finite element method has become more preferred and prevalent in geotechnical analysis. These approaches offer various advantages, including the ability to model slopes with a high degree of realism (complex geometry, loading sequences, the presence of reinforcement material, the action of water, laws for complicated soil behaviour), and to better depict soil deformations in situ. However, because of the greater number of variables available to the engineer, understanding the analytic output is crucial (Matthews et al., 2014).The finite element method (FEM) can be used to compute displacements and stresses caused by applied loads. However, it does not provide a value for the overall factor of safety without additional processing of the computed stresses. The principal uses of the finite element method for design are as follows (Matthews et al., 2014):

(1) Estimates of displacements and construction pore water pressures can be obtained using finite element analyses. These may be beneficial for construction field control or when surrounding structures are at risk of damage. If the measured displacements and pore water pressures differ significantly from those estimated, the explanation for the divergence should be addressed.

(2) Finite element analyses provide displacement patterns that may show potential and possibly complex failure mechanisms. The validity of the factor of safety obtained from limit equilibrium analyses depends on locating the most critical potential slip surfaces. In complex conditions, it is often difficult to anticipate failure modes, particularly if reinforcement or structural members such as geotextiles, concrete retaining walls, or sheet piles are included. Once a potential failure mechanism is recognised, the factor of safety against a shear failure developing in that mode can be computed using conventional limit equilibrium procedures.

(3) Estimates of mobilised stresses and forces are provided through finite element analyses. When materials have extremely divergent stress-strain and strength properties, i.e., when strain compatibility is an issue, the finite element method may be especially effective in determining what strengths should be employed.

The FEM can assist in identifying local locations where "overstress" may occur, resulting in cracking in brittle and strain-softening materials. The FEM is also useful in determining how reinforcement will respond on embankments. Finite element analyses may be beneficial in areas where new types of reinforcement are being employed or reinforcement is being used in ways that differ from what is known. The force in the reinforcement is a key input to the stability studies for reinforced slopes. The FEM can be useful in determining the force that will be used. If desired, the findings of finite element analyses can be used to compute safety factors equivalent to those computed using limit equilibrium analyses. Stress Reduction Technique To analyze slopes, the strength reduction method is applied. This method is based on the reduction of the cohesion (c) and the tangent of the friction angle (tan φ) of the soil. The parameters are reduced in steps until the soil mass fails. firstly, the initial stresses in slope are computed using the elastic finite element analysis. The vector of externally nodal forces consists of three parts: (1) surface force; (2) body force (total unit weight of soils); and (3) pore water pressure.

Secondly, stresses and strains are calculated by the elasto-plastic finite element analysis using the reduced shear strength criterion. The shear strength reduction factor F is initially selected to be so small, for example, 0.01, that the shear strength is large enough to keep the slope in the elastic stage. Stresses at some Gaussian points reach the yielding condition as the shear strength reduction factor F increases gradually (Nakamura et al., 2005). When the stress at any Gaussian point reaches the yielding condition, the increment of the shear strength reduction factor will make stresses at more Gaussian points reach the yielding condition because of the residual force induced by the decrease in the shear strength of the soil (Nakamura et al., 2005).

The shear strength reduction factor F grows incrementally until the slope's global failure exceeds it, indicating that the finite element computation diverges under a physically real convergence condition. The slope's lowest factor of safety is found between the shear strength reduction factor F at which the iteration limit is achieved and the one immediately preceding it. The approach described below can predict the factor of safety in a single loop and is simple to apply in a computer programme (Nakamura et al., 2005). One of the most significant advantages of SSR FEM is that the safety factor arises naturally from the analysis, without the user having to commit to any particular component of the mechanism in advance.

2.8.3. Kinematic analyses

Kinematic analyses were carried out on the stereonet to show the influence of discontinuity sets on stability and to indicate the types of potential failure modes. A programme called Dips 5.0, developed by Rocscience, was used for the kinematics analysis. A declination of 7.50 was added to the dip directions of the data to correct for the magnetic declination (ROCSCIENCE, 1999). The stability of a bedrock-composed slope is often controlled by the geologic structure within the bedrock. In such cases, the geometrical relationships between the geologic structures and the orientation of the overlying slope determine the kinematic stability of the slope. Kinematic refers to the geometrically possible motion of a body without consideration of the forces involved.

Kinematic analysis is concerned with movement direction and which movements are permissible and which are not. Kinematic analysis is commonly used in slope stability to determine if blocks or masses of rock can move along geologic structures and slide out of the face of a slope. Kinematic analysis is often used to examine two major forms of potential sliding: plane failure and wedge failure, and it was applied in this work. Plane failure occurs when a single, planar geologic structure tilts downward (dips) at a flatter inclination than the underlying slope face. Wedge failure occurs when a line of contact between two intersecting geologic features slides downward (plunges) at an inclination lower than that of the overlying slope face. These two failure mechanisms, sliding plane failure and wedge failure, are discussed in greater detail below. The following requirements must be met before considering the kinematic acceptability of planar modes of failure:

- The plane on which sliding occurs must strike near parallel to the slope face (within approx. ±20°).
- Release surfaces (that provide negligible resistance to sliding) must be present to define the lateral slide boundaries.
- The sliding plane must “daylight” in the slope face.
- The dip of the sliding plane must be greater than the angle of friction.
- The upper end of the sliding surface either intersects the upper slope, or terminates in a tension crack.

Similar to planar failures, several conditions relating to the line of intersection must be met for failure to be kinematically admissible:

(i) The dip of the slope must exceed the dip of the line of intersection of the two wedges forming discontinuity planes.

(ii) The line of intersection must "daylight" on the slope face.

(iii) The dip of the line of intersection must be such that the strength of the two planes is reached.

(iv) The upper end of the line of intersection either intersects the upper slope or terminates in a tension crack.

Furthermore, a toppling mode of failure may occur when the slope face's dip direction is approximately opposite the opposite orientation of the discontinuity plane's dip direction, but toppling will not occur when the difference between the strike of the slope face and the strike of the plane of the discontinuities is relatively large, say more than 200 (Wyllie and Mah, 2004). The following are the necessary circumstances for toppling failure to occur (Hoek and Bray, 1981): The layers' strike must be roughly parallel to the slope face. Differences in these orientations between 15 and 30 degrees have been quoted by various workers, but for consistency with other modes of failure, a value of 20 degrees seems appropriate. The dip of the layers must be into the slope face. In this study, stereographic projection and identifying the failure mode of rock slopes were determined using dips software.

2.9. **Slope Stability Analysis Software**

Today, a variety of computer-based geotechnical applications may be used to conduct slope stability evaluations. Limit equilibrium designs have been used in software for a long time. Both LEM and FEM-based software are commonly used in geotechnical computations.

Phase software: Phase2 Software, developed by Rocscience Inc., Toronto, Canada, has been utilised in geotechnical and mining engineering as a tool for the design and study of tunnel surface excavation and supports. Furthermore, it is based on the finite element method for analysing the stability of soil and rock slopes. This software includes various FEM models as well as four primary sub-procedures. Inputs, calculations, outputs, and curve charts are examples of these methods. The strength parameters are lowered automatically until the final calculation step yields a fully established failure mechanism. It is utilised in geotechnical applications to perform deformation and stability studies (Maula and Zhang, 2011).

Slide software: slide software, developed by Rocscience Inc., can be used to analyse slope stability studies for soil and rock slopes. It investigates natural and man-made slopes such as cuttings, embankments, and fills, as well as earth dams and retaining structures such as tie-back walls, soil nail systems, and rubbish dumps created by mining or industrial by-products. It comes with a two-dimensional limit equilibrium (LEM) computer tool for assessing the stability of circular or noncircular failure surfaces (Rocscience 2004, slide 6). External loading, groundwater, and forces such as surcharge and pseudo-static earthquakes might all be modelled in Slide programme for various investigations.

CHAPTER –THREE

3. MATERIAL AND METHOD

3.1. Introduction

Slope stability study entails doing a thorough site examination and identifying the geologic material's properties. A crucial surface is one that is prone to slipping. The surface is chosen based on the site's weak (loose) material and structure, slope, and the presence of water.

3.2. Data collection

Various data linked to and necessary for studying the slope's stability were gathered from various entities such as the National Metrological Service Agency and the Geological Survey of Ethiopia. This stage mostly collected secondary data, such as meteorological data, geological and topographic maps, and reports on the regional geology of the area. Horizontal seismic acceleration (Raghuvanshi, 2019) is an external driving force that acts along the failure plane. As a result, the seismic data for the study area was derived from Dulbal's (2020) Ethiopian seismic risk map for the hundred-year return period. Furthermore, rainfall is one of the most important variables in destabilising the slope's stability (Ayalew et al., 2004) The graph of mean monthly rain fall data collected at chencha stations in the study area versus the year over which the rain fall collected was plotted using Microsoft Excel.

3.3. Detail field survey

Following the reconnaissance survey, an extensive and thorough literature evaluation was conducted, followed by a complete field survey concentrating on the detailed investigation of slope stability in the study region. A sampling plan and sampling location were specified prior to the field research to minimise sampling errors. During this thorough examination, geological formations, lithologies, rock strength, and groundwater conditions on the slopes were determined. Furthermore, critical slope failures were identified and located based on field manifestations such as slope toe removal, tension crack development, slope face tilting, and the orientation of discontinuities, which favour rock slope failures and spring stains over the slope face. Six important slope sections were chosen in the field for slope stability study. Rock slopes were four of the key surfaces. Soil slopes, which are residual soil, are the other crucial surfaces. Fresh rock samples have been collected for a detailed laboratory test that demonstrates the severe state and is labelled, and disturbed soil samples of 20kg have been collected from two pits, each with a depth of 1-2m. The samples are used to determine the geotechnical qualities of the materials, most notably the strength parameters and unit weight. The dip and strike of joints were measured for structurally regulated slopes. To produce the geological map, GPS coordinates were obtained for each lithology, and the dip and strike of a geologic structure were measured and observed using a Bruno compass. The slope surface around the road segment is marked primarily by steep, difficult terrain; its geomorphological features reflect historic landslides, loose colluvium deposits, thick residual clay soil, and extensively worn and broken rocks caused by heavy and continuous rainfall. When compared to other parts, the colluvial soil surrounding the research area is more prone to sliding. The system has actually been covered by the soil in some places due to sliding caused by erosion. In the field, photographs of slopes that had already fallen on the road and those on the edge of failure were also taken (Six potential slope instabilities (four crucial rock slopes and two soil slope sections) were chosen for stability assessments based on field manifestation and eye observation (Fig 3.1), The majority of the rock slopes face the road.

Figure 3.1 Critical sections of soil and rock slopes A) soil slope section six, B) soil slope section three slope C) highly weathered basalt, d) ignimbrite E) slightly weathred basalt F) moderately to highly weathred basalt.

In every slope design and stability analysis, visual evaluation of slope saturation conditions and indirect manifestation of groundwater play a role. Groundwater has the greatest impact on slope stability through lowering strength due to the development of pore water pressure in discontinuities (Wyllie and Mah, 2004). When analysing the stability of rock and soil slopes, the absence of seepage in the slope face does not imply that groundwater does not exist in the slope (Hoek and Bray, 1981). To evaluate the relationship between precipitation and groundwater level in a slope, the average precipitation and peak event that causes instability must be established (Wyllie and Mah, 2004). In this study, the saturation conditions of the slope were visually determined, and the location of some springs emerging along the slope section was also recorded using the global positioning system (GPS). Some of the slopes in the road section are found near a spring or pond, but from the secondary borehole data, the groundwater is shown as dry.

Figure 3.2 Spring along the road section.

3.3.1. **In Situ Strength Tests**

The Schmidt hammer strength test in the field is used to estimate the uniaxial compressive strength (UCS) of the intact rock at the key slope section in this investigation (Barton & Choubey, 1977). Surface rebound hardness, which is related to compressive strength, is determined by the Schmidt rebound hammer test. It is made up of a spring-loaded mass in the form of a piston that releases when pressed orthogonally into a surface (Torabi et al., 2011). The tests were carried out in accordance with ASTM D5873 (2001). A Schmidt hammer was applied perpendicular to the surface and gradually pressured to hit it in the test. At each sample location, two trials were undertaken (each with ten readings). The average of the rebound values (R) was utilised for UCS determinations after listing the rebound values in ascending order. Finally, the empirical equation was used to calculate the uniaxial compressive strength of the rocks along the road's crucial slope portion (Barton & Choubey, 1977).

$$\mathrm{Log10}\,(UCS) = 0.00088 * \gamma * R + 1.01 \qquad \text{Eq(3.1)}$$

Where: UCS is the uniaxial compressive strength of rocks in Mpa, γ is the dry rock densities in KN/m3, and R average Schmidt hammer rebound value.

3.3.2. Laboratory analysis

Parameters	Method	Standard
Unit weight	Dry and saturated	AASHTO T-99
Strength parameters.	Direct shear method	ASTM D 3080
Specific gravity	Specific gravity test	ASTMD8541919
Moisture content	Natural Water content determination	ASTMD2216
Index property	Sieve analysis	ASTM D422
	Atterberg limit	ASTM4318
	Hydrometer	ASTM D7928H

Slope stability study entails determining the strength properties of materials in a laboratory. Various laboratory studies have been performed on soils and rocks. Particle size distribution, hydrometer, water content determination, specific gravity, compaction, and direct shear tests are all part of soil laboratory testing. The rock testing included point load, dry and saturated density, and intact Schmidt hammer.

3.4. **Physical property determination**

Based on their engineering, this strategy is used to identify and classify soils and rocks.A sieve and a hydrometer study were performed to determine index property.

3.4.1. **Index property determination**

Sieve analysis; the sieve analysis is used to determine the distribution of coarser grains with diameters higher than 75 m. The test was carried out in accordance with ASTM D422, a standard test protocol for assessing soil particle size. As a result, the following tests were performed at the laboratory: First, the dry soil samples were prepared and crushed into appropriate small sizes using a hammer and pestle grinder. After the sample preparation, the stack of sieves was cleaned with a brush and a set of sieves were placed with progressively smaller openings from top to bottom and the pan was placed at the bottom of the finest sieve. After 15 minutes, the soil retained on each sieve and pan was measured using a digital balance. The dry mass of soil grains from individual sieving was used to find the percent passing and accordingly percent retained in each sieve size. Finally, the recorded data was analysed on a Microsoft Excel datasheet, and the grain size distribution curve was generated from the diameter against percent finer sieve analysis result.

Hydrometer

This test is performed on soil samples with particle sizes less than 0.075mm. This test is used to determine the percentage of soil silt and clay size fractions. A 60-gram soil sample that passed a 0.075-mm sieve was collected for this test. The chemical sodium hexametaphosphate, with a weight of 5 g, was employed to spread soil.This test is carried out in accordance with the ASTM D 7928 standard.

Figure 3.3 Hydrometer analysis, dispersed soil in 1000ml cylinder

Atterberg Limit Test

The liquid limit (LL) and plastic limit (PL) of soil are determined using the Atterberg limit test. The moisture content in percent (%) at which the soil changes from liquid to plastic, and the moisture content in percent (%) at which the soil changes from plastic to semi-solid (Sharma and Bora, 2014). The test was carried out in accordance with the ASTM D 4318 (1998) standard. The Atterberg limit tests were performed on soil samples that passed sieve number 40 (0.425 mm), and the Casagrande test was performed with distilled water. The laboratory test was carried out in accordance with the following liquid and plastic limit test procedures:

Liquid limit

The test is performed to determine the liquid limit of soil according to ASTM 4318 by passing a 0.425-mm sieve sample through it. The soil was combined with water and allowed to evaporate. The wet soil was placed on a liquid limit device (Casagrande), and a grooving tool was used to cut through the sample along the top's symmetrical axis. After a series of blows, a 13-mm sample was taken near to the grove. The collected samples were placed in the can and placed in the oven to determine the moisture content.

➢ Plastic limit

The test is used to assess a soil sample's plastic limit. The sample must pass through a 0.425-mm sieve according to the ASTM 4318 standard. The soil is mixed with water and rolled on a glass plate until it reaches 3mm thread with the palm of your hand. The thread dirt was placed in the can and baked for 24 hours to determine the water content.

Finally, using equation 3.2, the plasticity index (PI) of the soil was calculated based on the liquid limit and plastic limit tests:

PI = LL-PL

Figure 3.4 Methodology for Atterberg test

3.4.2. **Density bottle method (Specific gravity)**

The test is aimed at determining the specific gravity of soil. For the test, the empty density bottle is weighted, and 10 grammes of oven-dried soil are added to it. The water is added to the soil in the density bottle, stirred, and weighted. The clean water in the density bottle was weighed after the stirred sample was removed. The standard used for this test was ASTM D 854-1919. Finally, the specific gravity can be calculated using eq. 3.3.

$$Gs = \frac{W2 - W1}{W4 - w1 - (W3 - W2)} \qquad \text{Eq(3.2)}$$

Where W1 denotes the weight of a clean and dry pycnometer; W2 denotes the weight of oven-dried soil and a pycnometer; W3 denotes the weight of a pycnometer filled with water; and W4 denotes the weight of a pycnometer filled with water and soil.

3.4.3. **Natural moisture content determination**

The test is used to determine the soil's moisture content. ASTM D 2216 was the standard reference used in this study. The moist soil is weighed and placed in an empty, weighted moisture container. The moisture can sample is left in the oven. This test is required to determine soil qualities. Finally, using equation 3.4, the natural moisture content was estimated.

$$\mathrm{W} = \mathrm{Mw} - Md/\mathrm{md} \times 100\% \qquad \text{Eq(3.3)}$$

where w is the natural moisture content in (%), Mw is the mass of wet soil samples in (g), and Md is the mass of oven-dried soil samples in (g).

3.5. **Mechanical Properties determination**

3.5.1. **Compaction test**

The maximum density and ideal moisture content of the soil used in the shear strength test are determined by compaction. Proctor tests are performed to see how soil compaction varies when moisture content changes. Two soil samples were tested in accordance with ASTM D698-07 (1998) on the key slope section of the study area. As a result, the laboratory test was carried out as follows: To begin, collect 5kg of soil sample that has been processed through a No. 4 sieve. Add the prescribed amount of water to the soil and thoroughly mix it in (Fig.). Calculate the weight of the compaction moulds in the base (M1).The soil sample was then blown into the cylinder mould in three layers, 25 blows for each layer.Remove the collar, trim, and level of excess compacted soil beyond the rim of the mold. Then the weight of the compacted soil within its molds and base was recorded (M2). Remove the collar and level any extra compacted soil beyond the mould's rim. The weight of the compacted dirt within the moulds and base was then measured (M2). Using a mechanical extruder, remove the compacted earth from the moulds. Then, using a knife, condense the crumbs and take a sample from the bottom and top of the moisture cans before placing them in an oven at 105 ° C for 24 hours. The bulk density and dry density of the soil are then calculated using the following equations: 3.8 and 3.9, respectively.

$$\gamma b = M2 - M1 / V \qquad \text{Eq(3.4)}$$

Where: γb - the bulk density of the soil M2- the mass soil after being compacted with mold, M1- the mass of the mold and V, is the volume of the mold.

The dry density of the soil is also calculated as the following equation.

$$\gamma d = \gamma b/(1 + w/100) \qquad \text{Eq(3.5)}$$

Where: γd is dry unit weight, γb is the bulk unit weight, W is the moisture contents of soils.

Finally, the results of the recorded data were analyzed on Microsoft Excel datasheet and plot the graph of the dry density versus moisture contents for analysis result (Fig 3.5)

Figure 3.5 Compaction test equipment

3.5.2. **Direct shear test**

The compacted soil was weighted and placed on the shear box. The box was positioned in front of the direct shear device. The gauges, horizontal displacement gauge and shear load gauge, were set to zero before starting the motor. The horizontal displacement and shear load were measured until the shear load reached the peaks and then dropped. The test was carried out using the ASTM D 3080 standard reference and three distinct shear loads: 100 kpa, 200 kpa, and 300 kpa. Finally, the Mohr-Coulomb failure criterion described the link between soil shear strength and normal stress at a point on a certain plane as follows in equation 3.7:

$$\tau = c + \partial \tan\varphi \qquad \text{Eq (3.6)}$$

Where: C is the cohesion and φ is internal angle friction of the soil particles.

Figure 3.6 Direct shear test and Top view of direct shear device

3.5.3. **Unit Weight of Soils**

The unit weight of soil is one of the input parameters used for soil slope stability evaluations. Both the saturated and dry unit weights of soil were determined from the laboratory test results of the soil sample from the study area. The in-situ unit weights of soils, both bulk () and dry (d), were computed as the product of the corresponding density and the acceleration of gravity (g). For this study, two typical soil samples were obtained from critical slope sections, and the corresponding unit weight was determined. The unit weight of the soil sample was calculated using the following method based on the bulk and dry density results: bulk unit weight = bulk density*g, and dry unit weight = dry density*g.

3.5.4. **Strength Test**

3.5.4.1. Point Load Test

The unconfined compressive strength of undamaged rock was determined using a point load strength test. The tests were carried out in accordance with ASTM D 2938. The test was performed under natural moisture content circumstances on at least four irregular rock samples collected at each crucial slope section.

Before beginning the test, a geological hammer and chisel were used to form and size uneven rock specimens for the point load testing machine Before the test, the height, breadth, and length of the irregular rock samples were measured (Fig. Then, place a rock sample in the test instrument and apply the load continually until failures emerge and the failure load (P) peak values are recorded. Later, the average of the corrected point load strength was converted to the rock's uniaxial compressive strength using the empirical equation proposed by(Broch & Franklin, 1972) , which demonstrated the relationship between the corrected point load strength and the rock's uniaxial compressive strength.

3.5.4.2. **Density and Unit Weight Rock**

The unit weight is used to calculate the weight and stress of a rock mass. One of the input factors utilised in computing the safety factor for rock slope stability evaluations was the unit weight of the rock. The test was carried out on at least three irregular rock samples taken from crucial rock slope portions at the Addis Ababa Science and Technology University Geotechnical Laboratory utilising buoyancy techniques in accordance with ISRM (1978) guidelines as follows:

The irregular rock samples were labelled and weighed (M1) under their natural moisture content before being oven-dried for 24 hours at 105°C, and the weight of the oven-dried rock samples was recorded (M2).

After filling the cylinder with water, the initial water volume (V1 in ml) was measured. The volume change (V2 in ml) of oven-dried samples was measured in a water-filled cylinder. Then Immerse an oven-dried irregular rock in a water-filled cylinder and compute the sample's modified volume as follows:

$$\Delta V = V2 - V1$$

Finally, the dry density (γd) and unit weight (γ) of each rock sample was determined using Equations 3.4 and 3.5, respectively.

$$pd = M2\Delta V \qquad Eq(3.7)$$

$$\gamma = pd \times g \qquad Eq(3.8)$$

where γd is the dry density of the rock samples in g/cm3, M2 is the mass of the rock samples after being oven-dried in g,, and ΔV is the difference between the water volume after the rock sample is placed and the water volume before the rock sample is placed in the cylinder. γ is the unit weight of rock in KN/m3, and g is the gravitational acceleration (in m/s^2).

Table 3.2 Analytical method adopted for rock sample.

Types of tests	Number of tests	Standard of tests
Point load test	14	ASTM D 2938
Unit weight	14	ISRM 1978

3.6. **Data processing and Analysis**

The data gathered from primary and secondary sources via desk study reconnaissance, compressive field survey, laboratory test, and literature review were packaged and processed in such a way that it could be accessible appropriately during subsequent slope stability analyses. Rocsciences software was used to collect and process all of the data required for stability assessments.

3.6.1. **Rock Mass Classifications Method**

One of the most widely used empirical classifications in rock engineering is rock mass classification (Salmanfarsi et al., 2020). They are methods for evaluating and quantifying the condition of rock-cut slopes based on critical criteria (Pantelidis, 2009). The rock quality and crucial rock slope stability analyses in this study were classified using the (Bieniawski, 1989) rock mass rating system. The quality of the rock mass was classified using five main rock mass rating parameters: uniaxial compressive strength of unbroken rock, rock quality designation (RQD), discontinuity spacing, discontinuity condition, and groundwater circumstances. n this work, the uniaxial compressive strength of complete rock was determined by performing a point load strength test on an uneven rock sample. The volumetric joint count method (Palmstrom, 1982 was used to calculate the Rock Quality Designation (RQD) index, which is the total number of discontinuities (Jv) present in a cubic metre of rock mass in the crucial slope section.

3.6.2. **Shear Strength Parameter of Rock mass**

The rock mass properties of a material that will be utilised as input parameters for the study, cohesion, friction angle, and Young's modulus, were determined using Roc Data programme. It is used to determine strength envelopes and other material parameters by examining the strength characteristics and constitutive behaviour of rock and soil materials. It took geological strength indices and unified compression strength data as input. The Heok Brown failure criterion was used to calculate the rock mass's shear strength and deformation parameters. (Hoek et al., 2002), estimated the cohesiveness (C) and internal friction angle of rock masses using Rocdata software and generalised Hoek-Brown failure criteria. Users can readily estimate rock mass characteristics and shear strength parameters using Rocdata software (Hoek, 2006). The Rocdata software used the Geological Strength Index (GSI), uniaxial compressive strength of intact rocks (UCS), material constant of intact rocks (mi), and disturbance factor (D) as input parameters. Furthermore, for slope application (Rocscierocks (mi),) the Rocdata software requires the unit weight of rock and slope height (H). The uniaxial compressive strength of rock entire rock was calculated in the laboratory using ASTM D5631-16 (1995) from the point load strength index. (Marinos & Hoek, 2000) computed the GSI in the field by taking into account the weathering conditions of the discontinuity surface rock mass structure and the interlocking of rock blocks. The material constant of intact rock (mi) was taken from the Rocdata software's standard table (Hoek et al., 2002). The disturbance factor was calculated using (Wyllie & Mah, 2004)criteria based on the degree of disturbance of the rock mass subjected to mechanical excavation. Furthermore, the rock unit weight was estimated in the lab using buoyancy techniques (ISRM, 1978), and the slope height was measured in the field using a tap metre. Finally, the Rocdata software output parameters were employed as input parameters in the slope stability studies.

Table 3.3 Input data for rock mass property determination in Rocdata software

Rock id	Rock type	UCS (Mpa)	GSI	Mi (for intact rock)
RSS1	Basalt	114	30	21
RSS2	Basalt	76.8	25	21
RSS4	Ignimbrite	146	58	26
RSS5	Basalt	93.36	25	21

3.7. Slope Stability Analysis Method

3.7.1. Kinematic Analysis Methods

To analyse the various failure mechanisms, such as planar, wedge, and toppling failure, kinematic analysis was performed using Dips software (Jaiswal et al., 2023). Field manifestations and kinematic analyses are the primary determinants of rock slope collapse modes (Park & West, 2001). Dips 6.0 software (Rocscience, 2004) was utilised in this study to investigate the kinematics of a rock slope for structurally controlled collapse. The stability of a rock slope was determined using plotted structural data and daylight envelopes. The displayed data can be utilised to determine the active failure mechanism as well as the possibility of a failure zone on a slope. Dips Software requires slope orientations, major joint set dip and dip directions, and friction angle as input parameters (Khanna & Dubey, 2021).The orientation of slopes and structural discontinuities (dip and dip direction) in important rock slope sections was measured in the field with a Brunton compass. Rocdata programme used nonlinear failure criteria to calculate the angle of friction along the failure plane (Barton and Bandis, 1990). Finally, the main plane's kinematic analysis was performed using the Dips software

(Rocscience, 2004, Dips 7) to determine the manner of slope failure in the research area's important rock slope portions. two slope segment displays a structurally controlled failure mode based on field visual estimation.

3.7.2. **Finite element method**

The reduction approach was used to calculate the safety factor, The soil parameters (tan) and (c) are gradually decreased until the structure fails. The shear strength reduction (SSR) approach was used in Phase 2 to calculate the safety factor of a simple homogeneous slope and a non-homogeneous slope. As input data, the approach established the factor of safety by clearly specifying cohesion, friction angle, unit weight, Young's modulus, and the material's slope geometry. Following the selection of the strength reduction method, the most significant step was to design the slope geometry. The material property option now includes the input parameters. After the geometry was formed, the input data were computed, and the computed data provided the strength reduction factor.

3.7.3. **Limit Equilibrium Method**

The limited equilibrium method calculates the safety factor by comparing the shear strength next to the sliding surface to the force required to keep the slope in equilibrium (Ullah et al., 2020).. Rocscience slide software was used to examine the stability of rock and soil slope failures using a limited equilibrium method. Because the Morgenstern-Price approach takes into account force and moment equilibrium, it can be used to analyse probable failure surfaces on both circular and noncircular surfaces (Kadakci Koca & Koca, 2020).. For this investigation, the slide software's limit equilibrium approach was utilised to model and compute the factor safety (Slide 6, Rocscience, 2004) for rock and soil-selected slope sections. The shear strength parameter of rock and soil (cohesion and angle of internal frictions), the unit weight of rocks, slope geometry, and external force (seismic load) are all input parameters for slide software. The shear strength of rock mass-selected slope section parameters determined from the Hoek-Brown failure criteria utilising Rocdata software unit there as the shear strength geometry (cohesion and friction angle) acquired from direct shear testing were investigated in this study. The unit weight of the rock was determined in a laboratory test using buoyancy techniques ISRM (1978), the slope geometry was estimated in the field using a tap metre, and the horizontal seismic acceleration angle) was derived from an Asfaw (1986) seismic risk map. Finally, the General Limit Equilibrium (GLEM)/Morgenstern Price method was utilized to calculate the limit equilibrium method's factor of safety for static dry, static saturated, dynamic dry, and dynamic saturated situations.

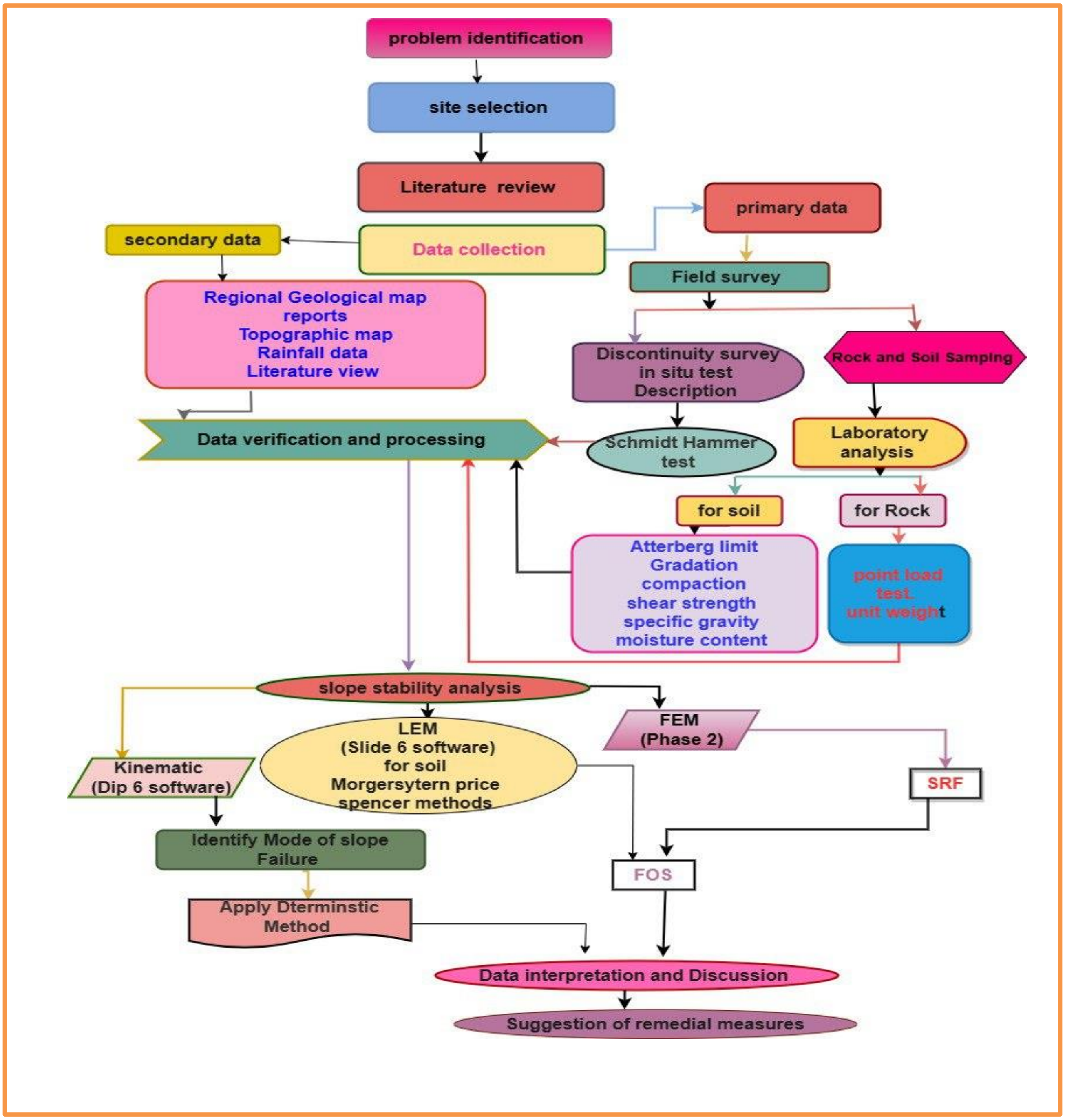

Figure 3.7 methdology

CHAPTER 4

4. GEOLOGY

4.1. Regional Geology and Stratigraphy

4.1.1. Regional Geology and Structural Setting.

The low-grade metamorphic phases of the Arabian-Nubian Shield, Palaeozoic deposits, and tertiary volcanism make up the terrains of southern and western Ethiopia. The Lower Complex is a group of low-grade metamorphic rocks made primarily of granitic gneisses and migmatites with biotite and amphibole-bearing gneisses. In contrast, the Palaeozoic deposits are primarily sandstone with conglomerate and intercalated siltstone (Davidson, 1983). This sandstone formed over the crystalline basement's unconformity with its Tertiary volcanic layer.The Ethiopian plateaus [North-Western, Southwestern, and South-Eastern], the Main Ethiopian Rift (MER), and the Afar Rift are then split into three primary geographic and geomorphologic components (Kazmin, 1979; Berhe et al., 1987).

The road project is located inside the East African continental flood basalt (CFB) province's southwestern Ethiopian plateau, where Tertiary volcanics unconformably topped the crystalline underlying rocks. The proposed slope portions, namely these volcanic flood basalts, are divided into two mapping units, which are classified as lower basaltic flows (older) and rhyolite flows (younger) based on stratigraphy and mode of occurrence. It also crosses Quaternary deposits in a few places.

Lower basalt flows: Lower basalt flows are dark grey, slightly vesicular, fine- to medium-grained basalt that lies directly on top of the Precambrian basement. Calcite fills several of the vesicles. On the Gamo highlands, it generates dense rivers. It is distinguished by thick basalt lava flows with columnar jointing and severe weathering. There are various lava flows on the way from Sawla to Bulki. Palesoil and a heavily worn mantle separate 60-metre-thick subhorizontal basalt flows.

Rhyolite flows: The crests and cliffs of the Gayla and Zala Mountains, as well as the top part of Gamo Mountain, are made of rhyolite. Rhyolite interfingers with basalt in various locations. It can also form domes. The domes were typically characterised by prominent, gently convex hills with steep slopes that protruded above the basalt plain to heights of 200 m. The rock has a fine-grained texture, is light grey in colour, and has a slickenside. West of Gayla Mountain, a small, thin area of rhyolite is also exposed. Rhyolite had a medium- to coarse-grained texture and a light pinkish grey, reddish brown, or purplish grey tint. It displayed a flow layer with alternating thin layers. Because of the flow layers, the rhyolite frequently displayed platy-weathering.

Regional Soil Covers

Because soils have different rates of penetration, soil parameters alter the relationship between runoff and rainfall. The primary parameters necessary to classify soils into Hydrologic Soil Groups (HSG) are permeability and infiltration. The suggested slope portions, according to the Soil Conservation Service (SCS), belong to the hydrologic soil group "B's," which includes Orthic Acrisols and Dystric Nitosols. They are loam soils or silt loam soils. Because of their modest penetration rates, soils have a moderately low runoff potential. These are mostly fairly deep to deep, well-drained soils with moderately fine to moderately coarse textures.The road corridor's soil is thick, clay-rich, dark reddish, moist, and low plastic. It becomes soft when it is saturated (which is most of the time due to the high and extended rainy seasons). The soil defines both the road foundations and the slope cuttings.

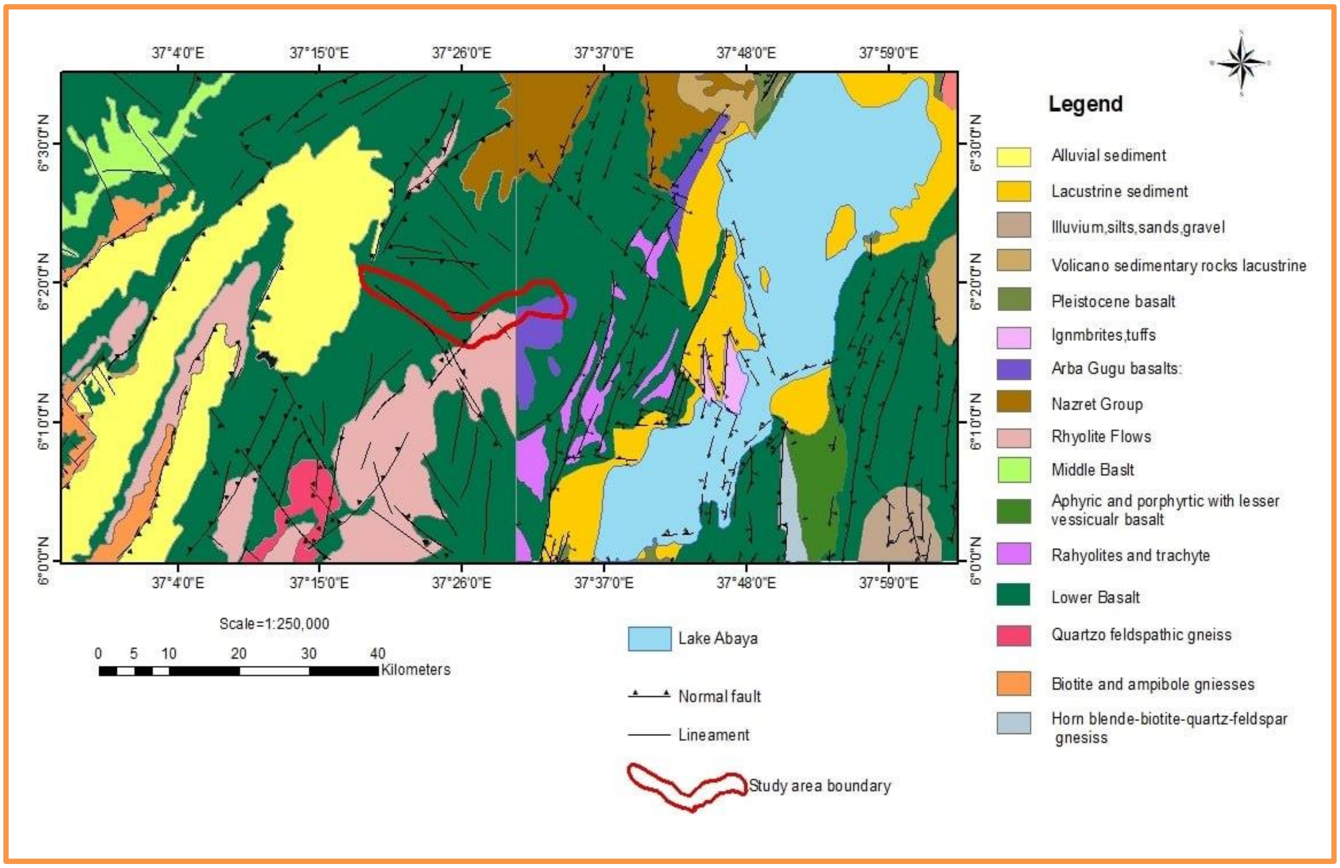

Figure 4.1 Regional Geological map of the 1:250,000 from Dila and Dime map sheets.

4.2.LOCAL GEOLOGY

The project area's geology is dominated by light-colored welded Rhyolitic-ignimbrite, Trachyte, post-rift basalt, Amaro-Gamo Basalt, and Scoriaceous Basalt, as well as an alluvium-colluvium mix of deposited rocks.

4.2.1. Light color Rhyolitic-ignimbrite

At the regional level, it is a light-colored welded rhyolitic-ignimbrite of Miocene volcanic origin that is part of the Dorze ignimbrite complex. This welded rhyolitic-ignimbrite rock formation encompasses the northern and southern parts of the 48+00 road chainage, as well as the project area's southwestern steep slope.

Figure 4.2 Light color Rhyolitic-ignimbrite

4.2.2. Light reddish trachytic basalt:

It is a light-reddish trachytic basalt, a Miocene-age syn-rift volcanic product. This rock unit is exposed in the project's steep slope area, particularly at the 29+00 chainage of the road alignment. This trachytic rhyolite lava flow was covered by residual soil and is locally intercalated with paleosoil horizons, scoriaceous basalt layers, and glassy basaltic material.

Figure 4.3 light-reddish color trachytic basalt

4.2.3. Slightly weathered massive basalt:

This rock unit is slightly weathered huge basalt that is covered by thin reddish residual soil. It is a vast Pleistocene post-rift volcanic product that exposed in a few portions of the project area, approximately 46+00 and 60+00 of the road section.

Figure 4.4 Slightly weathered massive basalt

4.2.4. Moderately-highly weathered basalt:

- This lower Oligocene-age volcanic product is moderately to highly weathered basaltic rock that covers a large part of the project area. It is amygdaloidal basalt and the oldest exposed rock formation.

Figure 4.5 Moderately-highly weathered basalt

4.2.5. Scoriaceous Basalt:

This rock unit is a Pleistocene post-rift volcanic product that creates a one-sided moderately plunged dome-like landform that covers the proposed road alignment from 48+500 to 49+300 chain ages.

Figure 4.6 Scoriaceous Basalt

4.2.6. Alluvium and Colluvium Deposited Material:

The steep sloppy part of the project area is washed down by erosion processes, supplying the local streams and surrounding flat area with loose sediment; thus, the plains with flat to rolling terrain are covered by a continuous supply of alluvium deposit, whereas the area near the foot of the steep slope is primarily characterised by alluvium and colluvium mixed loose material.

Figure 4.7 Alluvium and Colluvium Deposited Material.

Geological Structures

A sequence of sub-parallel basins can be seen in the project area. The North Omo, Berso, Sawla, Beto, and Mati-Dancha basins are made up of sub-parallel half-grabens that run west to east. The principal boundaries of these basins are steeply dipping faults that generate asymmetrical rifts (grabens). The majority of these basins appear as half grabens to correspond to the area's NW-SE and NE-SW trending faults, which generated steep escarpments and influenced the trap series.

• NW to NNW trending faults: the most noticeable collection of faults in the area. They are E-W fault-cut extensions of the Omo River Gorge. The E-W faults truncate it, exposing reddish-brown, severely crushed basaltic and rhyolitic breccias.

Throughout the map area, NE-oriented faults form conjugate patterns with the NNE structure. The area's NE to NNE and NW-trending structures are thought to have originated in the southern sector of the Main Ethiopian Rift and nearby rift zones.

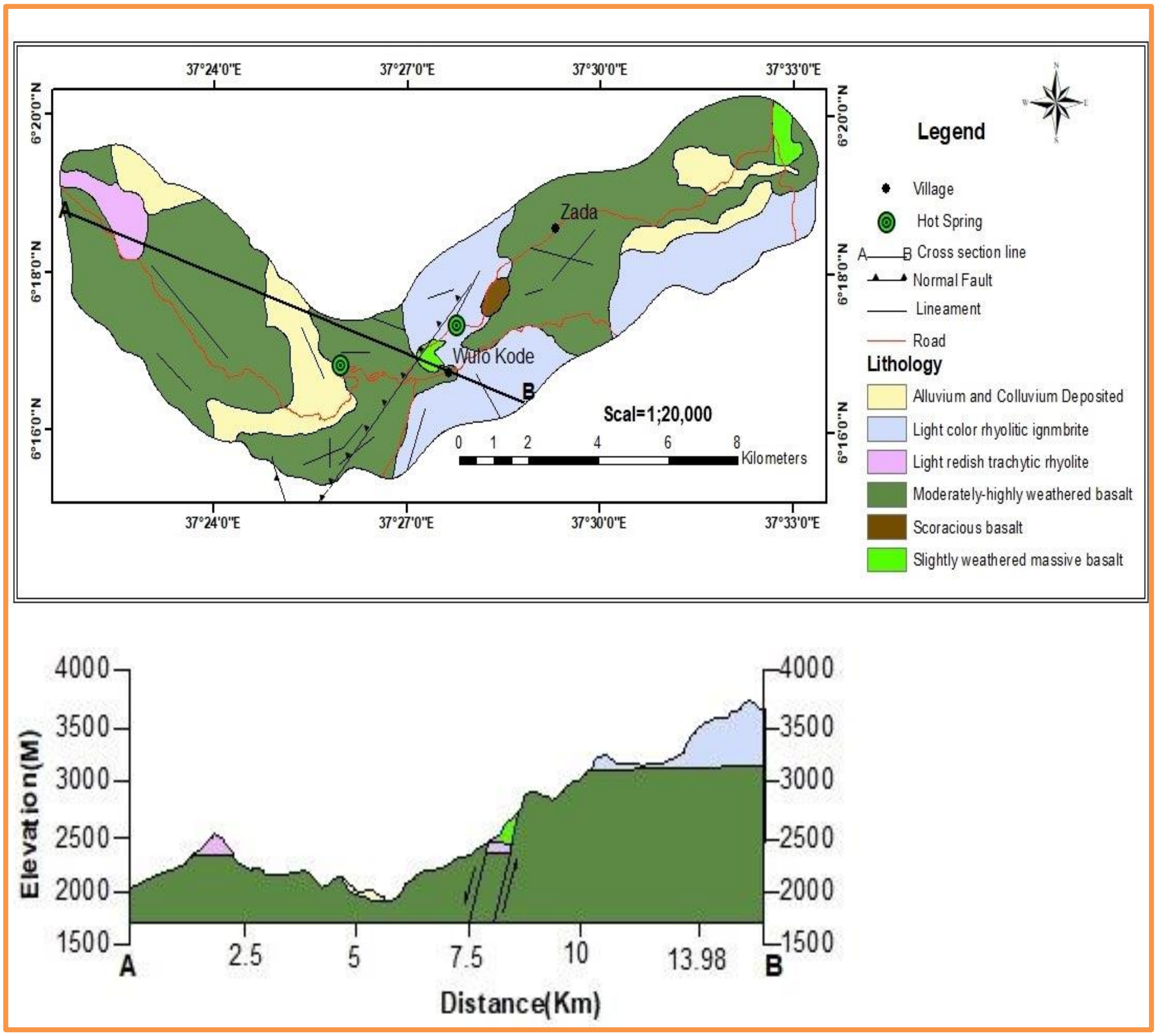

Figure 4.8 Geological map of Morka Gircha Chencha Road with its cross section.

CHAPTER 5

5. RESULT AND DISCUSSION

5.1. Engineering Geological Characterization of the Rock mass

5.1.1. In-Situ Rock Strength Test.

To calculate the factor of safety of the critical slope section in this work, a finite and a limit equilibrium analysis approach was used. Laboratory testing for rock and soil was entered into the software. Sieve, hydrometer, and compaction tests, direct shear test, Atterberg limit, specific gravity, and water content are all soil laboratory tests. The rock sample parameters were determined using dry and saturated density tests, point load testing, and Schmidt hammer tests,. The uniaxial compressive strength (UCS) of the intact rock at the key slope portion was evaluated in the field using the Schmidt hammer strength test (Barton & Choubey, 1977). This test was carried out in following with ASTM D5873 (2001) for the acquisition of rebound values. The representative average rebound value of rocks was translated into UCS using empirical formulae (Eq. 2.8) proposed by (Barton & Choubey, 1977).

Table 5.1 Schmidt Rebound and UCS values from different critical slope sections.

Slope sections	Schmidt hammer rebound value from each critical slope sections	Average of Rebound value for rock slopes	Ave (R)	UCS (Mpa)	According to ISRM (1979)
RSS1	40.5,32.5,38,40,44.5,43.5,42.1,40.2,42.5,42,	40.5	37.3	93	Medium strength
	24.7,20,17,34.5,37.5,46.5,40.5,32.5,43.5,43	34			
RSS4	52.5,52,47,46,44,45,52,54,43,55	49.1	44.7	107	Medium strength
	24,31.5,41,51.5,37,39,49,41,40,47.5	40.2			
RSS5	41,50,39,57,52.5,45.5,37,57,46,59	48.4	43.3	90	medium strength
	28,23.5,45,55,45,33,23.5,33,41,54	38.1			
RSS2	30.5,48,45,35,45,50,53,55,40,43	44.5	43.5	68.5	low strength
	40,42,50.5,52,45,40,33,42,38 ,43	42.5			

5.1.2. Rock Quality Designation (RQD)

According to(Palmstrom, 1982), the volumetric joint count (JV) for rock mass exposed at important slope sections along the road in the study area was used to assess rock quality designation in the current study. As a result, volumetric joint account measurements were taken on rock surfaces exposed along the road's crucial slope portions in the research region. Following the collection of measurements from each crucial slope section, the volumetric joint account was calculated using the average spacing of joints.

Table 5.2 summarizes the Rock quality designation index (RQD) determined from the joint count method

Slope section	JV (av)/1m*1m	RQD %	According to Deree (1988)
RSS1	17	58.9	Fair
RSS2	20	49	Fair
RSS4	15.25	64.7	Good
RSS5	16	60.2	Fair
RSS = Rock slope section and Jv, = volumetric joint account			

5.2. Laboratory Test results from the Rock samples

5.2.1. Point Load Tests

The rock strength classification of the research area and the point load strength test were done on a minimum of two to four irregular rock samples acquired from each designated key rock slope portion for this investigation. According to Deree and Miller 1966 the rocks classified as high strength to medium strength.

Table 5.3 Point load and uniaxial compressive strength test results of intact rocks

Slope sections	Sample ID	IS (50) Mpa	Ave, I S (50)	UCS (Mpa)	According to Deree and Miller 1966
RSS-4	RSS4-01	4.49	6,09	146.2	High strength
	RSS4-02	5.57			
	RSS4-03	4.99			
	RSS4-04	9.31			
RSS-2	RSS2-01	3.07	3.17	76.08	Medium strength
	RSS2-02	3.27			
RSS-5	RSS5-10	4.21	3.89	93.36	Medium strength
	RSS5-11	3.72			
	RS52-12	2.90			
	RSS5-13	4.73			
RSS-1	RSS1-01	4.35	8.93	114.4	High strength
	RSS1-02	13.2			
	RSS1-03	12.23			
	RSS1-04	5.96			

5.2.2. Density and Unit Weight Rocks

The observed samples were basalt, ignimbrite, and the density values for basalt, and basalts are higher than the density of ignimbrite.

Table 5.4 Dry and saturated unit weights of rocks from laboratory tests

Sample ID	Rock units	Dry unit weight γd (KN/m3)	Saturated unit weight γsat (kN/m3)
RSS1	Basalt	27.81	28.9
RSS4	Ignimbrite	23.19	24.83
RSS5	Basalt	28.54	28.78
RSS2	Basalt	21.3	26.14
RSS= rock slope section,			

5.3. Rock Mass Classifications

5.3.1. Geological Strength Index

GSI values determined in the field were also utilized to determine rock quality and as input parameters for finite element and limit equilibrium slope stability assessments.

Table 5.5 The Geological strength index (GSI) value of the critical rock slope section estimated in the field.

Slope sections	Rock units	Geological structure	GSI, a value estimated in the field.	Surface conditions
RSS1	MW, basalt	Blocky disturbed	30	Poor
RSS4	SW,ignimbrite	Very blocky	58	Good
RSS2	HW,basalt	Blocky/distributed	30	Poor
RSS5	SW, basalt	Blocky/distributed	25	Poor
GSI = Geological strength index, RSS = Rock slope sections, SW= slightly weathered, HW = highly weathered and MW = moderately weathered.				

5.4. Engineering Characterization of Soils.

The test was carried out in two test pits to determine the geotechnical qualities of the soil, with samples taken at 1m and 1.5m, respectively, for test pit 3 and test pit 6. The soil sample from test pit 3 was brown and had a specific gravity of 2.80. The soil is classified as high-plasticity clay soil, with a plastic limit of 30.97 and a liquid limit of 51.290. According to the AASHTO classification, the soil is clayey, with a water content value of 35.5%. The soil sample from test pit 6 was red and had a specific gravity of 2.74. The soil is classified as medium-plasticity clay soil, with a plastic limit of 32.09 and a liquid limit of 49.31. From the AASHTO classification the soil was classified as clayey soil which has a water content value of 30.83%.

5.4.1. Particle size distribution curve

The results of mechanical analysis (sieve and hydrometer analyses) are generally presented by semi-logarithmic plots known as particle-size distribution curves. This curve is obtained from the percentage finer results of both coarse- and fine-grained portions.

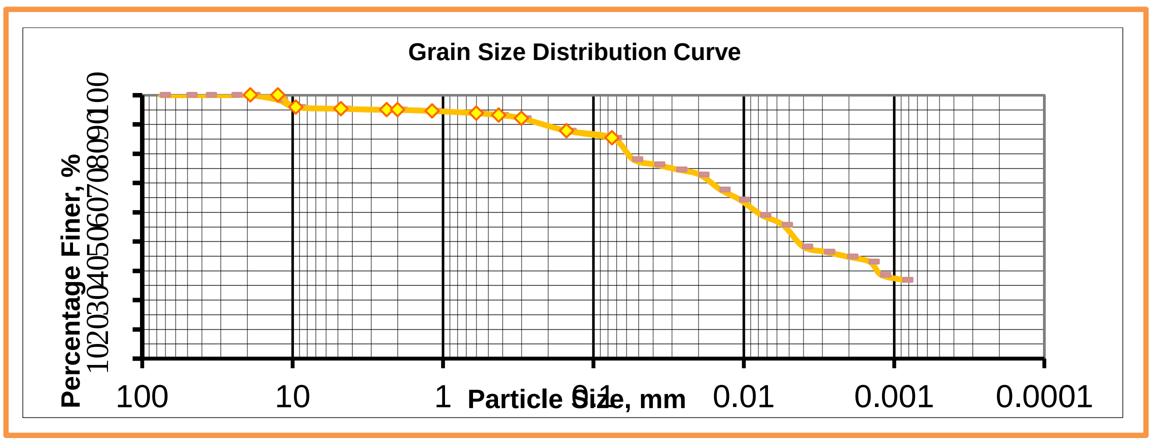

Figure 5.1 Particle size distribution curve

5.4.2. Atterberg Limit Test

The plasticity index was calculated using liquid and plastic limitations (Table 5.6) to estimate the range of the soils in the research area. As shown in Fig. 5.2, the plasticity index of the soils in the research region spans from 24.3% to 17.2%, indicating medium to high plasticity soils, and the liquid limit values range from 55.3% to 49.3%. Furthermore, the soil study area's lowest and maximum plasticity limitations are 30.97% and 32.09%, respectively, as indicated in Table 5.6 below.

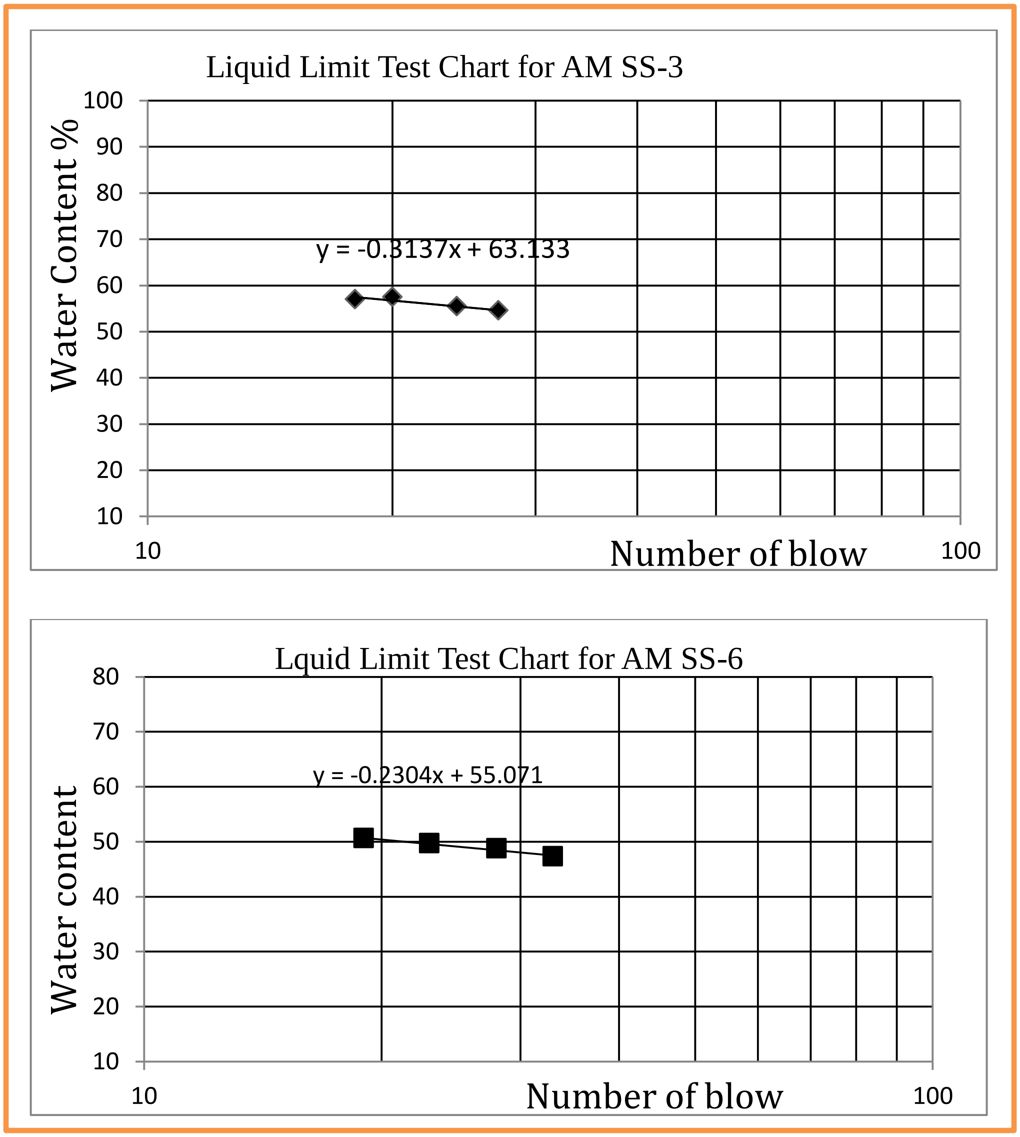

Figure 5.2 Liquid limit chart the critical soil slope of the study area a) SS1 and b) SS2

Table 5.6 Atterberg limit tests and plasticity index result of soil at critical slope sections.

Slope sections	Depth (m)	Sample types	Atterberg limit tests			Plasticity Class according to Das, (2002)
			LL	PL	PI	
SS3	1	Disturbed	55.3	31	24.3	High plasticity
SS6	1.5	Disturbed	49.3	32.1	17.2	Medium plasticity

5.4.3. Natural Moisture Contents

The in-situ water content of soils assessed using freshly excavated soil samples before exposing them to air is known as natural moisture content (w). Fresh soil samples were obtained from two crucial slope areas in line with ASTM D 2216 (1998). The natural moisture content of the soils in the key slope section ranged from 35.5% to 30.83% in the research region (Table 5.7).

5.4.4. Specific Gravity of Soils

A pycnometer and distilled water at a certain temperature were used to determine the specific gravity of soils in a designated slope segment of the study area. The specific gravity of the soil can be determined for each sample using the ASTM D 854 (1998) standard. Soil specific gravity ranged from 2.80 to 2.74 at selected slope portions in the research region (Table 5.7).

Table 5.7 Specific gravity and Natural moisture content of the soil slope sections.

Slope section	Depth of sample (m)	Natural moisture contents (NMC%)	Specific gravity (Gs)
SS3	1	35.5	2.80
SS6	1.5	30.83	2.74

5.4.5. Standard Compaction Tests

The Standard Proctor Compaction Test is used to assess the relationship between a specific soil sample's moisture content and dry density at a certain compactive effort. Using a typical proctor test, two soil samples were taken from the study area's crucial slope regions. Based on the compaction test findings, the maximum dry density (MDD) and optimum moisture content (OMC) of the soil utilised to remould the soil for the shear strength test were calculated. Fig. 5.3 depicts the laboratory test findings and accompaning compaction curves for the two crucial soil slope portions. Table 5.8 shows the results of maximum dry density (MDD) and optimum moisture content (OMC).

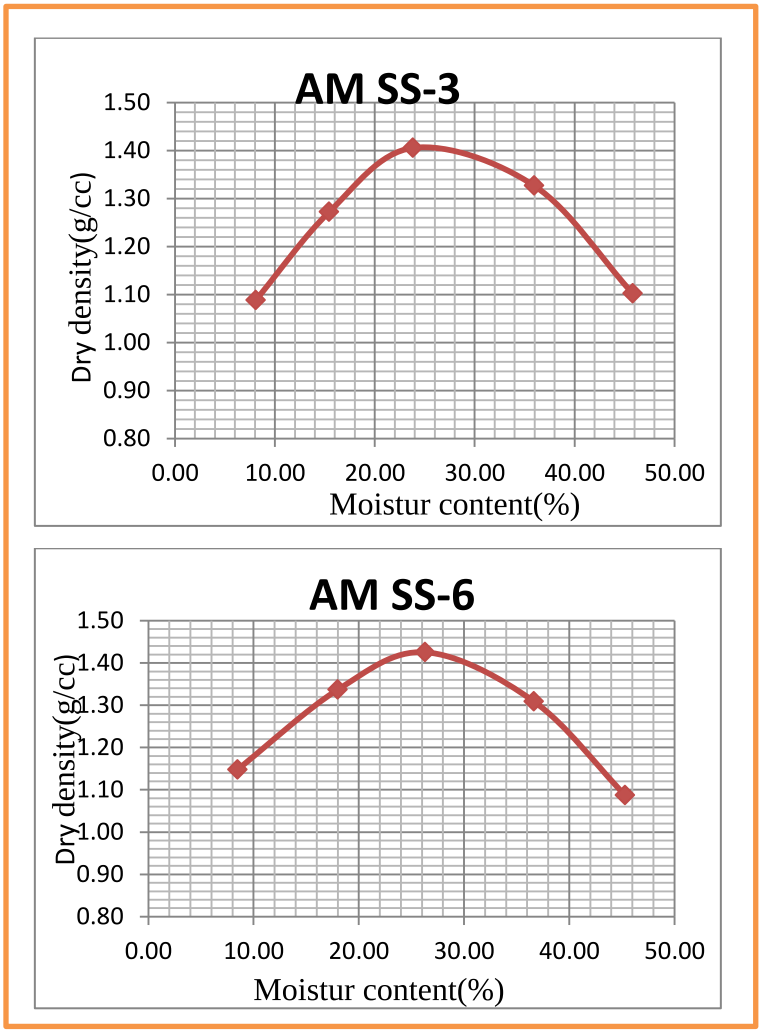

Figure 5.3 compaction curves of the soil critical soil slope section of the study area a) SS3 and b) SS6

Table 5.8 Maximum dry density and optimum moisture content of the soil slope section at SS3 and SS6

Slope sections	Soli description	MMD, (g/cm3)	OMC (%)
SS3	silty soil	1.39	24
SS6	Clayey silts with slight plasticity	1.46	26.84
SS = Soil slope sections, MDD = maximum dry density, and OMC = Optimum moisture contents			

5.4.6. Direct Shear Strength Tests

The direct shear test is one of the most frequent soil strength tests used to establish shear strength parameters for slope stability analysis. The shear strength characteristics, such as cohesion and angle of internal friction, of the selected critical soil slope section were obtained using direct shear testing in this study, as shown in Table 5.9. The direct shear test results (Table 5.9) show that the internal friction angles of soil slope sections three (SS3) and six (SS6) are 11.61and 9.02 respectively. The cohesiveness of the soils from slope sections three (SS3) and six (SS6) was found to be 23.0 KN/m2 and 24.08 KN/m2 (Fig. 5.4), respectively.

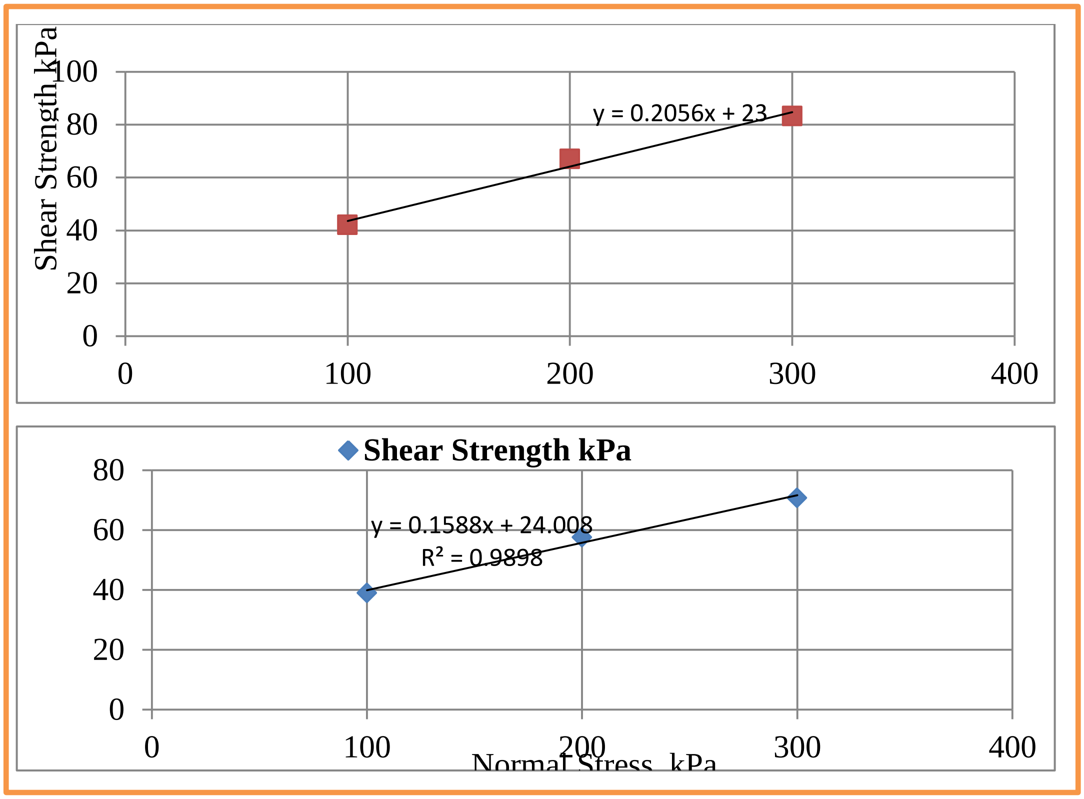

Figure 5.4 Shear Stress vs Normal stress of soil at a) SS3 and b) SS6

Table 5.9 Shear strength parameters of soils for the soil slope section at SS3 and SS6

Slope section	Soil description	Shear strength parameter	
		Cohesion, (C) Kpa	Angle of internal friction (ϕ)
SS3,	silty soils	23	11.61^{o}
SS6,	clayey silts with slight plasticity	24	9.02^{o}

5.5. Classification of Soils based on Unified Soil Classification (USC) System.

The UCS system categorised soils from a selected critical slope section along the road section of the study region using gradation analyses and Atterberg limit test findings (Table 5.10). Soil samples from the crucial slope part of the road in the study region, according to the USC system, fall into the MH/ML soil categories, signifying silty clay soils. Table 5.10 displays the comprehensive data as well as the UCS categorization of the soils for the research region.

Table 5.10 Classifications of Soils based on USC Classification System

Slope section	Percent amount of particle size			Atterberg limit			USCS soil classifications
	Fine materials (Silt and Clay%)	Gravel	Sand	LL%	PL%	PI%	
SS3	87.9	0.3	11.8	55.3	31	24.3	MH,silty soils
SS6	85.5	4.6	9.9	49.3	32.1	17.2	ML,clayey silts with slight plasticity
SS= Soil slope sections, USC = Unified Soil Classifications, LL = Liquid limit, PL = plastic limit, and PI = Plasticity Index.							

5.6. Stability analysis of rock slopes.

5.6.1. Kinematic slope stability analysis.

The kinematic analysis for this work was performed using Dips 6 software (Rocscience, 2004) to examine several slope failure modes such as planar, wedge, and toppling (Fig. 5.6). The data for the rock slope discontinuity was processed using the Dips software, which needed the orientation of the discontinuities (dip and dip direction of joints), the slope face orientation (dip and dip direction of slope), and the friction angle (Raghuvanshi, 2017; Khanna and Dubey, 2021). The dip and dip direction of joints, as well as the slope face orientation, were measured in the field, but the friction angle along the failure plane was calculated using Rocdata software.

Table 5.11 Input parameters used in Dips software for kinematic analysis.

Slope section	Slope face orientation	Joint set orientations (Dip and Dip direction)			
	Slope D/DD, (º)	JS1, (º)	JS2,(º)	JS3,(º)	Friction angle, (º)
Rss2	75/192	74/214	69/193	56/203	33
Rss4	86/275	65/216	67/264		39

The orientations of various joint sets obtained during the field survey were plotted on a lower hemisphere net using a stereographic projection that is contoured to determine the various pole concentrations (Fig. 5.6). According to the analysis, no wedge mode of failure was identified. The slope location at a critical rock slope section of RSS2 was subjected to the planar mode of failure (Fig. 5.6a). According to the result of the analysis, planar mode of failure, which is potentially located at RSS2, was vulnerable to planar failure due to discontinuity sets JS2 and JS3, in which the pole of the joint set fails inside the critical zone of planar mode of failure. Like this, at slope section RSS4, the pole of joint set two (PJS2) was plotted within the critical zone of the planar mode of failure (Fig. 5.6b). This showed that joint set JS2 was the cause of the planar failure at slope section RSS4. A detailed summary of the possible modes of failure at the critical slope section, as well as the joint set responsible for mode failure, is presented in Table 5.12. Finally, a deterministic method was used to conduct the stability analysis of the three modes of failure in order to calculate the factor of safety factor of safety.

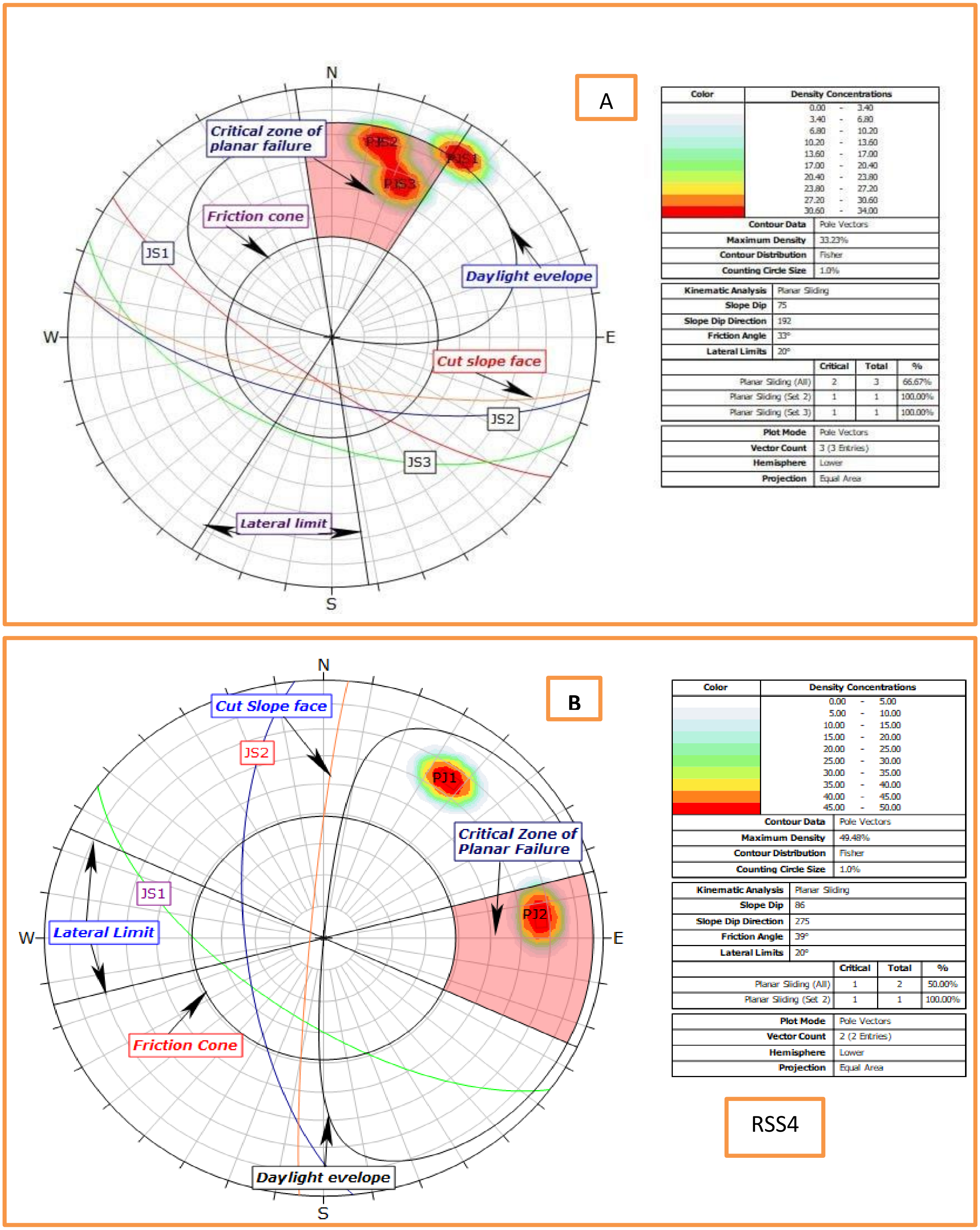

Figure 5.5 Kinematic analyses for planar modes of rock slope failure a)RSS2 b)RSS4.

Table 5.12 Mode of failures from kinematic analysis of rock slope sections

Slope Sections	Mode of failure from kinematic analysis rock slope sections
RSS-2	Planar failure due to joint set JS2 and JS3
RSS-4	Planar failure due to joint set JS2

5.6.2. Rock Slope Stability Analysis using LEM.

According to the kinematic analysis results (Fig 5.6), probable planar rock slope failure occurs at slope sections RSS2 and RSS4. A factor of safety slope stability assessment was conducted using Rocplane for planar. The software was used to analyze and interpret the factor of safety for the structurally controlled critical rock slope under static dry, static saturated, dynamic dry, and dynamic saturated conditions. For this analysis, shear strength parameters (cohesion and friction angle) of rock mass for the two structurally controlled critical selected rock slope sections were obtained from Barton-Bandis failure criteria using Rocdata software (Rocscience 2004, Rocdata, 3), and the unit weight of rock was obtained from the laboratory tests and summarized in Table 5.4. Furthermore, external loads such as horizontal seismic acceleration and groundwater conditions were considered during the stability analysis. In these sections, the stability slope describes the one mode of failure.

Table 5.13 Input parameter used in Rocplane software for planar mode of failure.

	Input parameter for Rocplane software to determine factor of safety the planar failure										
	Slope geometry			Failure plane				Shear strength		Forces	
	Joint set	Dip, (º)	H (m)	Dip, (º)	Wv	γr (t/m3)	USA, (º)	ϕ, (º)	C(t/m2)	γw (t/m3)	A
Rss2	Js2	75	16	69	10	2.66	10	31.20	0.51	1	0.07
	Js3	75	16	56	10	2.66	10	32.70	0.71	1	0.07
Rss4	Js2	86	12	67	1	2.53	8	39.78	1.73	1	0.07
Where γ = the unit weight of the rock, USA = the upper slope angle, ϕ = friction angle, c = cohesion, γw = water pressure, α = the seismic coefficient, H = the slope height and JS1= the joint set one, JS3 = joint set three and WV = the waviness of plane.											

The modeling of planar failures in Fig. 5.6 indicated that due to the presence of JS2 and JS3, planar failures are conceivable at rock slope section RSS2. The RocPlane software (Rocscience, 2004) was used to perform a factor of safety study on both JS2 and JS3 on rock slope section RSS2 (Fig. 5.7 and 5.8). As a result of the analysis, the FOS is smaller than one for rock slope section RSS2 for both joint set 2 (JS2) and joint set 3 (JS3). A slope that had a factor of safety less than one was unstable, according to slope stability study (Christian, 2004; Shariati and Fereidooni, 2021).

In this investigation, the evaluated factor of safety for both joints JS2 and JS3 for slope section RSS2 was less than one in all anticipated states. This implies that slope section RSS2 was unstable for static dry, dynamic dry, static saturated, and dynamic saturated conditions, as shown in Figs. 5.7 and 5.8. Similarly, the evaluated factor of safety for slope section RSS4 was greater than one in static dry and dynamic dry conditions, static saturated but unstable under dynamic saturated, as shown in Fig. 5.9 and The summary of the factor of safety analysis results and slope status at RSS2 and RSS4 under different anticipated conditions for the planar mode of failure is presented in Table 5.14. The slopes are unstable even in static dry condition that means it if failing with out any additional factor this is because groundwater manifested as spring along slope section plays greater role in destabilizing the slope. In addition, seismic acceleration and unfavorably oriented joints and slope also cause instability of the slope.

Table 5.14 Factor of safety and slope status under different condition for planar rock failure.

Slope Sections	Joint sets	Factor of safety planar formed in rock slope section RSS2 and RSS4 at different conditions.			
		Static dry (FOS)	Static saturated (FOS)	Dynamic dry (FOS)	Dynamic saturated (FOS)
RSS-2	JS2	0.54	0.26	0.47	0.24
	JS3	0.67	0.52	0.59	0.44
	Stability Condition	Unstable	Unstable	Unstable	Unstable
RSS-4	JS2	1.12	1.01	1.02	0.86
	Stability Condition	Stable	Stable	stable	Unstable

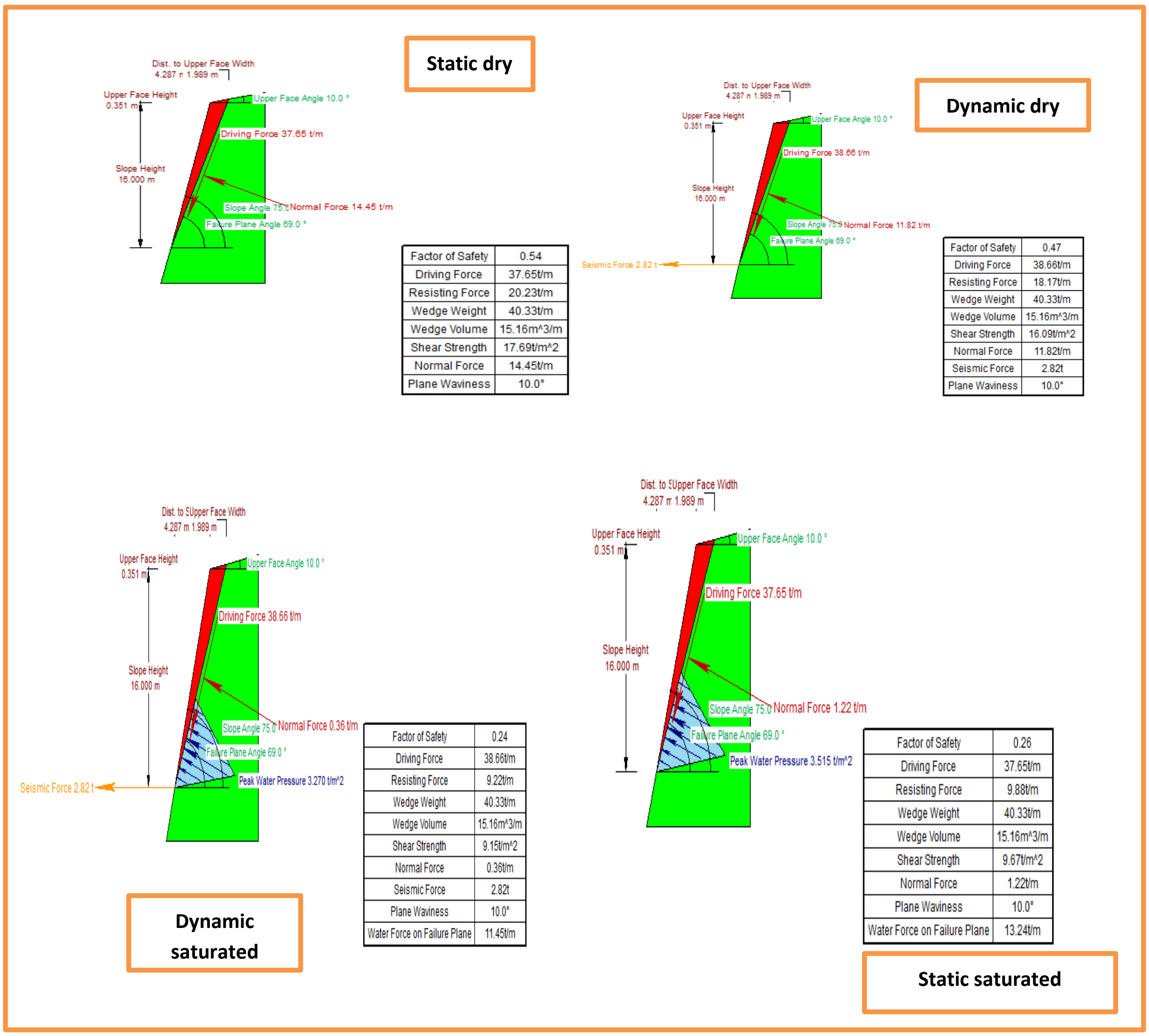

Figure 5.6 Slope stability analysis RocPlane software the planar failure rock slope section two (RSS2) forces acting on failure plane JS2 at different conditions.

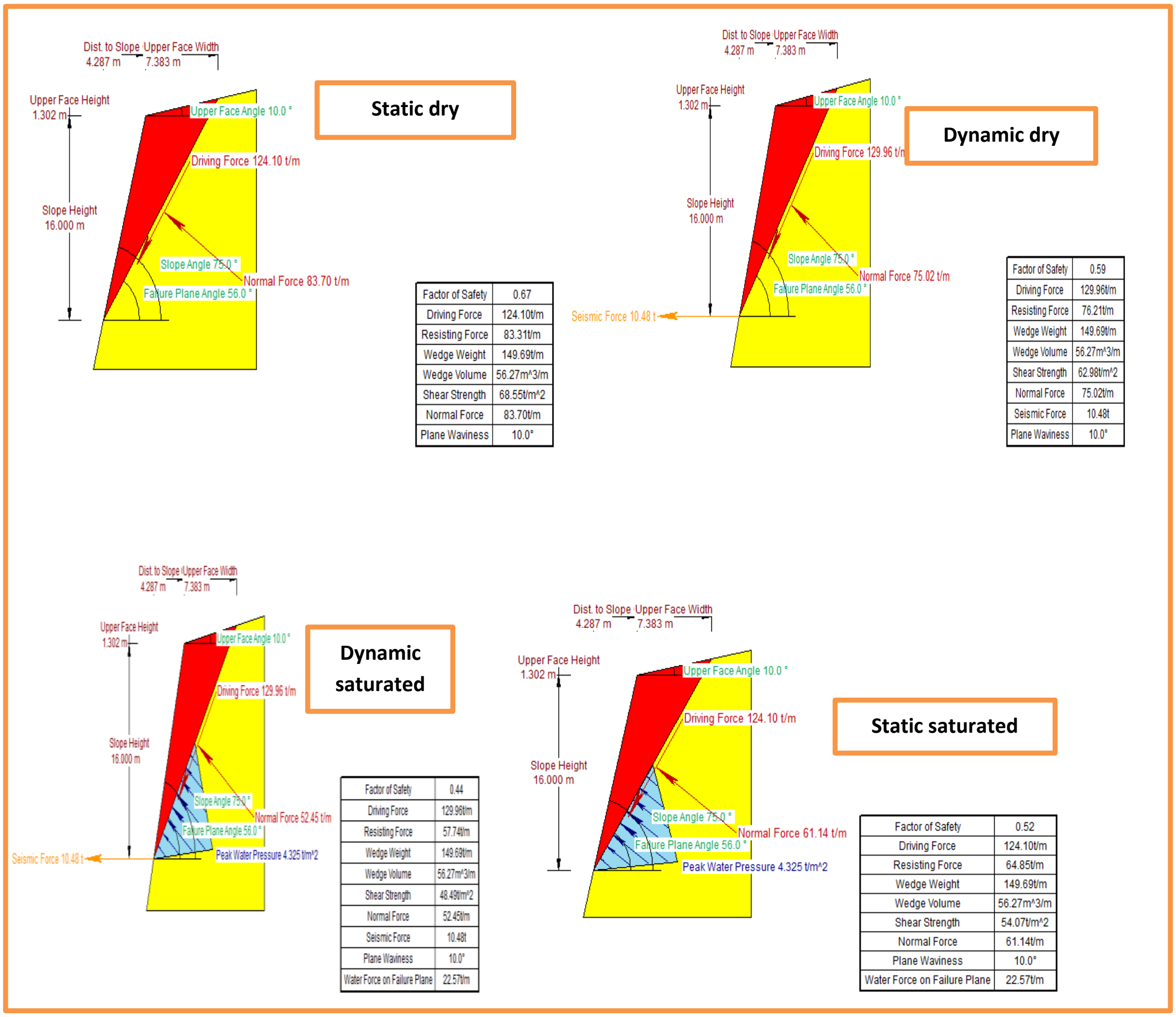

Figure 5.7 Slope stability analysis RocPlane software the planar failure rock slope section five (RSS2) forces acting on failure plane JS3 at different conditions

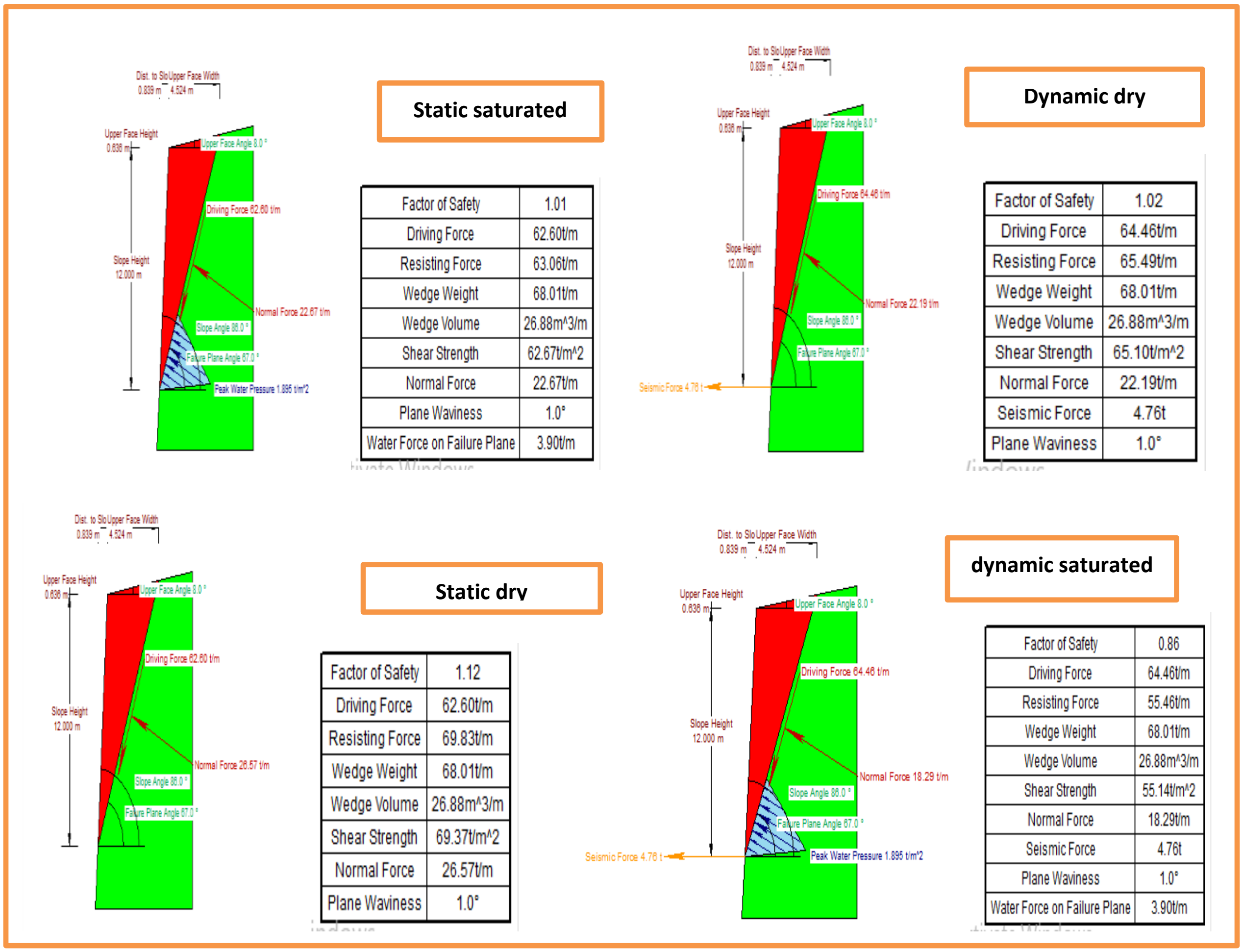

Factor of Safety	1.01
Driving Force	62.60t/m
Resisting Force	63.06t/m
Wedge Weight	68.01t/m
Wedge Volume	26.88m^3/m
Shear Strength	62.67t/m^2
Normal Force	22.67t/m
Plane Waviness	1.0°
Water Force on Failure Plane	3.90t/m

Factor of Safety	1.02
Driving Force	64.46t/m
Resisting Force	65.49t/m
Wedge Weight	68.01t/m
Wedge Volume	26.88m^3/m
Shear Strength	65.10t/m^2
Normal Force	22.19t/m
Seismic Force	4.76t
Plane Waviness	1.0°

Factor of Safety	1.12
Driving Force	62.60t/m
Resisting Force	69.83t/m
Wedge Weight	68.01t/m
Wedge Volume	26.88m^3/m
Shear Strength	69.37t/m^2
Normal Force	26.57t/m
Plane Waviness	1.0°

Factor of Safety	0.86
Driving Force	64.46t/m
Resisting Force	55.46t/m
Wedge Weight	68.01t/m
Wedge Volume	26.88m^3/m
Shear Strength	55.14t/m^2
Normal Force	18.29t/m
Seismic Force	4.76t
Plane Waviness	1.0°
Water Force on Failure Plane	3.90t/m

Figure 5.8 Slope stability analysis RocPlane software the planar failure rock slope section four(RSS4) forces acting on failure plane JS3 at different conditions.

5.6.3. Slope Stability Analysis of Homogenous Weathred Rocks using Limit Equilibrium Method

For this study, slope stability analysis of the two critical slope sections was performed using the limit equilibrium approach in terms of the factor of safety (FOS) by employing the General Limit Equilibrium (GLEM) or Morgenstern-Price method. The stability analysis of these two critical slope sections was evaluated by determining the factor of safety under various conditions. The analysis was done using slide software (Rocscience 2004, slide 6) within the Mohr-Coulomb model. The input parameters used in this software are material properties such as cohesion, angle of internal friction, and unit weight of rocks. For this study, shear strength parameters (cohesion and friction angle) of rock mass for the two critical selected slope sections were obtained from Hoek-Brown failure criteria using Rocdata software (Rocscience 2004, Rocdata3), and the unit weight of rock was obtained from the laboratory tests, which can be summarized in Table 5.6. Furthermore, external loads such as horizontal seismic acceleration and groundwater conditions were taken into account during the stability analysis. The study area is found in a high seismic zone, and the horizontal acceleration from seismic loading with a magnitude average (α) of 0.07g was used for dynamic dry and dynamic saturated conditions.

Table 5.15 Input parameters for limit equilibrium slope stability analysis of rocks for slide software

Slope sections	Materials	Strength Model	input parameter				Seismic horizontal acceleratio n (α) g
			Cohesion (Mpa)	friction angle, (º)	Unit weight (KN/m3)		
					Γdry	Γsat	
RSs1	Sw basalt	Mohr- coulomb	0.161	39.91	27.81	29.3	0.07
RSs5	Mw basalt	Mohr- coulomb	0.072	38.09	23.19	25.62	0.07
RSS is the rock slope sections, MW = Moderately weathered basalt, SW = slightly weathered basalt and HW = highly weathered basalt.							

The slope stability Analysis factor safety for non-Structurally Controlled critical selected four rock Slope Sections were determined using slide software through the Mohr-Coulomb model evaluated as the follows;

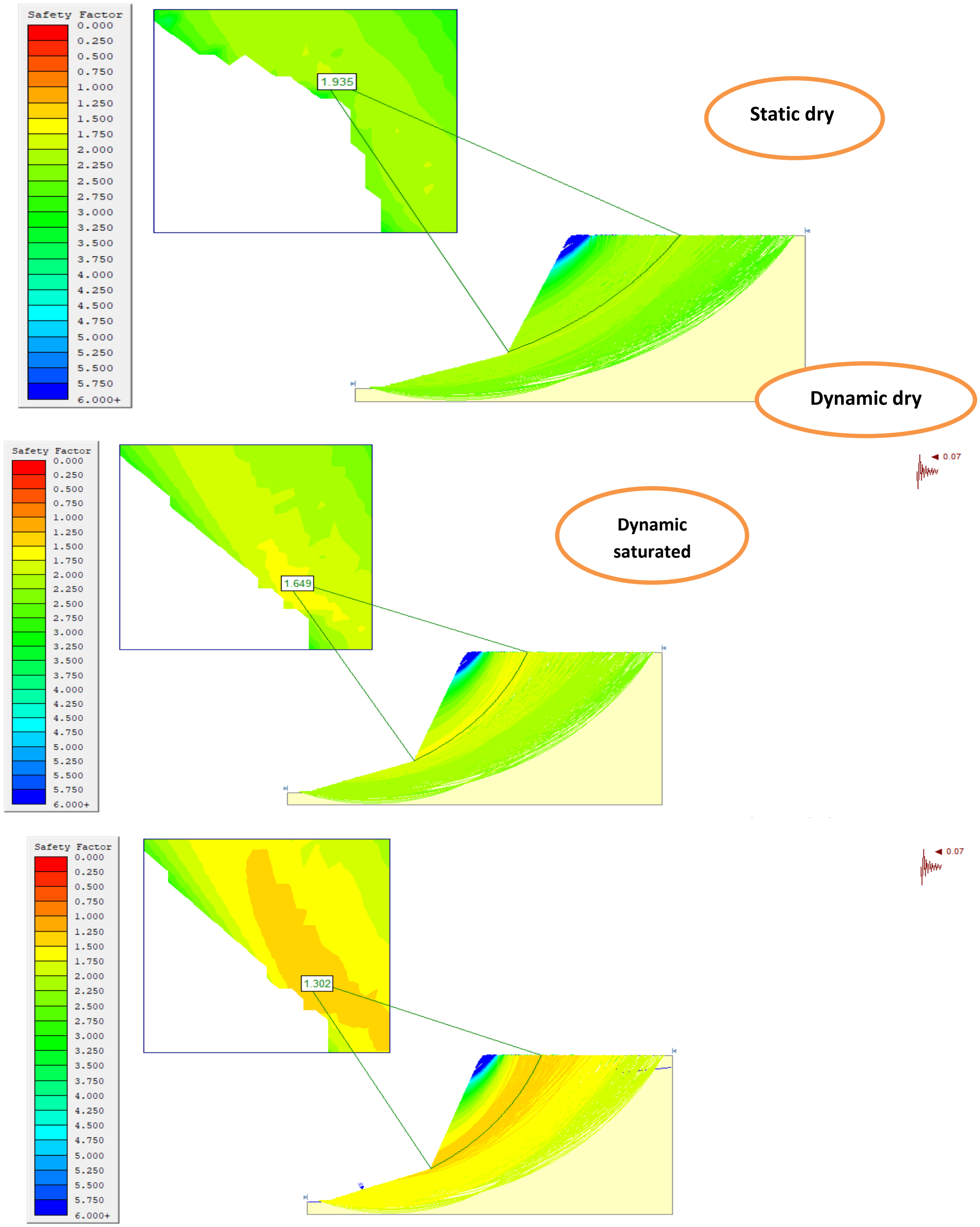
Safety Factor
0.000
0.250
0.500
0.750
1.000
1.250
1.500
1.750
2.000
2.250
2.500
2.750
3.000
3.250
3.500
3.750
4.000
4.250
4.500
4.750
5.000
5.250
5.500
5.750
6.000+
1.935
Static dry
Dynamic dry
Safety Factor
0.07
1.649
Dynamic saturated
Safety Factor
0.07
1.302

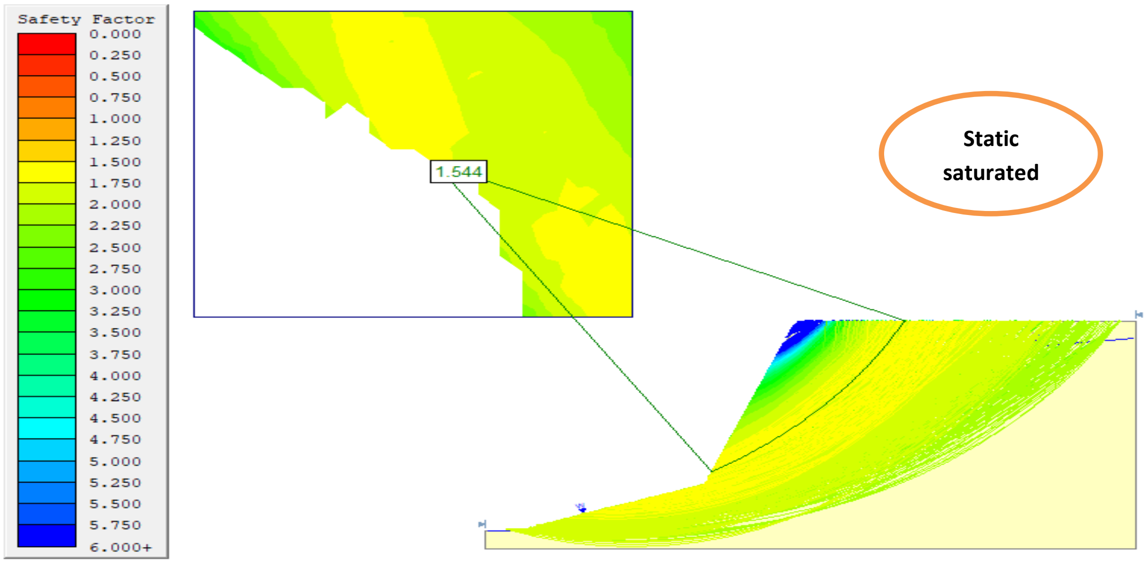

Figure 5.9 Slope stability analysis result using Limit equilibrium method for rock slope section RSS1 under a) static dry condition, b) Dynamic dry condition, c)dynamic saturated conditions, d) Static saturated conditions.

Based on the above analysis results, the factor of safety rock at slope section RSS1 is 0.388 and 0.341, respectively, under static and dynamic dry conditions (Figs.5.10). According to these results, rock slope section RSS1 is unstable in dynamic dry conditions and unstable in static dry conditions. However, the factors of safety that were determined under static saturated and dynamic saturated conditions for the rock slope section RSS1 were 0.163 and 0.220, respectively. This indicates that the rock critical slope section RSS1 is unstable in both saturated and dynamic saturated conditions.

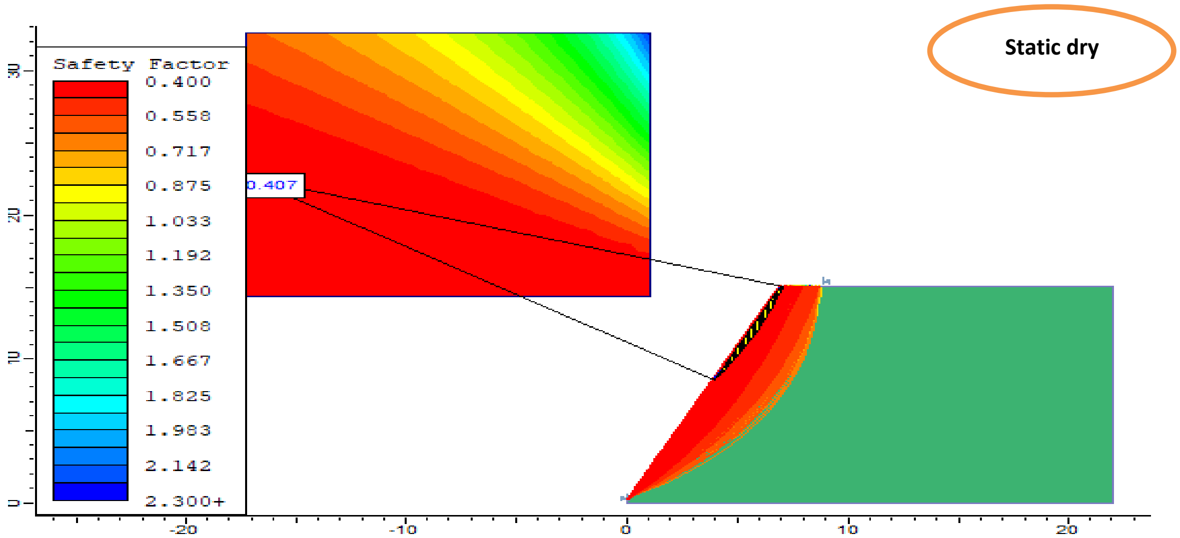
Static dry
Safety Factor
0.400
0.558
0.717
0.875
1.033
1.192
1.350
1.508
1.667
1.825
1.983
2.142
2.300+
0.407
-20
-10
0
10
20
30
20
10
0

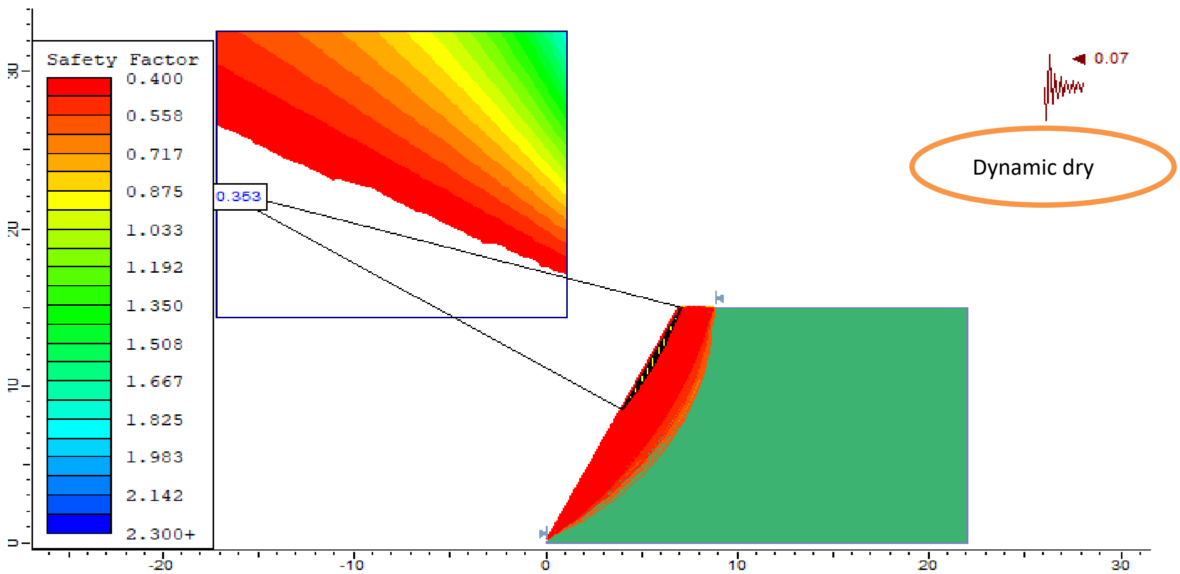
0.07
Dynamic dry
Safety Factor
0.400
0.558
0.717
0.875
1.033
1.192
1.350
1.508
1.667
1.825
1.983
2.142
2.300+
0.353
-20
-10
0
10
20
30
30
20
10
0

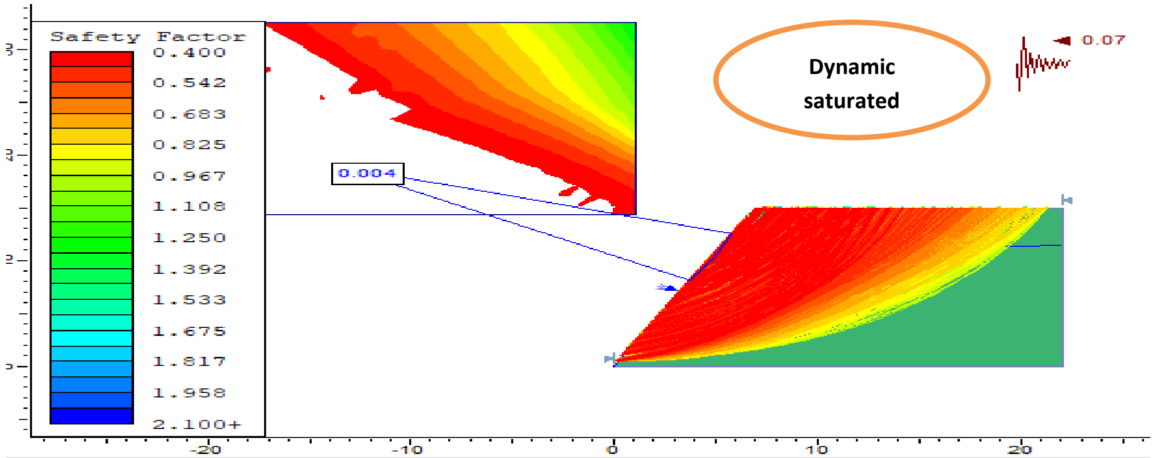

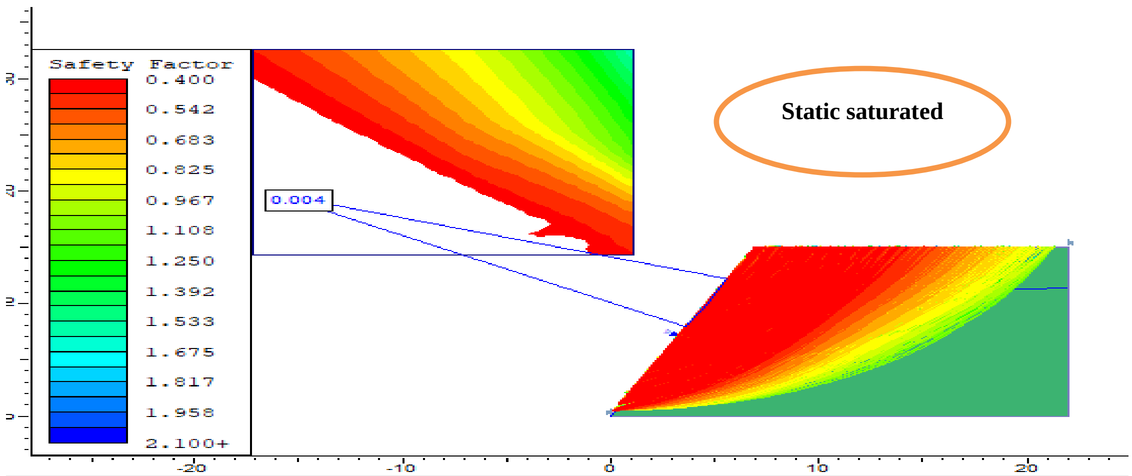

Figure 5.10 Slope stability analysis result using Limit equilibrium method for rock slope section RSS5 under a) static dry condition, b) Dynamic dry condition, c) Static saturated condition and d) dynamic saturated conditions.

The minimum factor of safety and critical slip surface of the rock at critical slope section RSS5 is determined using the general limit equilibrium methods by considering various conditions as indicated in Figure 5.11. Accordingly, the analysis results at the critical rock slope section RSS5 revealed that the factor of safety under static dry and dynamic dry conditions is 0.408 and 0.354, as shown in Figs. 5.11, respectively. Similarly, the factory of safety under static saturated and dynamic saturated conditions is 0.004, as shown in Figs. 5.11, respectively. This indicated that the rocks at critical slope section RSS5 were unstable in all conditions.

5.6.4. Slope Stability Analysis of Homogenous Soils Using Limit Equilibrium Method

The general limit equilibrium (GLE) or Morgenstern-Price approach was used to analyze the slope stability of two soil slope sections. Using Rocscience slide software, determining the critical potential slip surface in slope stability analysis using General Limit Equilibrium (GLE) or the Morgenstern-Price method is an essential measure for obtaining a minimum factor of safety in each slope section (Abramson et al., 2001). Furthermore, the general limit equilibrium approaches in the Rocscience Slide software satisfy all of the equilibrium conditions (Fredlund, 1987). The finite element approach and limit equilibrium were used in this work to assess the stability of two important selected soil slope portions along the road that were identified and observed in the field. The SS3 part of the soil slope has approximately 15 meters of height, 20 meters of length. Similarly, the soil slope section SS6 has approximately 10 m height.

Table 5.16 The input parameter for homogenous soil slope stability analysis

Slope section	Material	Unit weight (KN/m3)		Cohesions (KN/m2)	Angle of internal friction (degree)
		γsat	Γdry		
SS3	Silty soil	17	12.44	23	11.61
SS6	clayey silts with slight plasticity	16.5	12.54	24	9.02

SS = soil slope section, γdry = dry unit weight and γsat = saturated unit weight of soils.

For this study, the factor of safety (FOS) and slip surface were determined and interpreted for static dry, static saturated, dynamic dry, and dynamic saturated conditions using the General Limit Equilibrium or Morgenstern-Price LEM methods and the above input parameters in Table 5.16. The safety factor evaluation was carried out in static, dry conditions, representing the stability state without taking seismic load into account, and was assumed to be dry during the dry season in the study location. Furthermore, the safety factor evaluation was carried out under dynamic saturated conditions, which implies that the slope was subjected to seismic horizontal acceleration (= 0.07 g) in the study region and was assumed to be saturated under heavy rains (Lamessa and Meten, 2021).

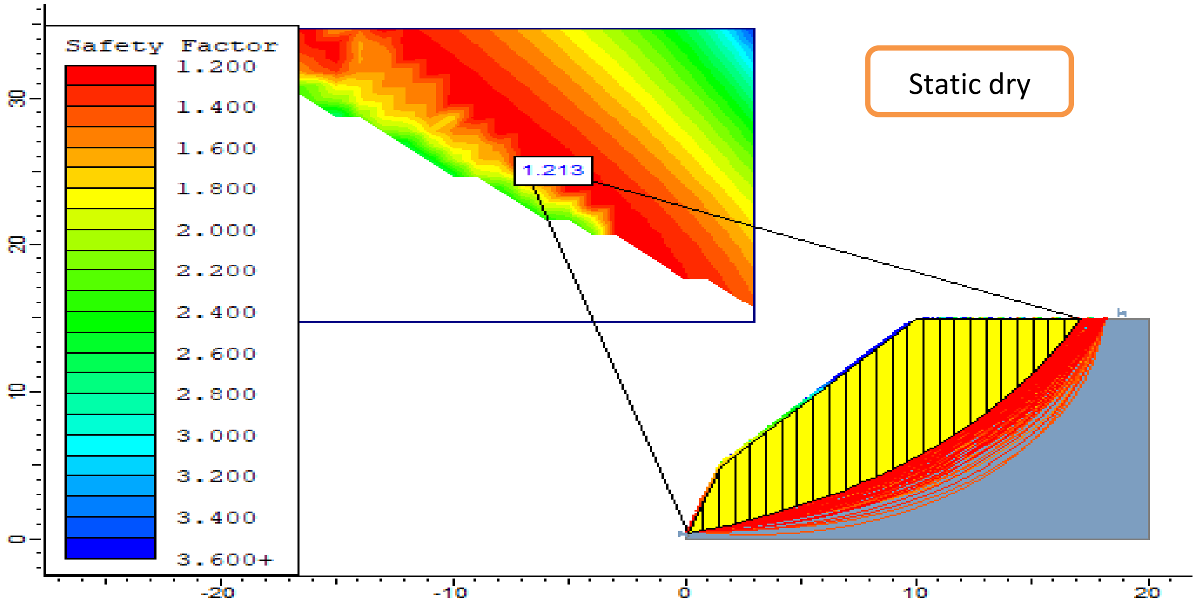

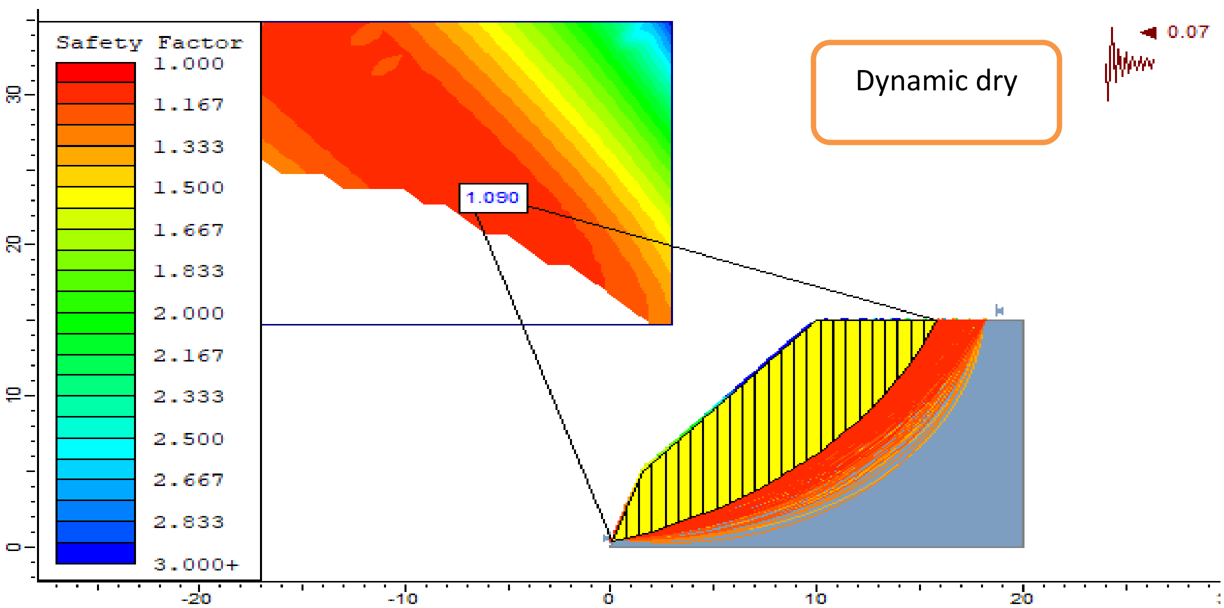

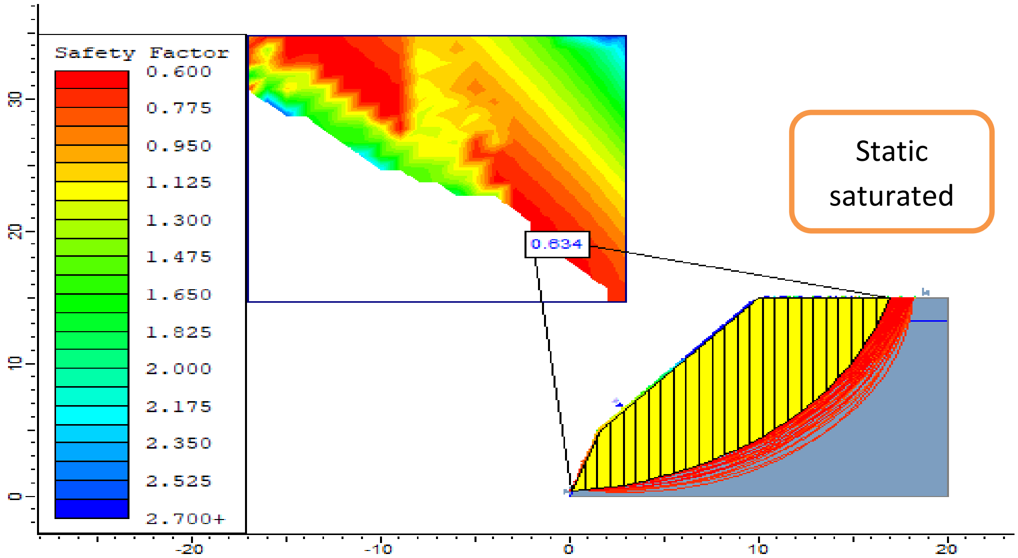

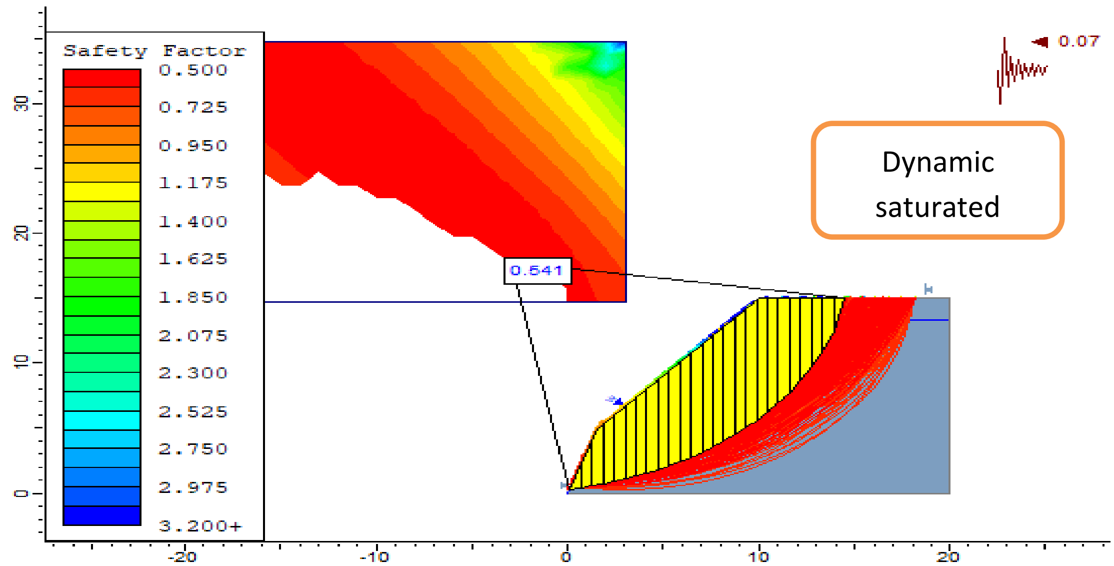

Figure 5.11 Slope stability analysis Limit equilibrium method for soil slope section SS3 at a)static dry, b) dynamic dry, c) static saturated and d) dynamic saturated conditions

The above analysis indicates that in static and dynamic dry conditions, slope section SS1 has a factor of safety of 1.213 and 1.090, respectively (Fig. 5.12). The results showed that the soil slope section SS1 is stable under static and dynamic drying conditions. However, the factor of safety that was determined under static saturated and dynamic saturated conditions of the slope section SS1 is 0.634 and 0.541 (Fig. 5.12 respectively). This indicates that the unstable slope is relatively small compared to static and dynamic dry slope conditions. Due to the groundwater, slope stability can be affected by increasing pore water pressure, increasing weight on a slope when the soil mass is fully saturated, decreasing effective stress, and losing shear strength parameters.

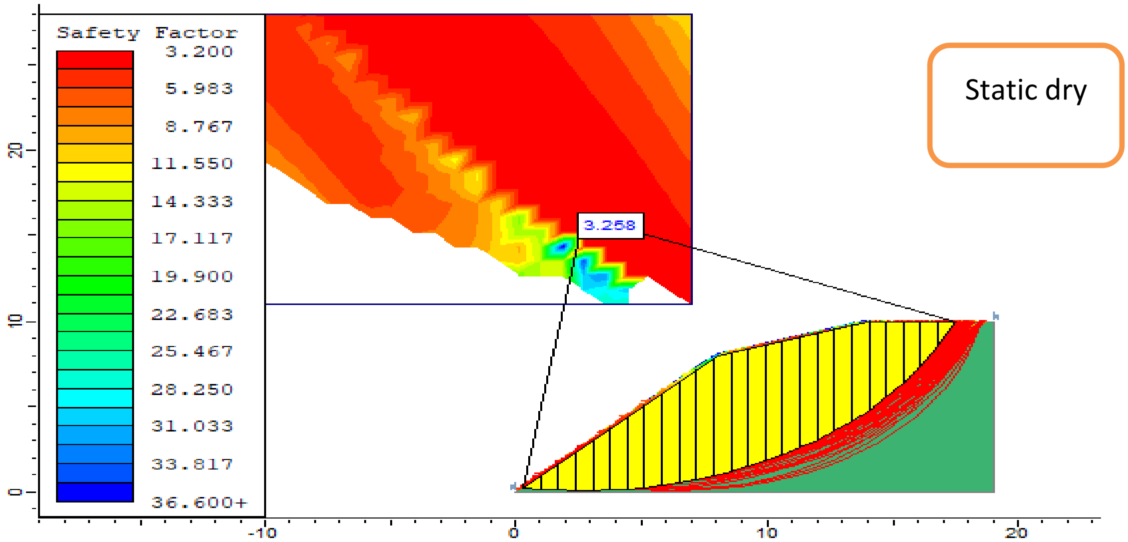
Safety Factor
3.200
5.983
8.767
11.550
14.333
17.117
19.900
22.683
25.467
28.250
31.033
33.817
36.600+
3.258
Static dry
0
10
20
-10
0
10
20

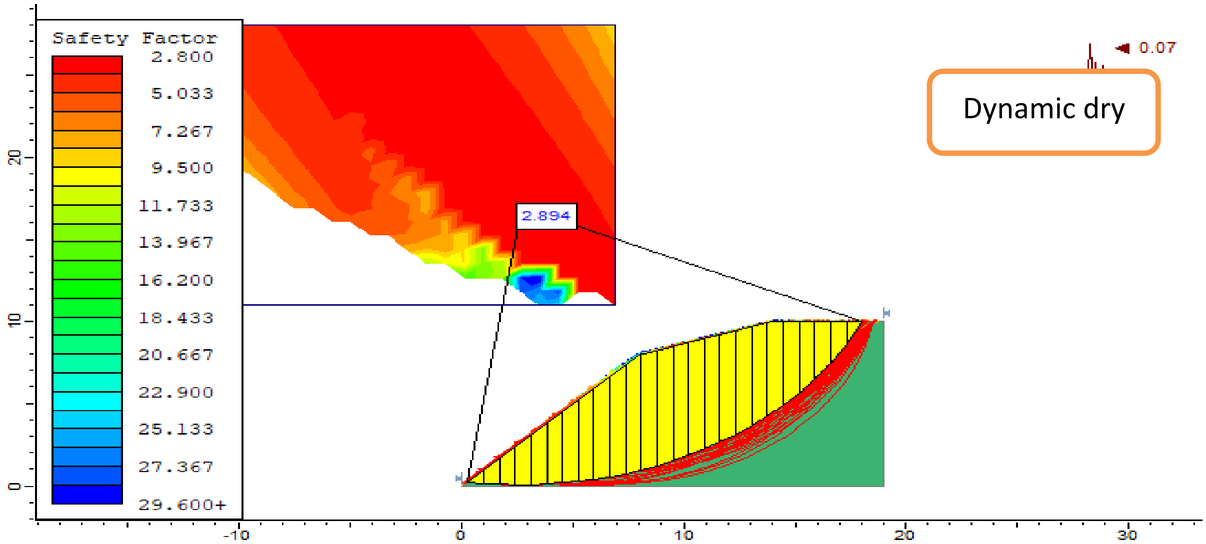
Safety Factor
2.800
5.033
7.267
9.500
11.733
13.967
16.200
18.433
20.667
22.900
25.133
27.367
29.600+
2.894
0.07
Dynamic dry
0
10
20
-10
0
10
20
30

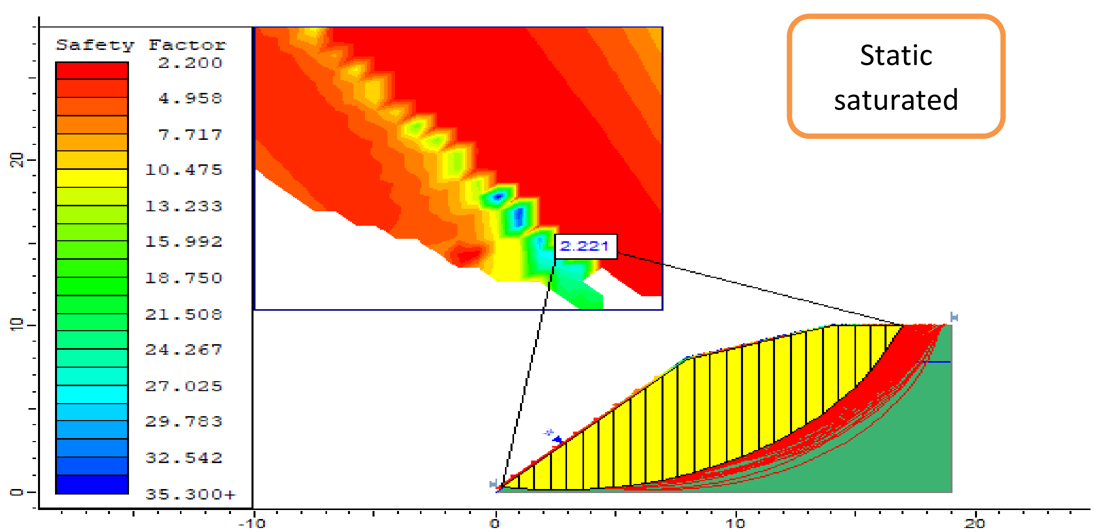
Safety Factor
2.200
4.958
7.717
10.475
13.233
15.992
18.750
21.508
24.267
27.025
29.783
32.542
35.300+
2.221
Static saturated
0
10
20
-10
0
10
20

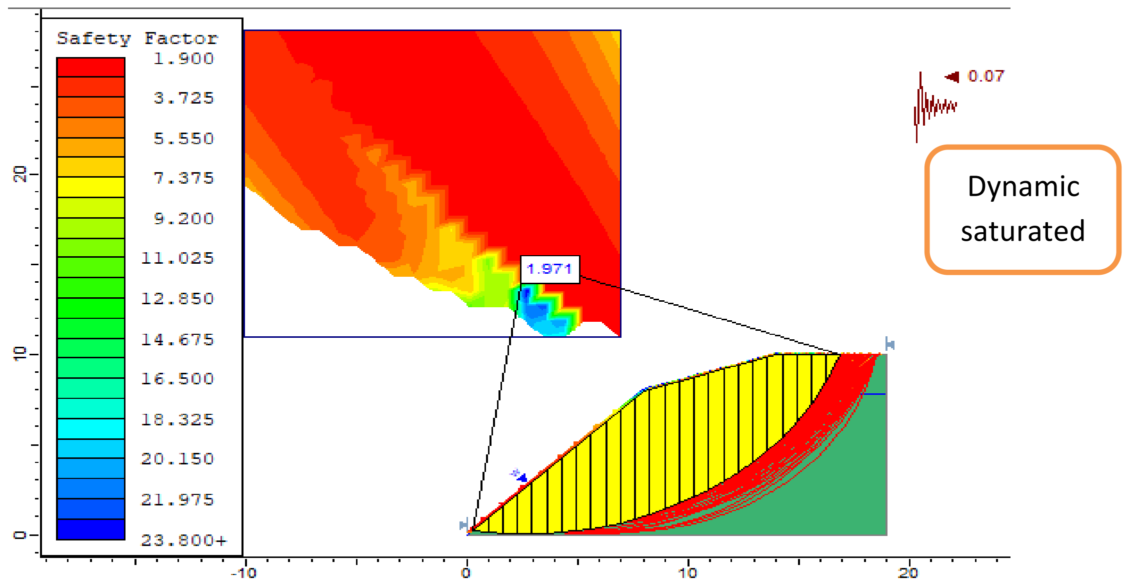

Figure 5.12 Slope stability analysis Limit equilibrium method for soil slope section SS6 at a)static dry, b) dynamic dry, c) static saturated and d) dynamic saturated conditions

Similarly, the factor of safety for a soil slope section SS6 is 3.258 and 2.894 under static and dynamic dry conditions (Figs. 5.13). This shows that soil slope section SS6 was stable in both static and dynamic dry conditions. Similarly, the factor of safety that was determined under static saturated and dynamic saturated conditions of the slope section SS6 is 2.221 and 1.971, respectively (Figs. 5.13). This indicates that the soil slope in Section 6 is stable in all conditions.

Table 5.17 Factor of safety and slope status under different anticipated condition of soil slope section SS3 and SS6.

Slope Sections	Method	Loading condition	The factor of safety (FOS)	Slope stability Conditions
(SS3)	GLEM/ Morgenstern-price method	Static dry	1.213	Unstable
		Static saturated	0.634	Stable
		Dynamic dry	1.090	Unstable
		Dynamic saturated	0.541	Stable
(SS6)	GLEM/ Morgenstern-price method	Static dry	3.258	Stable
		Static saturated	2.221	Stable
		Dynamic dry	2.894	Stable
		Dynamic saturated	1.971	Stable

5.6.5. Homogenous Weathred Rock Slope Stability Analysis Using Finite Element Method

For this study, the rock slope stability analysis of critical selected slope sections was performed by the finite element method. The finite element analysis was performed using the Phase2 software (Rocscience 2004, Phase2), and the slope stability condition can be expressed in terms of the Strength Reduction Factor (SRF) value. The critical shear strength reduction factor (SRF), which is equivalent to the factor of safety (FOS), was calculated using a finite-element-based numerical simulation in the Phase2 software program (Bushira et al., 2018; Charles et al., 2020). For this study, the critical rock selected slope section, the factory of safety, was estimated by limit equilibrium and finite element methods using the same material properties, slope angle, slope geometry, and boundary conditions. A finite element slope stability analysis was performed in this study in order to determine the critical strength reduction factor, or FOS, of the rock slope's static dry condition, static saturated condition, dynamic dry condition, and dynamic saturated condition. The input parameters used in stability analysis using the finite element method (FEM) are presented in Table 5.18 below.

Table 5.18 Input parameters for finite element stability analysis to compute critical strength reduction factor for phase software.

Slope section	Materials	Strength Model	C (Mpa)	ϕ,(º)	Erm (Mpa)	Ψ(º)	Unit weight (KN/m3)		V	α (g)
							Γdry	Γsat		
SS1	Sw basalt	Mohr-coulomb	0.161	39.91	1581.14	9.91	12.44	17	0.3	0.07
SS5	Mw basalt	Mohr-coulomb	0.072	38.09	1143	8.09	12.54	16.5	0.3	0.07

RSS = Rock slope section, C = cohesion, ϕ = angle of internal friction, Erm= deformation modulus, γ = Unit weight of rocks, V = Poisson ratio and α = seismic horizontal acceleration, Ψ = Dilatancy angle of rocks, MW = moderately weathered, SW =Slightly weathered, Hw = highly weathered lower basalts.

Stability analysis of non-structurally controlled four critical rock slope sections on critical strength reduction factor (SRF) was determined using phase2 software through the Mohr-Coulomb model as shown in Fig. 5.14 below.

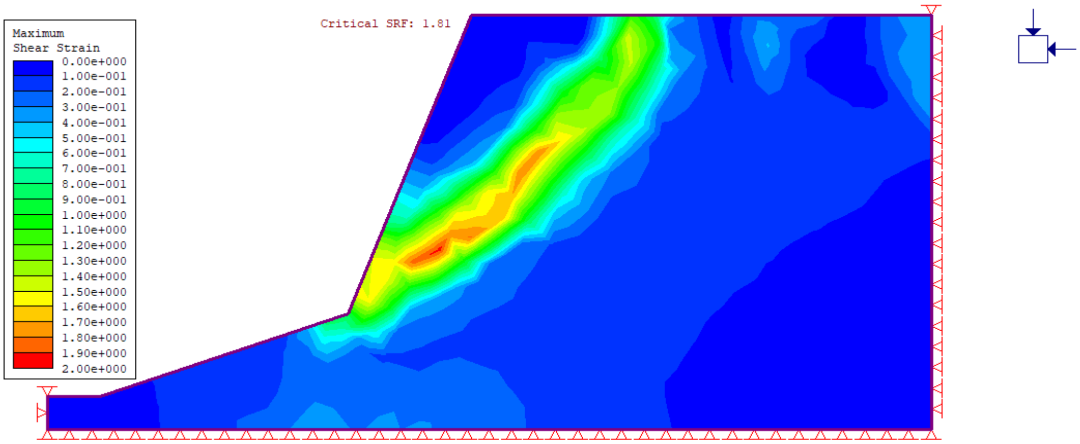
Maximum
Shear Strain
0.00e+000
1.00e-001
2.00e-001
3.00e-001
4.00e-001
5.00e-001
6.00e-001
7.00e-001
8.00e-001
9.00e-001
1.00e+000
1.10e+000
1.20e+000
1.30e+000
1.40e+000
1.50e+000
1.60e+000
1.70e+000
1.80e+000
1.90e+000
2.00e+000
Critical SRF: 1.81

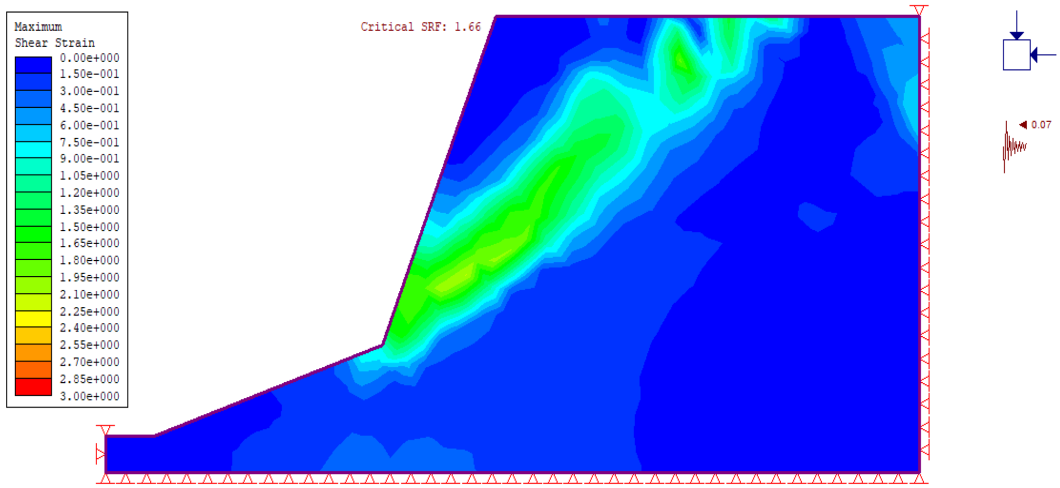
Maximum
Shear Strain
0.00e+000
1.50e-001
3.00e-001
4.50e-001
6.00e-001
7.50e-001
9.00e-001
1.05e+000
1.20e+000
1.35e+000
1.50e+000
1.65e+000
1.80e+000
1.95e+000
2.10e+000
2.25e+000
2.40e+000
2.55e+000
2.70e+000
2.85e+000
3.00e+000
Critical SRF: 1.66
0.07

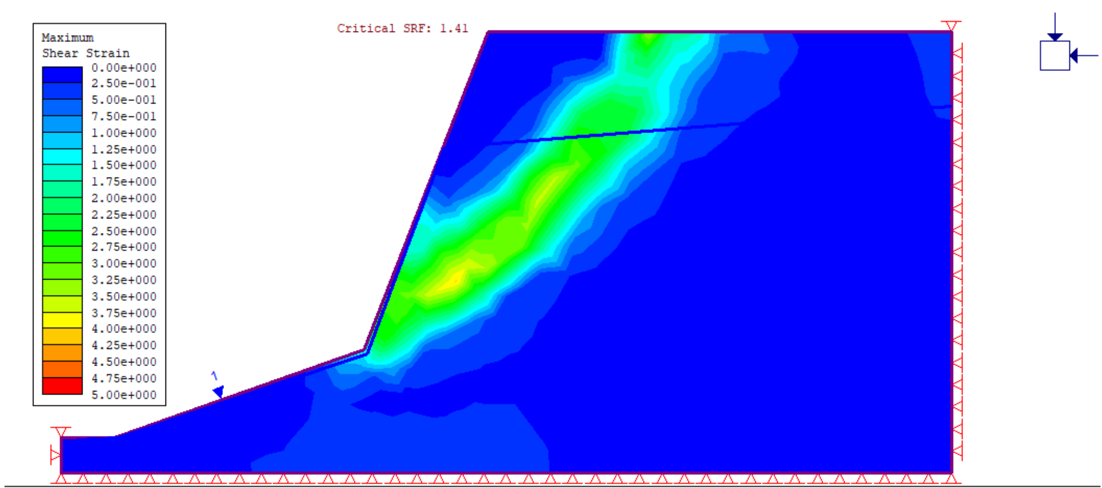
Maximum
Shear Strain
0.00e+000
2.50e-001
5.00e-001
7.50e-001
1.00e+000
1.25e+000
1.50e+000
1.75e+000
2.00e+000
2.25e+000
2.50e+000
2.75e+000
3.00e+000
3.25e+000
3.50e+000
3.75e+000
4.00e+000
4.25e+000
4.50e+000
4.75e+000
5.00e+000
Critical SRF: 1.41

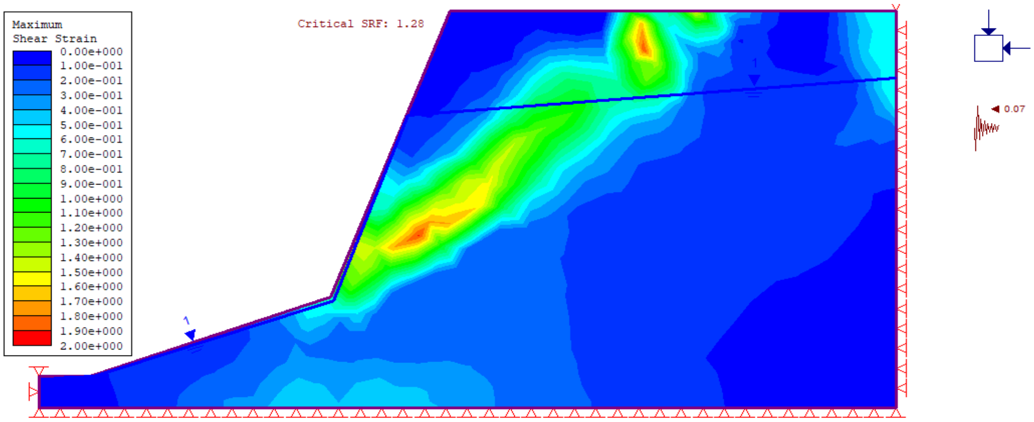

Figure 5.13 Slope stability analysis finite element method for rock slope section RSS1 under a) static dry, b) dynamic dry, c) static saturated and d) dynamic saturated conditions.

According to the results of the analysis, the SRF of RSS1 is 0.27 at static dry conditions and 0.18 at dynamic dry conditions, as shown in Figs. 5.14, respectively. In addition, the critical strength reduction factor (SRF) for the static saturated and dynamic saturated slope sections shown in Figs. 5.14 is 0.163 and 0.123, respectively. According to Christian (2004) and Shariati (2021), when the slope is supposed to be static dry, static saturated, dynamic dry, or dynamic saturated, the critical SRF, or FOS, is less than one, indicating that the slope is unstable. This implies that the rock-critical slope section RSS1 was unstable in all anticipated conditions. This demonstrated that groundwater can affect slope stability by increasing pore water pressure, increasing weight on a slope when the rock mass is saturated, and reducing the shear strength parameter (Kabeta 2021).

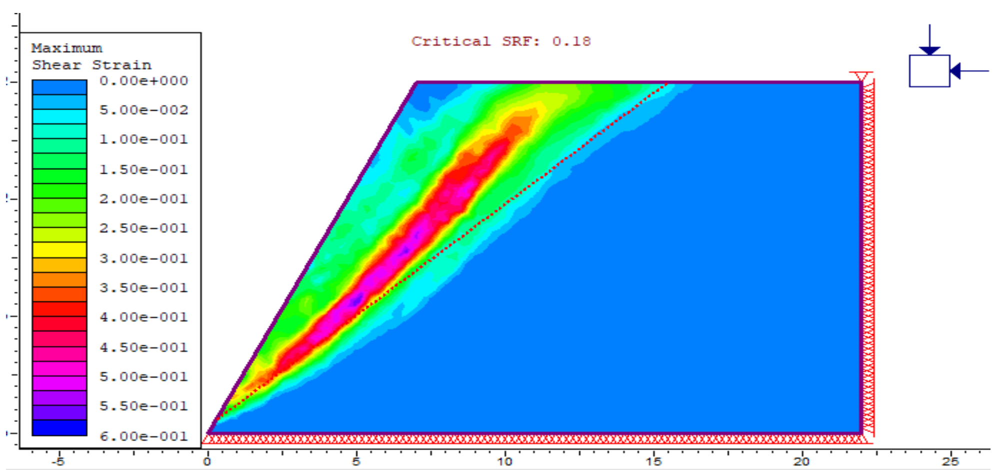

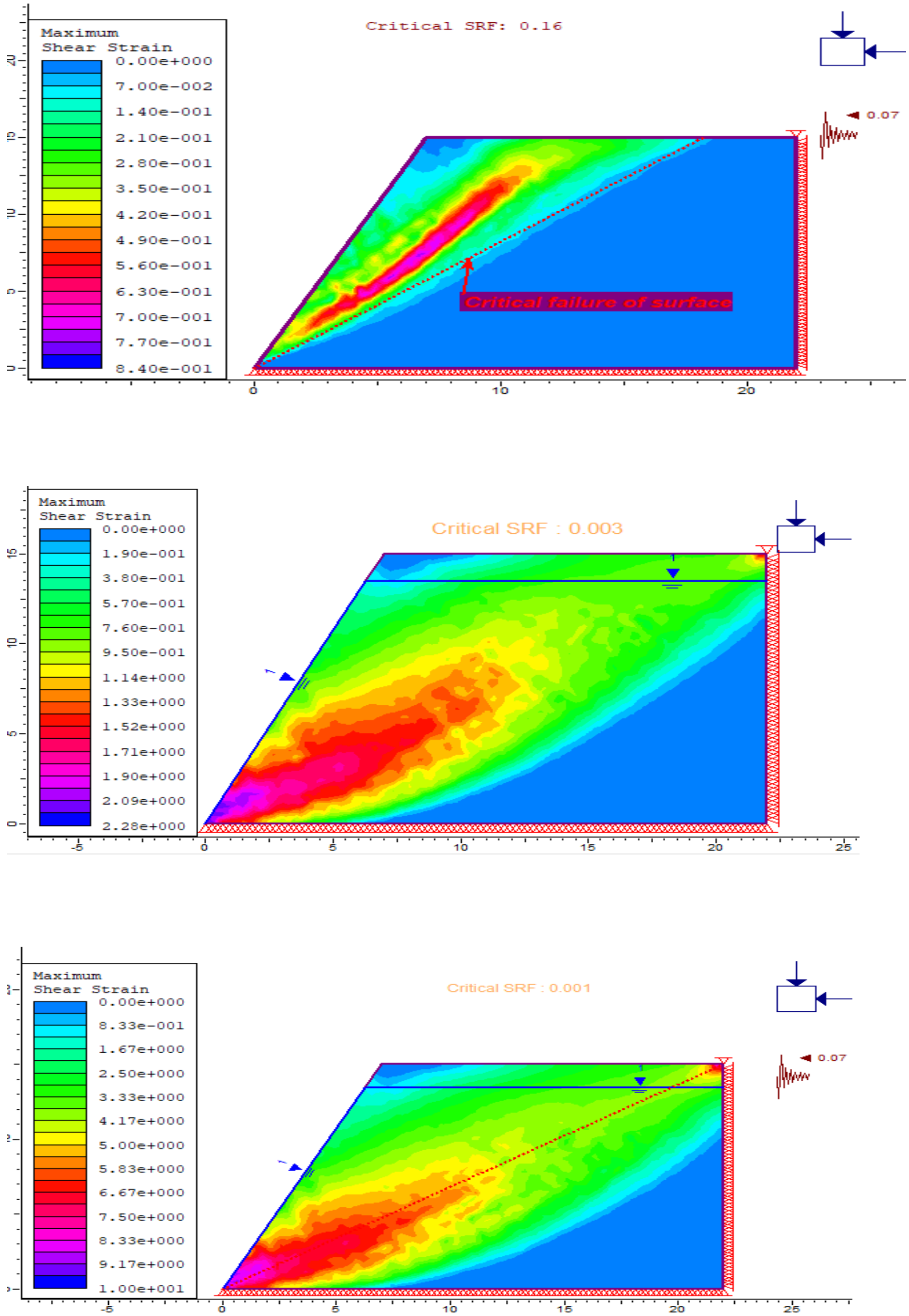

Figure 5.14 Slope stability analysis finite element method for rock slope section RSS4 under a) static dry condition b) dynamic dry condition c) Static saturated condition and d) dynamic saturated conditions

The analysis results suggest that the SRF of RSS5 is 0.18 at static dry conditions and 0.16 at dynamic dry conditions, as illustrated in Figs 5.15, respectively. Furthermore, the critical strength reduction factor (SRF) for the static saturated and dynamic saturated slope sections shown in Figs. 5.15 respectively, is 0.03 and 0.01. When the slope is meant to be static dry, static saturated, dynamic dry, or dynamic saturated, the critical SRF, or FOS, is less than one, suggesting that the slope is unstable, according to Christian (2004) and Shariati (2021). This means that the rock-critical slope segment RSS5 was unstable under all expected scenarios. This demonstrated that the Groundwater can influence slope stability by raising pore water pressure, increasing weight on a slope when the rock mass is saturated, and decreasing the shear strength parameter (Bekele & Meten, 2023).

5.6.6. Slope Stability Analysis of Homogenous Soil using Finite Element method

The factory of safety for the two soil critical slope portions is evaluated using limit equilibrium and finite element methods with the same material parameters, slope angle, and slope geometry as in the previous study. The analysis was performed to determine whether the slope was stable or unstable. Cohesion, internal friction angle, soil unit weight, Poisson's ratio (v), dilatancy angles, and Young's modulus are the input parameters for the two soil slope sections utilized in finite element modeling. Laboratory experiments are used to establish the internal friction angle, cohesiveness, and unit weight of the two soil slope sections (SS3 and SS6). The correlation and recommendation of literature were utilized to establish the deformation modulus of a soil (Es) and Poisson's ration (v) that are employed for numerical modeling (Terzaghi and Pecks, 1967; Bowles, 1996).

Table 5.19 Input parameters for soil slope stability analysis using finite element method for phase software.

Slope sections	Materials	Unit weight (KN/m2)		C (Mpa)	ϕ(º)	Ψ (º)	V	Es (KN/m2)
		Γsat	Γdry					
SS3	Silty soils	17	12.44	23.0	11.61	0	0.3	8760
SS6	clayey silts with slight plasticity	16.5	12.54	49.55	17.3	0	0.4	12804
$_{\gamma}$dry = dry unit weight of soil, $_{\gamma}$sat = the saturated unit weight of soil, C = cohesion, ϕ = angle of internal friction, ψ = dilatancy angle, v = Poisson's ratio and Es = young modulus.								

The safety factors for the selected the two critical soil slope sections (SS1and SS2) were determined in Phase2 software (Rocscience, 2004) using the Mohr-Coulomb model discussed as stated belows.

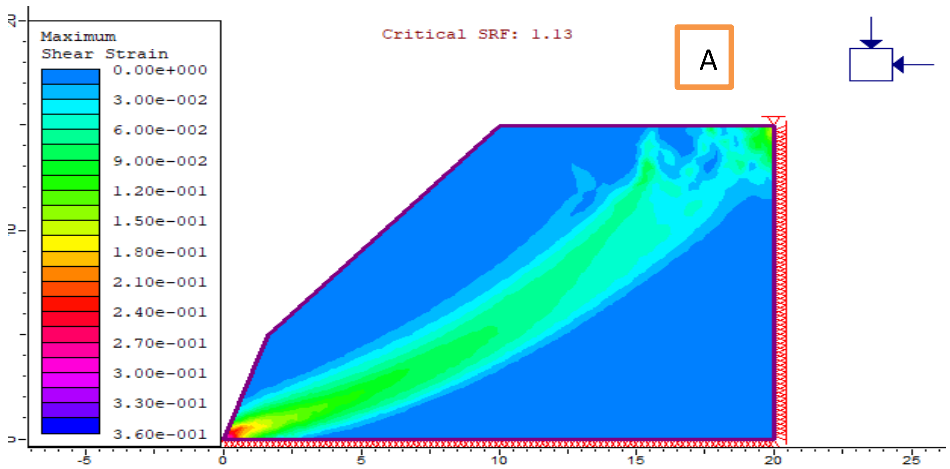

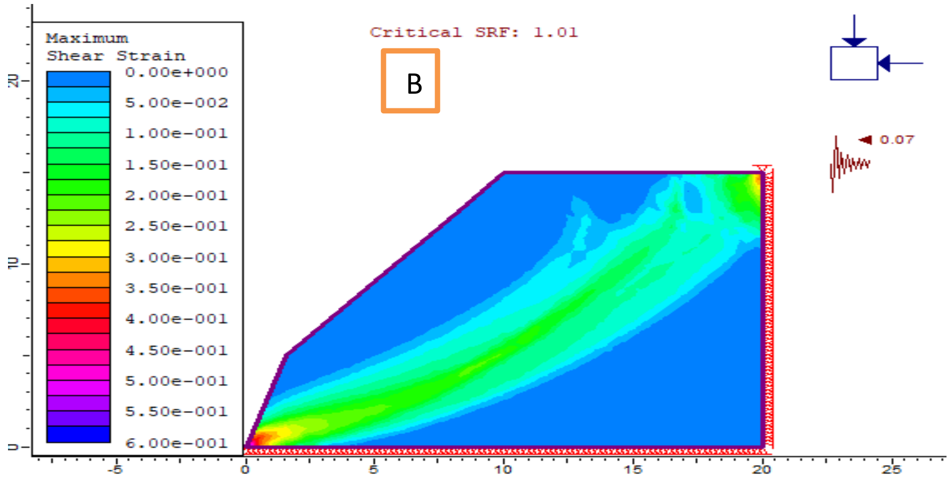

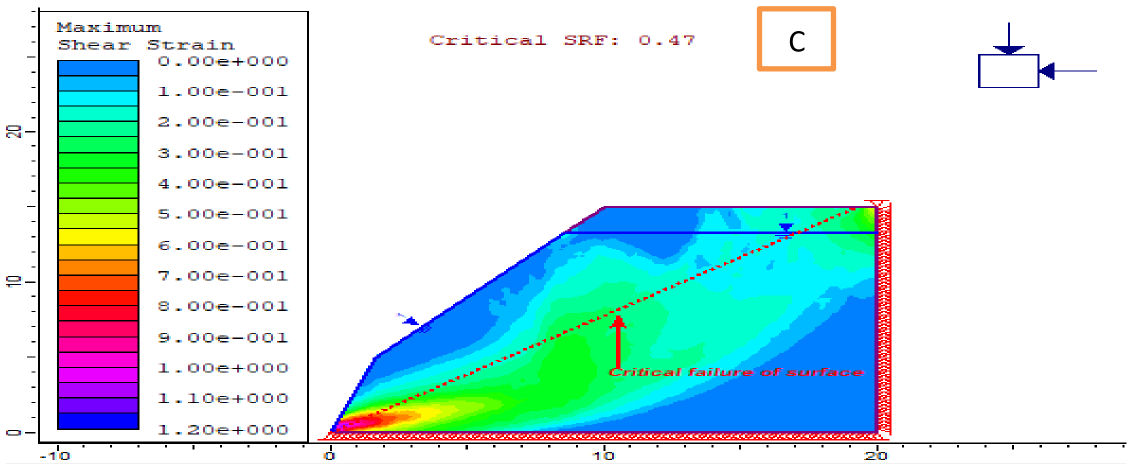

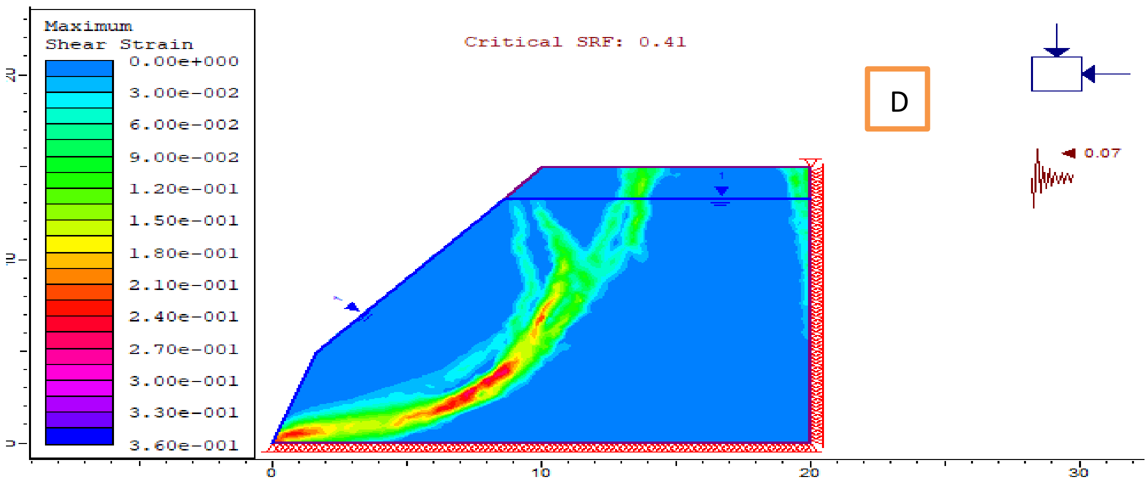

Figure 5.15 Slope stability analysis finite element method for soil slope section SS2 under

a) static dry condition, b) Dynamic dry condition, c) Static saturated condition, and d) dynamic saturated conditions.

According to the above analysis results the factor of safety a soil at slope section SS3 is 1.13 and 1.01 under static and dynamic dry conditions (Figs.5.16) respectively. This shows that soil slope section SS3 was stable in both conditions. However, the factor of safety that was determined under static saturated and dynamic saturated conditions of the soil slope section SS3 is 0.47 and 0.41 less than one respectively (Figs.5.16). This indicates that the soil at critical slope section SS3 is unstable. This demonstrating that pore water pressure has a greater effect on destabilizing these slope sections than seismic activity.

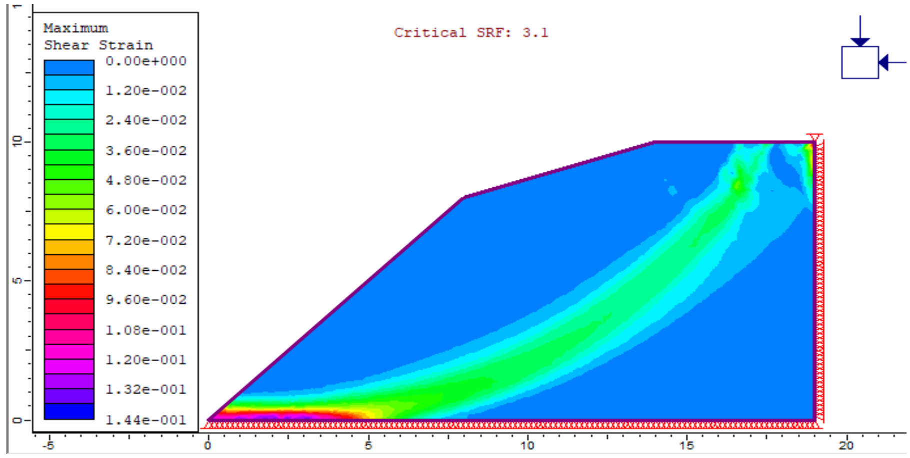
Maximum
Shear Strain
0.00e+000
1.20e-002
2.40e-002
3.60e-002
4.80e-002
6.00e-002
7.20e-002
8.40e-002
9.60e-002
1.08e-001
1.20e-001
1.32e-001
1.44e-001
Critical SRF: 3.1

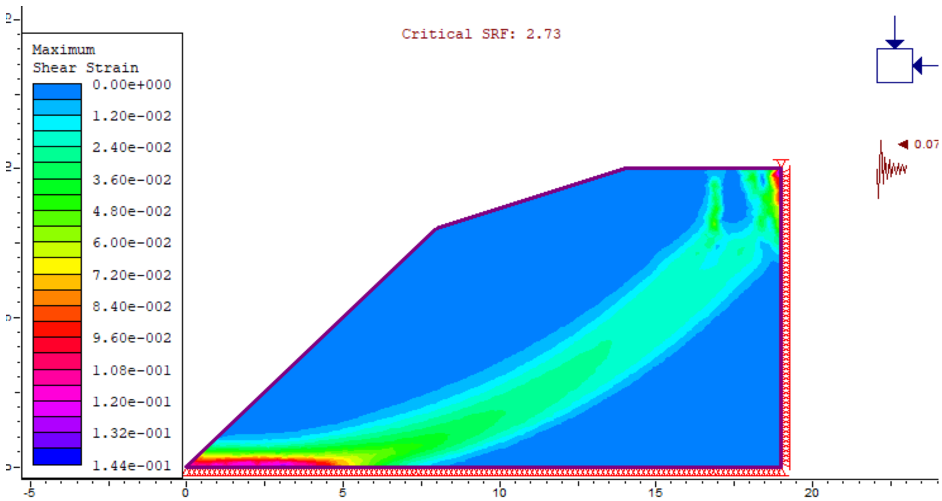
Maximum
Shear Strain
0.00e+000
1.20e-002
2.40e-002
3.60e-002
4.80e-002
6.00e-002
7.20e-002
8.40e-002
9.60e-002
1.08e-001
1.20e-001
1.32e-001
1.44e-001
Critical SRF: 2.73
0.07

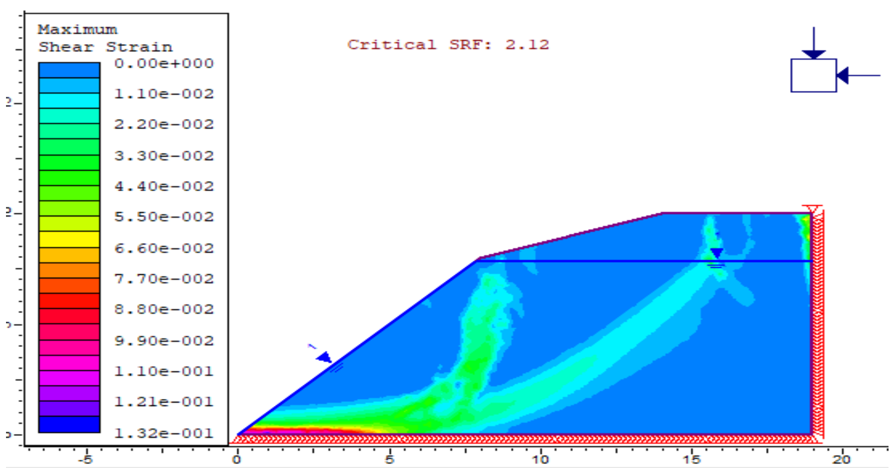
Maximum
Shear Strain
0.00e+000
1.10e-002
2.20e-002
3.30e-002
4.40e-002
5.50e-002
6.60e-002
7.70e-002
8.80e-002
9.90e-002
1.10e-001
1.21e-001
1.32e-001
Critical SRF: 2.12

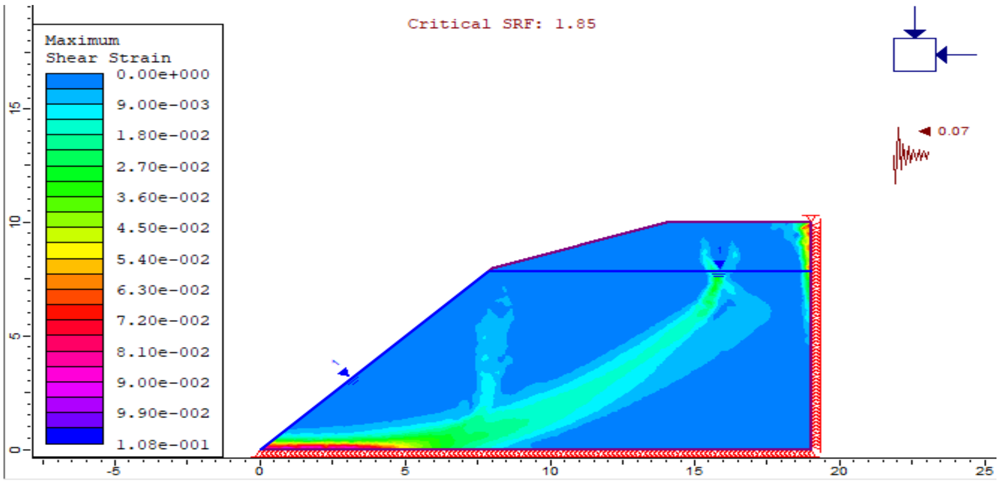

Figure 5.16 Slope stability analysis finite element method for soil slope section SS6 under a) static dry condition, b) Dynamic dry condition, c) Static saturated condition,and d) dynamic saturated conditions.

The above analysis result the minimum factors of safety or strength reduction factor determined from the FEM analyses of the soil slope section SS6 is 3.1and 2.73 for static dry and dynamic dry condition as shown in (Figs.5.16). , the strength reduction factor that was determined under static saturated and dynamic saturated conditions of the soil slope section SS6 is 2.12 and 1.85 as shown in (Figs.5.16). This indicates that the soil slope section SS2 was stable in all conditions.

5.7. Comparison of limit equilibrium method and finite element method

The analysis for different slope sections in the study area was done by limit equilibrium and finite element method. The factor of safety for the sections is close to the strength reduction factor of the same section. To compare the LEM and FEM the Moregerstorn and SRF of the slope respectively were selected for different sections. In this study, comparisons were made between the FEM strength reduction technique and factor safety the results were obtained the from limit equilibrium method (LEM) using General Limit Equilibrium methods. Accordingly, the factor of safety results computed by FEM was quite close to those computed using limit equilibrium methods. However, the factor safety obtained from LEM is slightly higher than FEM. It has been demonstrated that FEM results provide more information regarding the failure surface, such as stress, strain, deformation, and displacements, at any position along the slope section. A comparison of the results obtained from FEM and LEM modeling shows that the estimated probable failure surface is similar. Furthermore, the values of the factor of safety in both LEM and FEM decrease as the slope angle increases.

Table 5.21 Comparison of LEM with FEM for RSS1

Methods	Dry static Condition	Dry dynamic Condition	Wet static Condition	Wet dynamic Condition
FOS (LEM)	1.935	1.65	1.544	1.302
SRF (FEM)	1.81	1.65	1.41	1.28

Table 5.22 Comparison of LEM with FEM for RSS5

Methods	Dry static Condition	Dry dynamic Condition	Wet static Condition	Wet dynamic Condition
FOS (LEM)	0.408	0.354	0.04	0.004
SRF (FEM)	0.18	0.16	0.003	0.001

Table 5.23 Comparison of LEM and FEM for soil-3

Methods	Dry static Condition	Dry dynamic Condition	Wet static Condition	Wet dynamic Condition
FOS (LEM)	1.213	1.090	0.634	0.541
SRF (FEM)	1.13	1.01	0.47	0.41

Table 5.24 Comparison of LEM and FEM for soil-6

Methods	Dry static Condition	Dry dynamic Condition	Wet static Condition	Wet dynamic Condition
FOS (LEM)	3.258	2.894	2.221	1.971
SRF (FEM)	3.1	2.73	2.12	1.85

5.8. Remedial Measures

Based on the actual stability state of the slope as assessed by numerical evaluation and field inspection, effective corrective actions were suggested in this study. the four main categories of slope failure remedial treatments are: altering the slope's geometry; supplying drainage; designing retaining structures; and internal soil reinforcement. To ensure the stability of the important slope parts of the research area, it is advised to modify the slope geometry, provide drainage and engineered retaining structures, and reinforce the internal soil.

5.8.1. Modification of Slope Geometry

The slope in the study region ranges from moderately steep to very steep, which encourages slope instability since it increases tangential gravity force due to the highest value of shear stress. One of the most crucial factors affecting the slope's stability is its shape (Popescu, 2001). By lowering the slope angle and slope height as well as removing material from the research area's landslide, the slope geometry can be altered. The slope height and slope angle are important factors impacting the stability conditions of the researched slopes for this study, per the analysis results. These aspects were taken into account, and mitigation strategies to lessen their instability were proposed. Using the LEM approach and the application slide software, slope stability assessment for remedial work was carried out (Slide 6 Rocscience 2004). The slope's stability was evaluated using the factor of safety (FOS). Slide software was used to examine the recommended corrective solutions for slope modification geometry, such as the impact of slope height and slope angle (Slide 6, Rocscience, 2004).

5.8.2. Reducing of Slope Angle and Slope Height

Slope angle and height have an impact on a slope's stability because they increase shear stress while decreasing shear strength on the likely failure plane(Shiferaw, 2021). For various slope heights and slope angles, a numerical model was used to simulate the impact of these characteristics. The worst condition of the unstable rock slope section five (RSS5) was used to analyze the influence of slope angle under various circumstances. To assess the impact of slope angle on the factor of safety and slope stability, the critical slope section RSS5 was modelled at slope angles of 65, 50, and 35. To demonstrate how the slope angle affects slope stability, the value of the factor of safety was computed using slide software (Rocscience, 2004, slide 6). By lowering the slope angle from the initial condition (65) to 50 and 35, the factors of safety were computed. The outcome in Figure 5.18 demonstrates unequivocally that the factor of safety on a slope is greatly increased by a decreasing slope angle (D. Chatterjee & Murali Krishna, 2019)

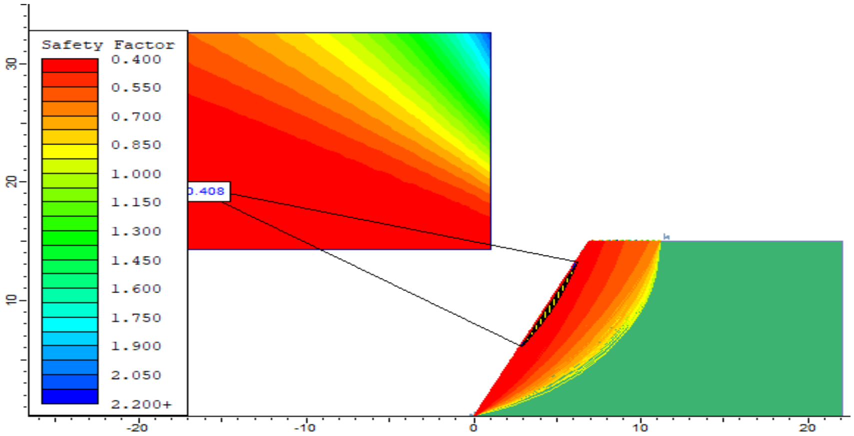

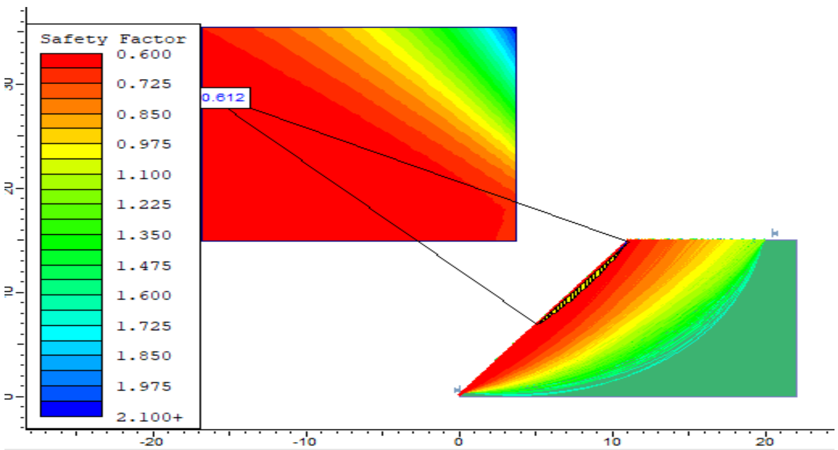

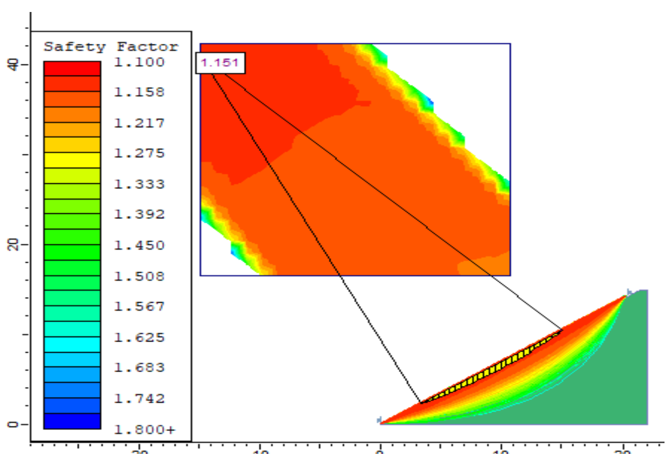

Slope angle in degree	FS
65	0.408
50	0.612
35	1.15

Figure 5.17 Effect of slope angle on factor of safety slope analysis using slide software, a) at 72º, b) at 50º and c) at 36.

By analyzing the slope at various heights, the influence of slope height was also studied. According to research, lowering the slope height at the start tends to increase the factor of safety at a lower rate (Raghuvanshi et al., 2014). On the same premise, it is understood that both slope height and slope angle lower the factor of safety slope. The slope height correlation study, as shown in the figure below, demonstrates that there is an inverse link between slope height and factor safety. Under different situations, the influence of slope height was examined using the worst conditions of unstable rock slope sections one and five (RSS1 and RSS5).The evaluation result using slide software (Rocscience,2004) was plotted and presented in Fig.5.28 below

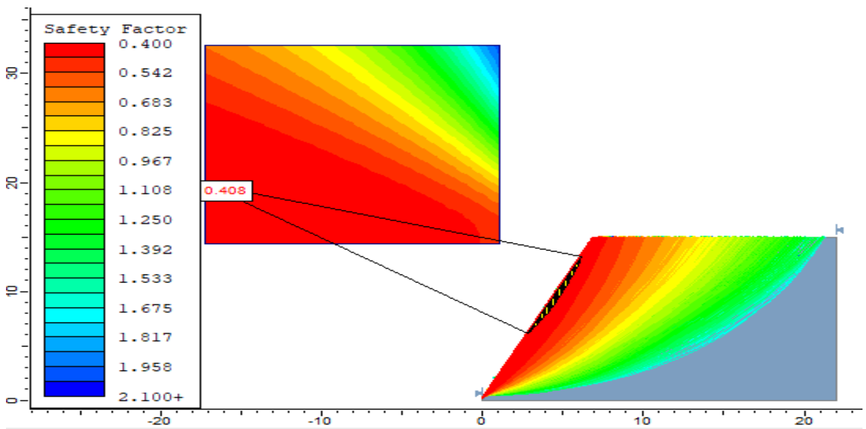

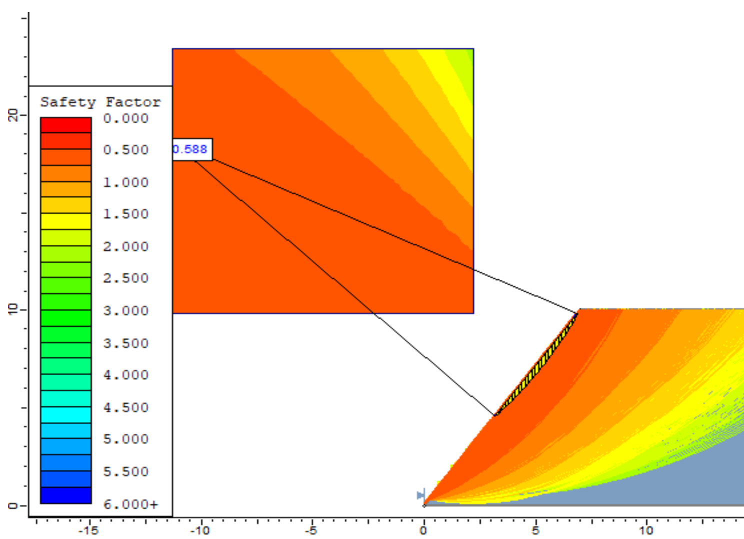

V/H Ratio	FS
0.68	0.408
0.45	0.588
0.22	1.134

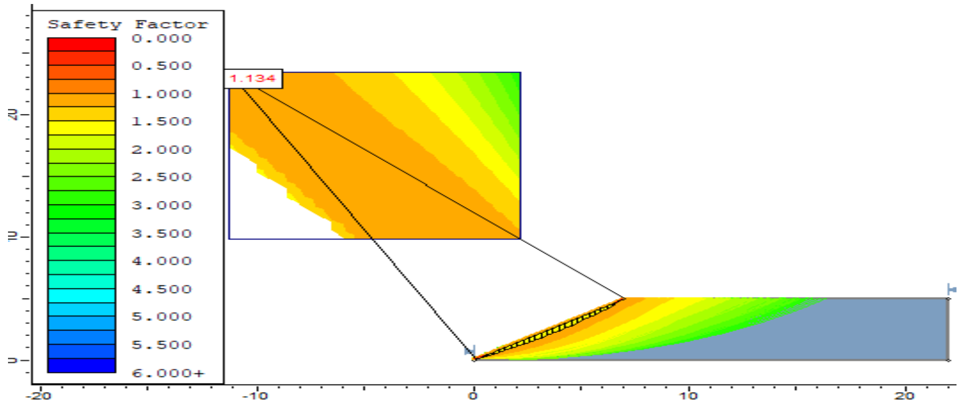

Figure 5.18 Effect of slope height on rss5 factor of safety slope stability analysis using slide software

5.8.3. Rock bolt applied to RSS3 for planar mode of failure due to JSS1 and JSS2

About 2 rock bolts with length of 3m each were applied to the unstable slope section RSS3 with planar mode failure due to JS2 at angle of 45º each , bolt capacity of 88t/m each and resultant active bolt force of 176t/m. After the rock bolts with these properties are applied to the slope section, the factor of safety has increased from 0.24 to 1.26 with the resisting force 138.86 t/m and driving force to 110.25 t/m as shown in Figure 5.20.

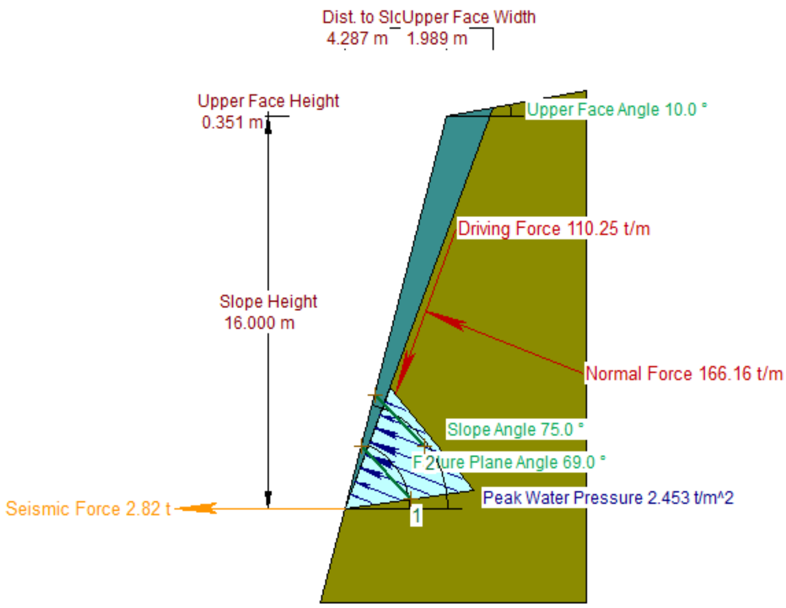

Factor of Safety	1.26
Driving Force	110.25t/m
Resisting Force	138.86t/m
Wedge Weight	40.33t/m
Wedge Volume	15.16m^3/m
Shear Strength	109.56t/m^2
Normal Force	166.16t/m
Seismic Force	2.82t
Plane Waviness	10.0°
Active Bolt Force	176.00t
Active Bolt Angle	315.0°
Passive Bolt Force	0.00t
Passive Bolt Angle	0.0°
Water Force on Failure Plane	6.44t/m

Bolt Properties:

#	Angle	Capacity	Length	AnchLength
1	45.0 °	88.00t/m	3.000 m	2.701 m
2	45.0 °	88.00t/m	3.000 m	2.451 m

Figure 5.19 A designed and installed rock bolt for JS2 of RSS2

Similarly, about 2 rock bolts with length of 4m each were applied to the unstable slope section RSS3 with planar mode failure due to JS2 at angle of 45° each , bolt capacity of 97t/m each and resultant active bolt force of 194t/m. After the rock bolts with these properties are applied to the slope section, the factor of safety has increased from 0.44 to 1.22 with the resisting force 212.42t/m and driving force to 173.60 t/m as shown in Figure 5.20.

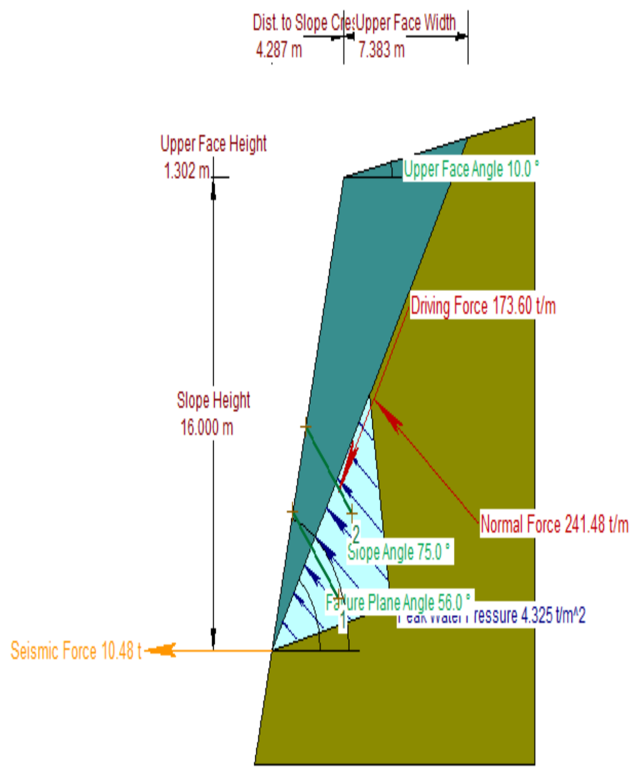

Factor of Safety	1.22
Driving Force	173.60t/m
Resisting Force	212.42t/m
Wedge Weight	149.69t/m
Wedge Volume	56.27m^3/m
Shear Strength	169.84t/m^2
Normal Force	241.48t/m
Seismic Force	10.48t
Plane Waviness	10.0°
Active Bolt Force	194.00t
Active Bolt Angle	313.0°
Passive Bolt Force	0.00t
Passive Bolt Angle	0.0°
Water Force on Failure Plane	22.57t/m

Bolt Properties:

#	Angle	Capacity	Length	AnchLength
1	47.0 °	97.00t/m	4.000 m	2.381 m
2	47.0 °	97.00t/m	4.000 m	1.390 m

Figure 5.20 A designed and installed rock bolt for JS3 of RSS2

5.8.3.1. Rock bolt applied to RSS4 for planar mode of failure due to JSS2

About 2 rock bolts with length of 3m each were applied to the unstable slope section RSS3 with planar mode failure due to Js2 at angle of 45º each , bolt capacity of 120t/m each and resultant active bolt force of 240t/m. After the rock bolts with these properties are applied to the slope section, the factor of safety has increased from 0.85 to 1.27 with the resisting force 198.79 t/m and driving force to 156.71 t/m as shown in Figure 5.20

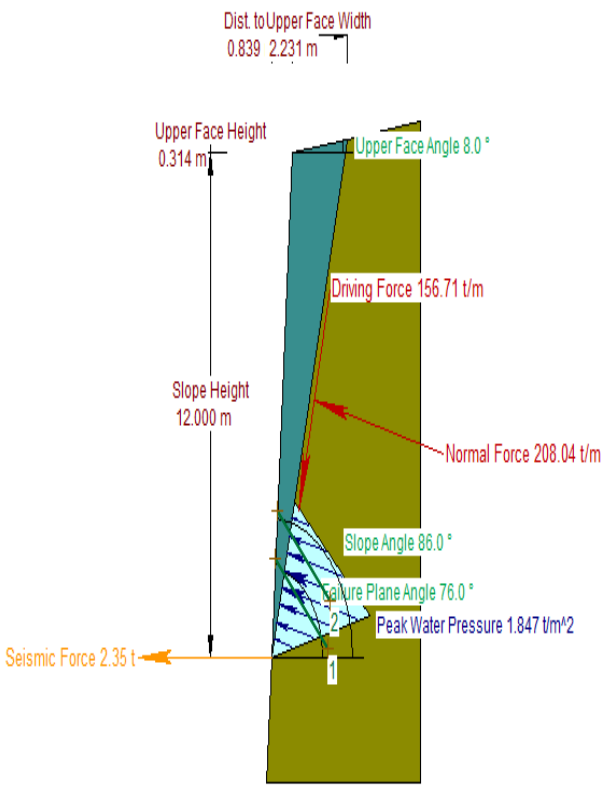

Factor of Safety	1.27
Driving Force	156.71t/m
Resisting Force	198.79t/m
Wedge Weight	33.53t/m
Wedge Volume	13.25m^3/m
Shear Strength	195.16t/m^2
Normal Force	208.04t/m
Seismic Force	2.35t
Plane Waviness	1.0°
Active Bolt Force	240.00t
Active Bolt Angle	315.0°
Passive Bolt Force	0.00t
Passive Bolt Angle	0.0°
Water Force on Failure Plane	3.52t/m

Bolt Properties:

#	*Angle*	*Capacity*	*Length*	*AnchLength*
1	45.0 °	120.00t/m	3.000 m	2.529 m
2	45.0 °	120.00t/m	3.000 m	2.297 m

Figure 5.21 A designed and installed rock bolt for JS2 of RSS4

5.8.4. Flattening Slope Angle Using 2D Slide Software

The steep slope is highly susceptible to sliding due to the gravity effect when compared with the gentle slope section. The effect of slope angle was evaluated using the worst condition of the dynamic saturated soil slope sections.

The original slope angle was modeled as (1H: 1V) and the analysis was then carried out by subsequently reducing the slope angle from (1H: 1V) to (1.5H: V), (2H: 1V) and (2.5H: 1V) by keeping the height (V) constant. This analysis was carried out using Slide 6.0 software (Slide 6.0 Rocscience, 2004) using the Morgersteren-price technique.

5.8.5. Flattening Slope Angle Using 2D Slide Software for SS3

According to the analysis shown below (fig 5.14), the factor of safety which was initially 0.54 at 50 and 75 at the top and bottom angel respectively made it unstable, with slope angles at 40 and 73 at the top and bottom angel respectively increased to 0.72 which made slope unstable,with slope angels at 32 and 68 at top and bottom angel respectively increased to 0.91 which made again slope unstable. with slope angel at 30 and 67 at top and bottom angel respectivelly increased to 1.14 which made slope stable.

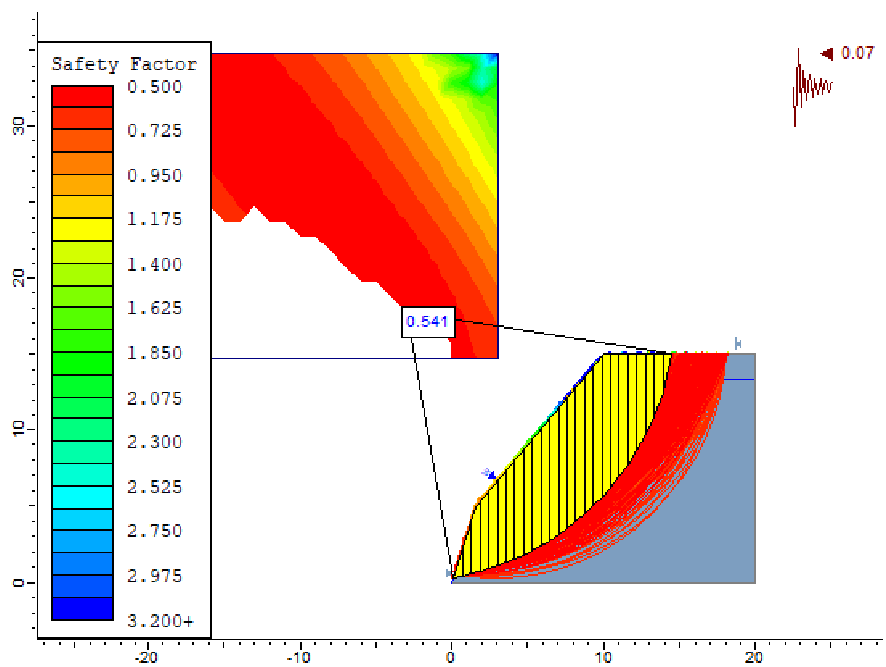

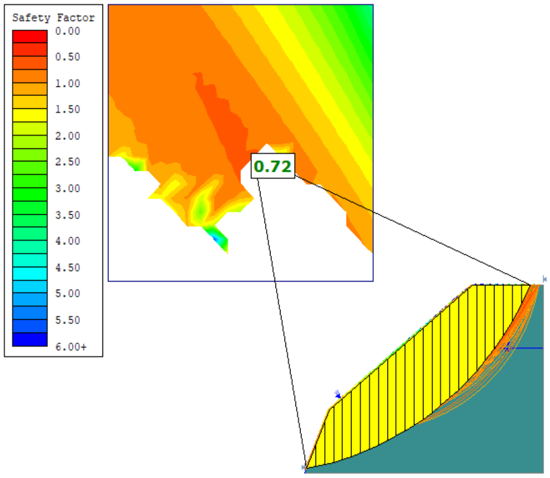
Safety Factor
0.00
0.50
1.00
1.50
2.00
2.50
3.00
3.50
4.00
4.50
5.00
5.50
6.00+
0.72


0.07

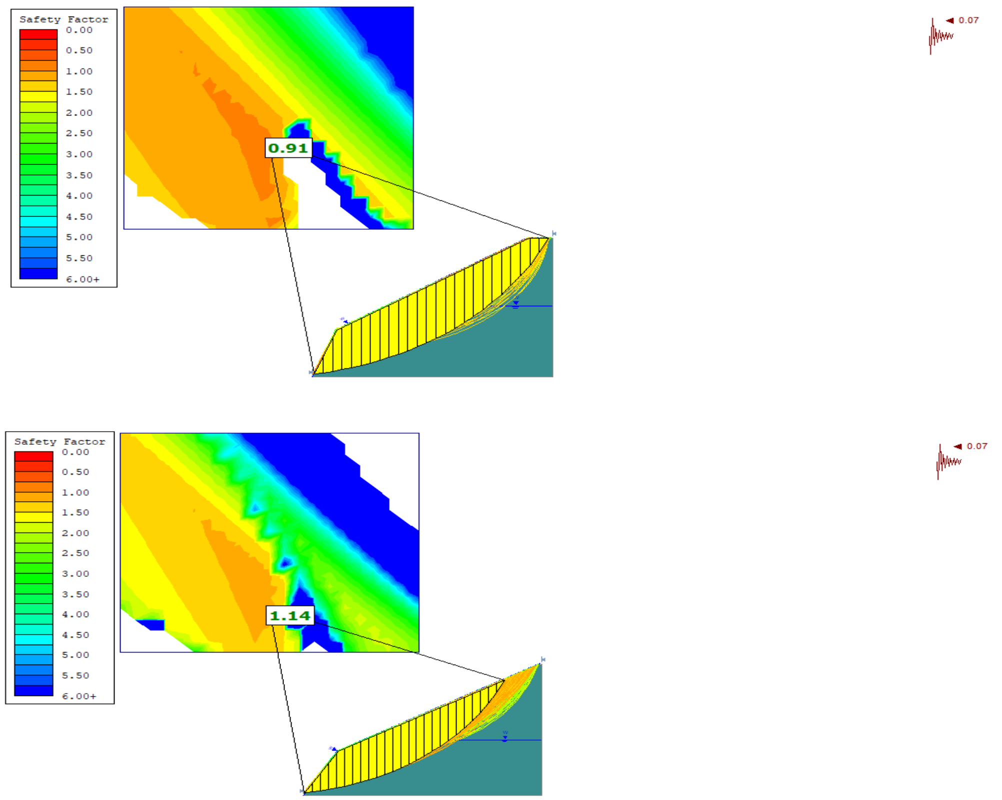

Figure 5.22 Effect of slope flattening on the factor of safety at SS3

Slope angel		Slope ratio	H/V Ratio	FOS in slide 2
Top	Tan(50)	1H:1V	1	0.54
Bottom	tan(75)			
Top	tan(40)		1.5	0.72
Bottom	Tan(73)	1.5H:1V		
Top	tan(32)	2H:1V	2	0.91
Bottom	tan(68)			
Top	Tan(30)			
Bottom	Tan (67)	2.5H:1V	2.5	1.14

5.8.6. Providing engineering Retaining Structures

Providing engineering constructions such as gabion retaining walls for slope failure regions along the Morka road segment Building gabions along one side of the slope to manage soil movement and supplying embankments along the failing slope, the size of which is determined by the gradient that provides a stable slope at selected crucial soil slope section two. Furthermore, gravity retaining walls, reinforced earth retaining structures with strip metallic reinforcement elements, rock slope face retention nets, rockfall stopping systems, and protective rock against erosion can be applied to the slope rock to reduce the likelihood of rock failure on the road.

In general, some rock slope parts in the research region are stable in the face of current and expected severe conditions. However, loose block instability was observed in some slope portions, particularly in basaltic rock strata. The removal of such rock blocks is essential as a precautionary measure. Furthermore, retention measures such as designed ditches, broad shoulders, berms, steel barriers, and nets may be placed in addition to retaining walls to prevent further rock falling or sliding, particularly on slopes in basaltic rock units.

5.8.7. Providing Drainage

Providing drainage for surface and subsurface water appears to be the most effective remedial solution for active landslide problems in order to reduce pore water pressure and subsoil saturation (Lim et al., 2017). The research site was almost on a hill, with no drainage to prevent erosion after severe rains. As a result, the unstable slope is prone to sliding. To address these concerns, providing surface drainage along the top side of the slide area from west to east and north to south, as well as controlling runoff, will lessen the continuity of the slope failure in the Morka Gircha Chencha road's selected key soil slope section.

CHAPTER SIX

6. CONCLUSION AND RECOMMENDATION

6.1. Conclusion

The project route has steep, difficult terrain; its geomorphological features reflect historic landslides, loose colluvium deposits, thick residual clay soil, and extensively worn and broken rocks caused by intense and persistent rainfall. Extensive field surveys, laboratory analysis, kinematic analysis, limit equilibrium, and finite element methods were used to locate and study the important rock and soil slope sections. Identifying modes of failure and crucial slope sections was done during the field survey, as well as in-situ measurements such as slope dip direction,Schmidt hammer rebound value on exposed rock surfaces, and collecting representative soil and rock samples. Furthermore, soil and rock samples collected from the study area were examined for strength and index qualities in the laboratory. The kinematic, deterministic, equilibrium limit, and finite element approaches were used to analyze slope stability. The limit equilibrium and finite element techniques were tested in the critical slope part of the research area under static dry, static saturated, dynamic dry, and dynamic saturated loading conditions. In general, the following findings were reached from the current study's analysis results:

- Engineering geological evaluations of field manifestations revealed that the rock masses along the road sections were moderately to badly worn and fractured, with four important rock slope parts and two key soil slope sections identified.
- The majority of the rocks along the road sections are medium- to high-strength basalt rock, according to in-situ Schmidt hammer and laboratory point load testing on representative rock samples.
- The kinematic analysis results show that one sort of failure mechanism among the discontinuities in joint sets seen in the field is planar at slope sections RSS2 and RSS4. Deterministic stability calculations for planar using Rocplane revealed that the factor of safety was less than one in all expected scenarios at RSS2 but RSS4 was stable except under dynamic saturated condition.

- The finite element and limit equilibrium stability analysis methods were used to study two key rock slope sections under changing conditions. The investigation found that RSS1 stable for all condition but RSS5 are unstable under all expected situations.
- According to gradation analyses and Atterberg limit results, the soils in the study area slope sections have a high plasticity index ranging from 24.3% to 17.2% and a high liquid limit ranging from 55.3% to 49.3%. The results of the LEM analysis of soil slope sections revealed that soil slope SS3 is stable in static dry and dynamic dry conditions, but unstable in static saturated and dynamic saturated conditions. In all conditions, the soil slope section SS6 is stable.
- A comparison of FEM and LEM utilizing findings from slide software and phase2 software revealed that LEM produces a somewhat higher FOS. Furthermore, it has been demonstrated that the finite element slope stability analysis provides more meaningful information about the failure surface, such as stress, strain, deformation, and displacement at every point in a slope section.
- In their natural condition, the overall results demonstrate that half of the proposed slope cut design ratios produced unstable results when the anticipated safety factor was used. Furthermore, the reverse analysis of all sections reveals that the main cause of instability is the slope face tilt (topography) and water-saturated slope materials that may occur during slope cut, while the natural slope is supposed to be stable.

6.2. Recommendation

The following recommendations were made based on the results and conclusions of the current study;

- Under all expected conditions, the rock at slope portions RSS2 was unstable and RSS4 was stable except under dynamic saturated condition. The slope can be stabilized and protected from future failure by installing shotcrete, rock bolts, and retaining walls with anchors to these slope section.
- Rocsciences software, such as Rocplane, Slide, and Phase2, can design and install suitable support systems, such as rock bolts, anchors, and shotcrete, to raise the safety factor and stabilize the slope.
- Further detailed geotechnical investigations, geophysical and topographic surveys should be performed to better evaluate the influence of critical factors for slope instability.
- In the future, every effort should be done to conduct this type of assessment in that mountainous area of the country where slope rock failure problems are a major concern. Additionally, other researchers use various methodologies to enhance the reliability of the current research result.

The following additional recommendation should be considered with the cut design ratio:

1. Embedding of shrubs or grass on successive horizontal levels into the cut slope (planting of locally accessible type of vegetation) for ss6.
2. Install a cascade and/or chute at an appropriate place along the cut slope, as needed for Rss2.
3. Whenever possible, provide a concrete line ditch on the cut bench in an easily erodible portion as a guide to the cascade and/or chute for rock section part.
4. Provide a paved furrow ditch at the top of the cut section to reduce erosion for Rss5.

Furthermore, for any ditches provided, ensure that surface water is appropriately collected in the ditch and does not infiltrate into the slope. Waste disposal on the roadside is a key concern while stabilizing and developing the cut parts. One of the triggering factors for the failing slopes, as we discovered during our site inspection, was improper trash disposal. As a result, waste should only be disposed of in designated areas.

The final recommendation is that all corrective procedures be carried out during the dry season to prevent the reactivation and worsening of the pavement and slope collapses.

REFERENCES

Abramson, L. W., Lee, T. S., Sharma, S., & Boyce, G. M. (2001). *Slope stability and stabilization methods*. John Wiley & Sons.

Abzalov, M., & Abzalov, M. (2016). Geotechnical Logging and Mapping. *Applied Mining Geology*, 87–95.

Addis, M. A., Barton, N. R., Bandis, S. C., & Henry, J. P. (1990). Laboratory studies on the stability of vertical and deviated boreholes. *SPE Annual Technical Conference and Exhibition*.

Alejano, L. R., Gómez-Márquez, I., & Martínez-Alegría, R. (2010). Analysis of a complex toppling-circular slope failure. *Engineering Geology*, *114*(1–2), 93–104.

Aleotti, P., & Chowdhury, R. (1999). Landslide hazard assessment: summary review and new perspectives. *Bulletin of Engineering Geology and the Environment*, *58*(1), 21–44.

Ayalew, L. (1999). The effect of seasonal rainfall on landslides in the highlands of Ethiopia. *Bulletin of Engineering Geology and the Environment*, *58*(1), 9–19.

Ayalew, L., Yamagishi, H., & Ugawa, N. (2004). Landslide susceptibility mapping using GIS-based weighted linear combination, the case in Tsugawa area of Agano River, Niigata Prefecture, Japan. *Landslides*, *1*, 73–81.

Azimian, A. (2016). A new method for improving the RQD determination of rock core in borehole. *Rock Mechanics and Rock Engineering*, *49*, 1559–1566.

Barton, N. (1973). Review of a new shear-strength criterion for rock joints. *Engineering Geology*, *7*(4), 287–332.

Barton, N. (1976). The shear strength of rock and rock joints. *International Journal of Rock Mechanics and Mining Sciences & Geomechanics Abstracts*, *13*(9), 255–279.

Barton, N., & Choubey, V. (1977). The shear strength of rock joints in theory and practice. *Rock Mechanics*, *10*, 1–54.

Bekele, A., & Meten, M. (2022). Modeling rock slope stability using kinematic, limit equilibrium and finite-element methods along Mertule Maryam–Mekane Selam road, central Ethiopia. *Modeling Earth Systems and Environment*, *0123456789*. https://doi.org/10.1007/s40808-022-01563-8

Bekele, A., & Meten, M. (2023). Modeling rock slope stability using kinematic, limit equilibrium and finite-element methods along Mertule Maryam–Mekane Selam road, central Ethiopia. *Modeling Earth Systems and Environment*, *9*(2), 1559–1585.

Beyene, B. M., & Assefa, S. M. (2022). Slope deformation analysis along a gravel road from Arib Gebaye to Mekdela-Amba woreda, Northern Ethiopia. *Modeling Earth Systems and Environment*, 1–10.

Bieniawski, Z. T. (1979). The geomechanics classification in rock engineering applications. *4th ISRM Congress*.

Bieniawski, Z. T. (1989). *Engineering rock mass classifications: a complete manual for engineers and geologists in mining, civil, and petroleum engineering*. John Wiley & Sons.

Bishop, A. W. (1955). The use of the slip circle in the stability analysis of slopes. *Geotechnique*, *5*(1), 7–17.

Broch, E., & Franklin, J. A. (1972). The point-load strength test. *International Journal of Rock Mechanics and Mining Sciences & Geomechanics Abstracts*, *9*(6), 669–676.

Chatterjee, D., & Murali Krishna, A. (2019). Effect of slope angle on the stability of a slope under rainfall infiltration. *Indian Geotechnical Journal*, *49*(6), 708–717.

Chatterjee, K., & Dey, A. (2021). Stochastic analysis of rockfall along a Himalayan slope. *Proceedings of the Indian Geotechnical Conference 2019: IGC-2019 Volume V*, 651–658.

Chen, Z., Wang, X., Haberfield, C., Yin, J.-H., & Wang, Y. (2001). A three-dimensional slope stability analysis method using the upper bound theorem: Part I: theory and methods. *International Journal of Rock Mechanics and Mining Sciences*, *38*(3), 369–378.

Cheng, Y. M., & Lau, C. K. (2014). *Soil Slope stability analysis and stabilization–new methods and insights*. Spon Press.

Chowdhury, R., & Flentje, P. (2011). *Practical reliability approach to urban slope stability*.

Çobanoğlu, İ., & Çelik, S. B. (2008). Estimation of uniaxial compressive strength from point load strength, Schmidt hardness and P-wave velocity. *Bulletin of Engineering Geology and the Environment*, *67*, 491–498.

Deere, D. U., & Deere, D. W. (1989). *Rock Quality Designation (RQD) after Twenty Years.* DEERE (DON U) CONSULTANT GAINESVILLE FL.

Dehls, J. F., Fischer, L., Böhme, M., Saintot, A., Hermanns, R. H., Oppikofer, T., Lauknes, T. R., Larsen, Y., & Blikra, L. H. (2012). Landslide monitoring in western Norway using high resolution TerraSAR-X and Radarsat-2 InSAR. *Landslides and Engineered Slopes: Protecting Society through Improved Understanding; Eberhardt, E., Froese, C., Turner, K., Leroueil, S., Eds*, 1321–1325.

Eberhardt, E., Stead, D., Coggan, J. S., & Willenberg, H. (2003). Hybrid finite-/discrete-element modelling of progressive failure in massive rock slopes. *10th ISRM Congress*.

Ermias, B., Raghuvanshi, T. K., & Abebe, B. (2017). Landslide Hazard zonation (LHZ) around Alemketema town, north Showa zone, Central Ethiopia-a GIS based expert evaluation approach. *Int J Earth Sci Eng*, *10*(1), 33–44.

Fellenius, W. (1936). Calculation of stability of earth dam. *Transactions. 2nd Congress Large Dams, Washington, DC, 1936*, *4*, 445–462.

Fredlund, D. G. (1987). Slope stability analysis incorporating the effect of soil suction. *Slope Stability*, 113–144.

Goodman, R. E. (1989). *Introduction to rock mechanics* (Vol. 2). Wiley New York.

Griffiths, D. V, & Lane, P. A. (1999). Slope stability analysis by finite elements. *Geotechnique*, *49*(3), 387–403.

Hack, R. (2002). An evaluation of slope stability classification. *ISRM International Symposium-EUROCK 2002*.

Hammah, R. E., Curran, J. H., Yacoub, T., & Corkum, B. (2004). Stability analysis of rock slopes using the finite element method. *Proceedings of the ISRM Regional Symposium*

EUROCK.

Hamza, T., & Raghuvanshi, T. K. (2017). GIS based landslide hazard evaluation and zonation–A case from Jeldu District, Central Ethiopia. *Journal of King Saud University-Science*, *29*(2), 151–165.

Hoek, E., & Bray, J. D. (1981). *Rock slope engineering*. CRC Press.

Hoek, E., Carranza-Torres, C., & Corkum, B. (2002). Hoek-Brown failure criterion-2002 edition. *Proceedings of NARMS-Tac*, *1*(1), 267–273.

International Union of Geological Sciences Working Group on Landslides, C. on L. R. (Chairman: M. P., & Popescu, M. (2001). A suggested method for reporting landslide remedial measures. *Bulletin of Engineering Geology and the Environment*, *60*, 69–74.

Jaiswal, A., Verma, A. K., & Singh, T. N. (2023). Evaluation of slope stability through rock mass classification and kinematic analysis of some major slopes along NH-1A from Ramban to Banihal, North Western Himalayas. *Journal of Rock Mechanics and Geotechnical Engineering*.

Janbu, N., Bjerrum, L., & Kjaernsli, B. (1956). *Soil mechanics applied to some engineering problems*. Norwegian Geotechnical Institute.

Kabeta, W. F., & Lemma, H. (2023). Modeling the application of steel slag in stabilizing expansive soil. *Modeling Earth Systems and Environment*, 1–8.

Kadakci Koca, T., & Koca, M. Y. (2020). Comparative analyses of finite element and limit-equilibrium methods for heavily fractured rock slopes. *Journal of Earth System Science*, *129*(1), 49.

Kazmi, D., Qasim, S., Harahap, I. S. H., Baharom, S., Mehmood, M., Siddiqui, F. I., & Imran, M. (2017). Slope remediation techniques and overview of landslide risk management. *Civil Engineering Journal*, *3*(3), 180–189.

Khanna, R., & Dubey, R. K. (2021). Comparative assessment of slope stability along road-cuts through rock slope classification systems in Kullu Himalayas, Himachal Pradesh, India. *Bulletin of Engineering Geology and the Environment*, *80*, 993–1017.

Kliche, C. A. (1999). *Rock slope stability*.

Lamessa, G., & Meten, M. (2021). Stability analysis of rock slope along selected road sections from Gutane Migiru town to Fincha sugar factory , Oromiya , Ethiopia. *SN Applied Sciences*, *3*(2), 1–16. https://doi.org/10.1007/s42452-020-04026-w

Lim, K., Li, A.-J., Schmid, A., & Lyamin, A. V. (2017). Slope-stability assessments using finite-element limit-analysis methods. *International Journal of Geomechanics*, *17*(2), 6016017.

Marinos, P., & Hoek, E. (2000). GSI: a geologically friendly tool for rock mass strength estimation. *ISRM International Symposium*.

Matthews, C., Farook, Z., & Helm, P. (2014). Slope stability analysis – limit equilibrium or the finite element method ? *Ground Engineering*, *May*, 22–28.

MISGANA, A. (2018). *ASSESSMENT AND EVALUATION OF EXISTING WATER RESOURCES DEVELOPMENT SCHEMES FOR POWER PRODUCTION: THE CASE OF MEGECH AND RIBB PROJECTS*.

Morgenstern, N. R. u, & Price, V. E. (1965). The analysis of the stability of general slip surfaces. *Geotechnique*, *15*(1), 79–93.

Nakamura, T., Ohyama, T., Waki, T., Kinuta, S., Wakabayashi, K., Takano, N., & Yatani, H. (2005). Finite element analysis of fiber-reinforced fixed partial dentures. *Dental Materials Journal*, *24*(2), 275–279.

Norrish, N. I., & Wyllie, D. C. (1996). Landslides: Investigation and Mitigation. Chapter 15-Rock slope stability analysis. *Transportation Research Board Special Report*, *247*.

Palmstrom, A. (1974). Characterization of jointing density and the quality of rock masses. *Intern. Rep. Norw. AB Berdal*, *26*(3).

Palmstrom, A. (1982). The volumetric joint count—a useful and simple measure of the degree of rock mass jointing. *International Association of Engineering Geology. International Congress*. *4*, 221–228.

Palmstrom, A. (2005). Measurements of and correlations between block size and rock quality designation (RQD). *Tunnelling and Underground Space Technology*, *20*(4), 362–377.

Pantelidis, L. (2009). Rock slope stability assessment through rock mass classification systems. *International Journal of Rock Mechanics and Mining Sciences*, *46*(2), 315–325.

Park, H., & West, T. R. (2001). Development of a probabilistic approach for rock wedge failure. *Engineering Geology*, *59*(3–4), 233–251.

Rafiei Renani, H., & Martin, C. D. (2020). Slope stability analysis using equivalent Mohr–Coulomb and Hoek–Brown criteria. *Rock Mechanics and Rock Engineering*, *53*(1), 13–21.

Raghuvanshi, T. K. (2019). Plane failure in rock slopes–A review on stability analysis techniques. *Journal of King Saud University-Science*, *31*(1), 101–109.

Raghuvanshi, T. K., Ibrahim, J., & Ayalew, D. (2014). Slope stability susceptibility evaluation parameter (SSEP) rating scheme–an approach for landslide hazard zonation. *Journal of African Earth Sciences*, *99*, 595–612.

Rahim, A., Nasae, T. M., Hareyani, Z., Ngoroyemoto, T. F. K., Hasim, I., Sapawie, M. F., & Hussin, H. (2022). Evaluation of the effect of rock joints on the stability of underground tunnels. *IOP Conference Series: Earth and Environmental Science*, *1071*(1), 12006.

ROCSCIENCE, I. N. C. (1999). Dips version 5.02. *Toronto, Canada*.

Salmanfarsi, A. F., Awang, H., & Ali, M. I. (2020). Rock mass classification for rock slope stability assessment in Malaysia: a review. *IOP Conference Series: Materials Science and Engineering*, *712*(1), 12035.

Searom, G. (2017). *Landslide hazard evaluation and zonation in and Around Hagereselam Town*. Addis Ababa University, Ethiopia.

Shiferaw, H. M. (2021). Study on the influence of slope height and angle on the factor of safety and shape of failure of slopes based on strength reduction method of analysis. *Beni-Suef University Journal of Basic and Applied Sciences*, *10*(1), 31.

Singh, T. N., & Singh, D. P. (1992). Prediction of instability of slopes in an opencast mine over old surface and underground workings. *International Journal o/Surface Mining*, *Reclamation and Environment*, *6*(2), 81–89.

Torabi, S. R., Ataei, M., & Javanshir, M. (2011). Application of Schmidt rebound number for estimating rock strength under specific geological conditions. *Journal of Mining and Environment*, *1*(2).

Ullah, S., Khanb, M. U., & Rehmana, G. A. (2020). Brief review of the slope stability analysis methods. *Geological Behavior (GBR)*, *4*(2), 73–77.

Wang, X., Cheng, T., & Gan, R. Z. (2007). Finite-element analysis of middle-ear pressure effects on static and dynamic behavior of human ear. *The Journal of the Acoustical Society of America*, *122*(2), 906–917.

Woldearegay, K. (2013). Review of the occurrences and influencing factors of landslides in the highlands of Ethiopia: With implications for infrastructural development. *Momona Ethiopian Journal of Science*, *5*(1), 3–31.

Woldegiorgis, H. (2008). Landslide hazard zonation mapping in Blue Nile Gorge. *Unpublished MSc Thesis, Addis Ababa University, Addis Ababa, Ethiopia*.

Wyllie, D. C., & Mah, C. (2004). *Rock slope engineering*. CRC Press.

Zare, M., & Jimenez, R. (2015). On the development of a slope instability index for open-pit mines using an improved systems approach. *ISRM Regional Symposium-EUROCK 2015*.

Zhang, Y., Chen, G., Wu, J., Zheng, L., & Zhuang, X. (2012). Numerical simulation of seismic slope stability analysis based on tension-shear failure mechanism. *Landslides*, *9*, 0–25.

Zhang, Y., Liu, X., Liu, X., Wang, S., & Ren, F. (2019). Numerical characterization for rock mass integrating GSI/Hoek-Brown system and synthetic rock mass method. *Journal of Structural Geology*, *126*, 318–329.

APPENDINCES

Soil property determination

Appendix A: Natural moisture content determination of test pit-6 and test pit-3 Natural water content is determined from laboratory tests. Natural soil is put in the oven and the dry sample is measured and water content is the mass of water to the ratio of the mass of soil. it is expressed in percentages.

Sample Number:	AM SS-6		
Moisture can and lid number	C-9	B-3	D-5
MC = Mass of empty, clean can + lid (grams)	24.1	24.2	24
MCMS = Mass of can, lid, and moist soil (grams)	98.3	83.7	89.2
MCDS = Mass of can, lid, and dry soil (grams)	80.7	69.8	73.8
MS = Mass of soil solids (grams)	56.6	45.6	49.8
MW = Mass of pore water (grams)	17.6	13.9	15.4
w = Water content, w%	31.0954	30.4825	30.9237
Average W%	30.83		

Sample Number:	AM SS-3		
Moisture can and lid number	D-9	D-10	C-4
MC = Mass of empty, clean can + lid (grams)	24.4	24.2	24
MCMS = Mass of can, lid, and moist soil (grams)	76.2	73.6	75.5
MCDS = Mass of can, lid, and dry soil (grams)	62.6	60.7	62
MS = Mass of soil solids (grams)	38.2	36.5	38
MW = Mass of pore water (grams)	13.6	12.9	13.5
w = Water content, w%	35.6021	35.3425	35.5263
Average W(%)	35.49		

Appendix B: Specific gravity determination test pit-6 and test pit-3

The specific gravity of soil was determined from the weight of soil to the weight of water using the density bottle procedure.

Specific Gravity for AM SS-6		
Sample Number	A	B
Pycnometer #	1	2
C. Mass of Dry Soil (No. 10 sieve)	50	50
D. Mass of Pycnometer full of water	344.6	340.9

E. Mass of pycno + Soil +full of water (Distil)	376.4	372.7
T⁰c	26	26
T⁰c correction	0.9968	0.9968
F. Specific Gravity=C/(C+(D-E))	2.74	2.74
Average Specific Gravity ((1+2)/2)	2.74	

Specific Gravity for AM SS-3		
Sample Number	C	D
Pycnometer #	1	2
C. Mass of Dry Soil (No. 10 sieve)	50	50
D. Mass of Pycnometer full of water	344.6	340.9
E. Mass of pycno + Soil +full of water (Distil)	376.7	373.2
T⁰c	26	26
T⁰c correction	0.9968	0.9968
F. Specific Gravity=C/(C+(D-E))	2.78	2.82
Average Specific Gravity ((1+2)/2)	2.80	

Appendix C: Atterberg limit test results at SS3 and SS6

Liquid Limit					
Sample Number:	AM SS-3				
Moisture can and lid number		A-2	A17	B-5	A11
Number of Drops (N)		18	20	24	27
MC = Mass of empty, clean can + lid (grams)		24	24.1	23.9	23.6
MCMS = Mass of can, lid, and moist soil (grams)		58.7	54.5	53.6	55.6
MCDS = Mass of can, lid, and dry soil (grams)		46.1	43.4	43	44.3
MS = Mass of soil solids (grams)		22.1	19.3	19.1	20.7
MW = Mass of pore water (grams)		12.6	11.1	10.6	11.3
w = Water content, w%		57.01357	57.51295	55.49738	54.58937

Plastic Limit Test				
Sample Number:	AM SS-3			
Moisture can and lid number		C-3	E-22	E-7
MC = Mass of empty, clean can + lid (grams)		13.1	13	24.5
MCMS = Mass of can, lid, and moist soil (grams)		17.3	18.6	29.1
MCDS = Mass of can, lid, and dry soil (grams)		16.3	17.3	28

MS = Mass of soil solids (grams)	3.2	4.3	3.5
MW = Mass of pore water (grams)	1	1.3	1.1
w = Water content, w%	31.25	30.23256	31.42857
Average Moisture Content w%	30.97		

Liquid Limit				
Sample Number: AM SS-6				
Moisture can and lid number	C-2	D-1	A13	C-3
Number of Drops (N)	19	23	28	33
MC = Mass of empty, clean can + lid (grams)	24.2	23.9	23.4	24.1
MCMS = Mass of can, lid, and moist soil (grams)	59	54	60	57.7
MCDS = Mass of can, lid, and dry soil (grams)	47.3	44	48	46.9
MS = Mass of soil solids (grams)	23.1	20.1	24.6	22.8
MW = Mass of pore water (grams)	11.7	10	12	10.8
w = Water content, w%	50.649351	49.75124	48.78049	47.36842

Plastic Limit Test			
Sample Number: AM SS-6			
Moisture can and lid number	A-7	C-1	E-7

MC = Mass of empty, clean can + lid (grams)	13	24	24
MCMS = Mass of can, lid, and moist soil (grams)	18.3	28.5	28.6
MCDS = Mass of can, lid, and dry soil (grams)	17	27.4	27.5
MS = Mass of soil solids (grams)	4	3.4	3.5
MW = Mass of pore water (grams)	1.3	1.1	1.1
w = Water content, w%	32.5	32.35294	31.42857
Average Moisture Content w%	32.09		

Appendix D: Soil Particle Size Analysis Result.

	Test pit Location SS3		Test pit Location SS6	
Sieve No.	Opening (mm)	% Passing	Opening (mm)	% Passing
4	4.75	99.7	4.75	95.4
10	2.36	98.5	2.36	95.0
16	2	98.1	2	95.0
20	1.18	96.4	1.18	94.6
40	0.6	94.5	0.6	93.9
60	0.425	93.3	0.425	93.2
100	0.3	92.2	0.3	92.1
200	0.15	89.8	0.15	87.8
	0.075	87.9	0.075	85.5
	-------	87.8	-------	85.5

Appendix E Compaction test data and result

Compaction test Raw data for test pit-3 and test pit-6

Sample No.	AM SS-3				
Moisture content Vs dry density computation table					
Determination No.	1	2	3	4	5
Mass of Mold, g	4321.1	4321.1	4321.1	4321.1	4321.1
Mass of mold + Compacted Soil, g	5430.4	5707.2	5964.2	6024	5852
Mass of Compacted soil, g	1109.3	1386.1	1643.1	1702.9	1530.9
Volume of Mold, cm3	943	944	944	944	944
Bulk density, g/cm3	1.18	1.47	1.74	1.80	1.62
Water Contenet, %	8.08	15.43	23.82	35.96	47.11
Dry density, g/cm3	1.09	1.27	1.41	1.33	1.10
TR	1	2	3	4	5
Conatainer No	B-10	W-2	C-6	D-4	B-9
Mass of container, g	23.5	24.3	24.2	23.7	24.2
Mass of container + wet soil, g	55.6	64.7	71.5	82.3	57.3
Mass of ontainer + Dry soil, g	53.2	59.3	62.4	66.8	46.9
Mass of Water, g	2.4	5.4	9.1	15.5	10.4
Mass of Dry soil, g	29.7	35	38.2	43.1	22.7
Water content, %	8.08	15.43	23.82	35.96	45.81

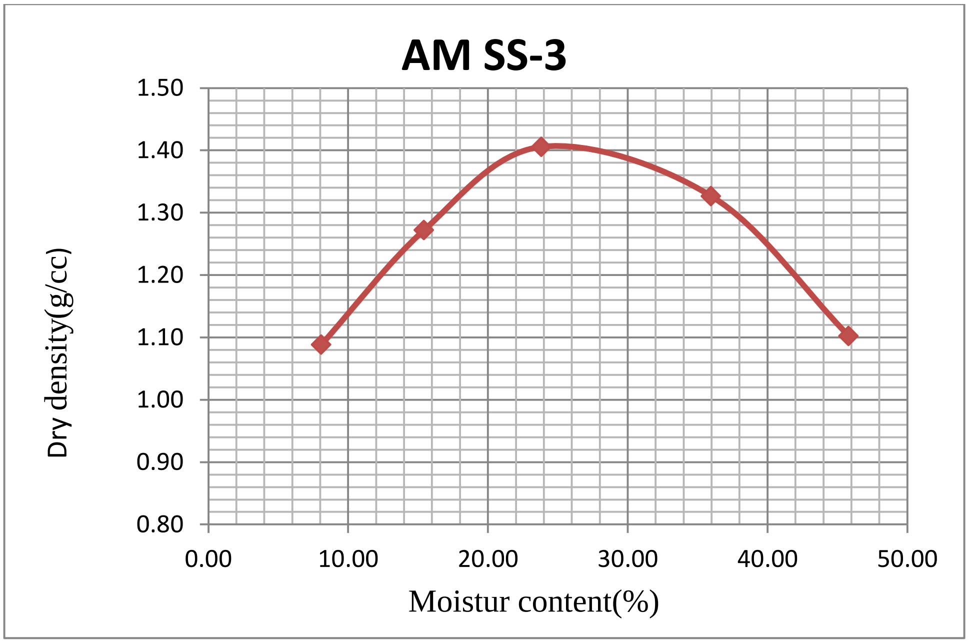

Compaction test Raw data for test pit-6

Sample No.	AM SS-6				
Moisture content Vs dry density computation table					
Determination No.	1	2	3	4	5
Mass of Mold, g	4321.1	4321.1	4321.1	4321.1	4321.1
Mass of mold + Compacted Soil, g	5492.4	5810	6020.3	6009.6	5812.5
Mass of Compacted soil, g	1171.3	1488.9	1699.2	1688.5	1491.4
Volume of Mold, cm3	943	944	944	944	944
Bulk density, g/cm3	1.24	1.58	1.80	1.79	1.58
Water Contenet, %	8.22	17.99	26.29	36.64	45.30

Dry density, g/cm3	1.15	1.34	1.43	1.31	1.09

TR	1	2	3	4	5
Conatainer No	C-5	C-1	C-1	D-8	B-7
Mass of container, g	24.2	23.7	24	23.6	24
Mass of container + wet soil, g	71.6	57.8	77.8	96.7	67.3
Mass of ontainer + Dry soil, g	67.9	52.6	66.6	77.1	53.8
Mass of Water, g	3.7	5.2	11.2	19.6	13.5
Mass of Dry soil, g	43.7	28.9	42.6	53.5	29.8
Water content, %	8.47	17.99	26.29	36.64	45.30

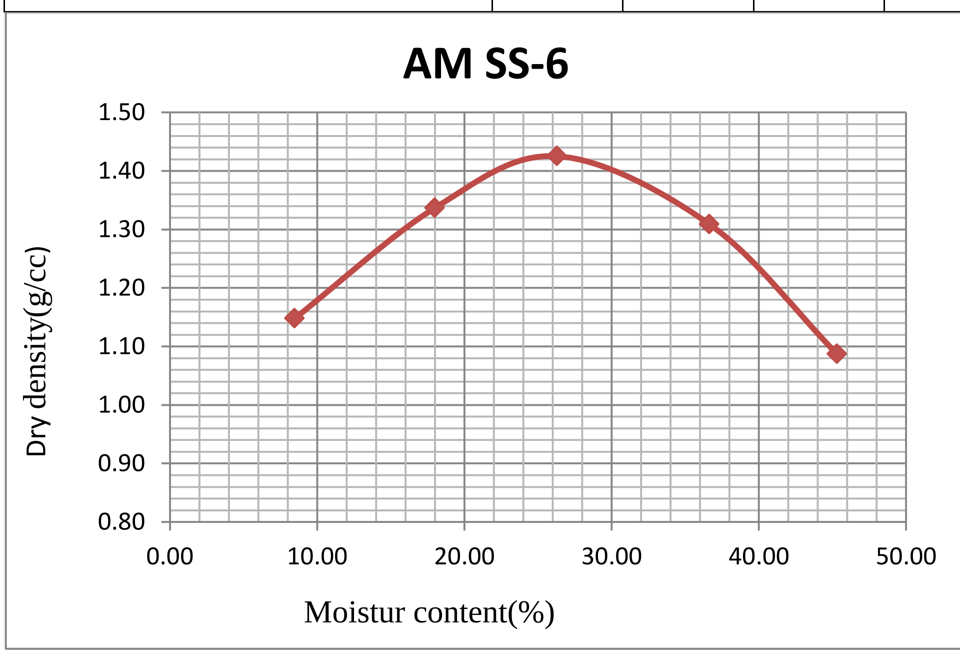

Appendix G Raw data and results for direct shear test for test pit -3 and for test pit -6

Direct shear test for test pit -3

Normal Stress kPa	Shear Stress kPa
100	42.1113448
200	67.032
300	83.23834709
Paramters	
C	23.00
ϕ	11.61

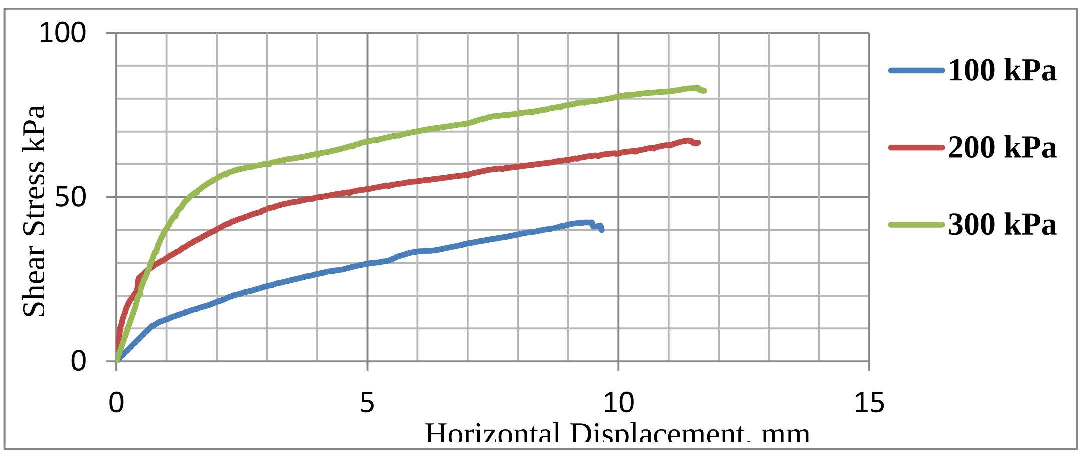

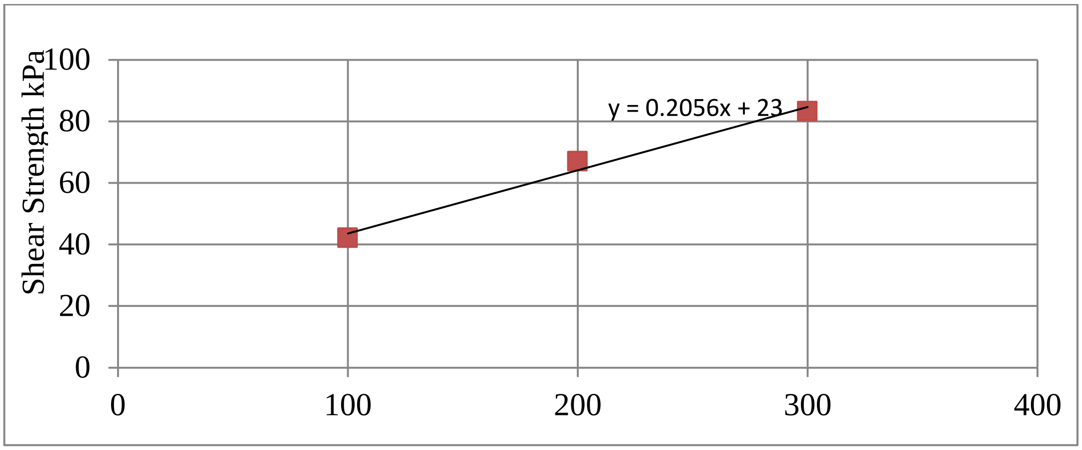

Direct shear test pit -6

Normal Stress kPa	Shear Stress kPa
100	38.95494306
200	57.61816
300	70.70632
Parameters	
C	24.0
ϕ	9.02

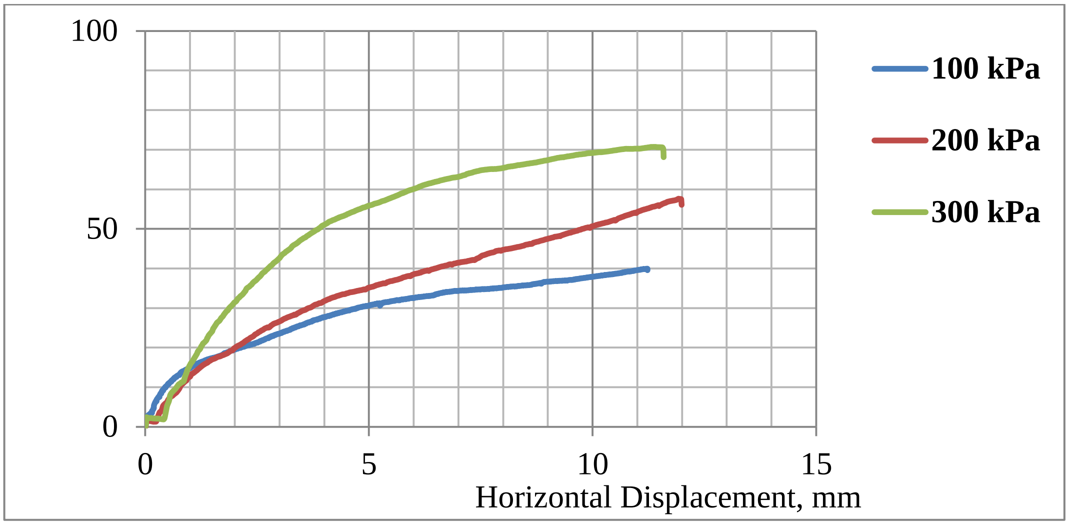
100
50
0
0
5
10
15
Horizontal Displacement, mm
100 kPa
200 kPa
300 kPa

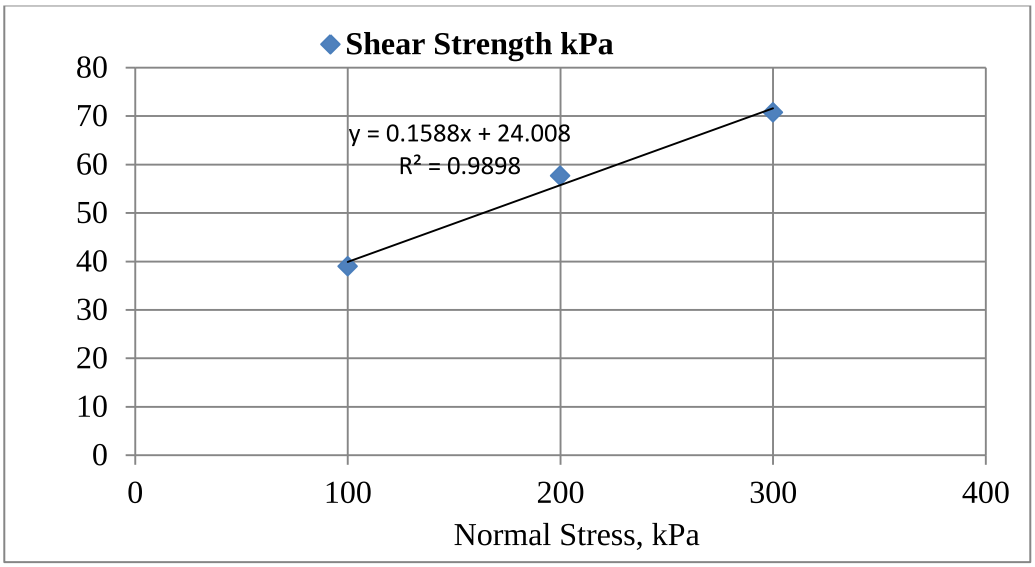
Shear Strength kPa
80
70
60
50
40
30
20
10
0
y = 0.1588x + 24.008
R² = 0.9898
0
100
200
300
400
Normal Stress, kPa

Rock material characterization

Appendix H: Raw data point load test

TEST RESULT OF POINT LOAD TEST											
Sample ID (BH)	Depth [m]	W1, mm	W2, mm	D, mm	A, mm2	De, cm	Q, Mpa	P, kN	Is, Mpa	Is(50), Mpa	UCS, Mpa
SS-4(1)	-	88	64	69	5240	81.7	25.0 0	2405 0	3.60	4.49	
SS-4(2)	-	75	55	61	3960. 5	71.1	25.0 0	2405 0	4.76	5.57	146.16
SS-4(3)	-	79	58	50	3420. 5	66	20.0 0	1924 0	4.41	4.99	
SS-4(4)	-	89	53	23	1630. 3	45.6	21.0 0	2020 0	9.71	9.31	
sS-2(1)		74. 3	87. 9	48	2650	76.7 3	25.0 0	1500 0	2.54	3.07	76.08
ss-(2)		92. 2	85. 5	56. 4	3210	73.8 2	20.0 0	1500 0	2.75	3.27	
SS-5(1)	-	82	54	63	4280. 4	73.9	20.0 0	1924 0	3.53	4.21	
SS-5(2)	-	77	51	54	3450. 6	66.3	15.0 0	1443 0	3.28	3.72	
SS-5(3)	-	61	48	52	2830. 4	60.1	10.0 0	9620	2.67	2.90	

SS-5(4)	-	70	60	39	2530.5	56.8	15.00	14430	4.47	4.73	93.36
SS-1(1)	-	69	57	65	4090.5	72.2	20.00	19240	3.69	4.35	
SS-1(2)	-	68	50	28	1650.2	45.9	30.00	28860	13.72	13.2	
SS-1(3)	-	59	44	28	1440.2	42.8	25.00	24050	13.12	12.23	
SS-1(4)	-	65	36	54	2720.7	58.9	20.00	19240	5.54	5.96	114.44

Appendix I: Dry density determination

Sample id	Slope section rock	M(g)	V1(ml)	V2(ml)	V2-V1(ml)	P=M/V g/cm	=p*g kn/m	Average of dry density
S101	RSS1	357.3	600	730	130	2.75	26.9	27.81
S102		215.9	600	675	75	2.9	28.42	
S103		198.1	070	670	70	2.83	27.73	
S104		304.7	465	570	105	2.90	28.42	
S409	RSS4	209.8	562	650	88	2.38	23.32	23.19
S410		193.0	560	650	90	2.14	20.97	
S411		227.2	600	700	100	2.27	22.25	
S412		361.8	500	635	135	2.68	26.25	
S501	RSS5	303.9	600	700	100	3.1	30.38	28.54
S502		358.2	600	725	125	2.86	28.02	
S503		234.1	500	580	80	2.92	28.16	
S504		208.7	626	700	74	2.82	27.63	
S201	RSS2	189.3	500	595	95	1.987	19.492	21.3
S201		271.9	500	615	115	2.35	23.10	

Appendix J: Saturated density determination

Sample id	Slope section rock	M(g)	V1(ml)	V2(ml)	V2-V1(ml)	P=M/V g/cm	=p*g kn/m	Average of saturated density
S101	RSS1	360.5	500	625	125	2.88	28.2	28.9
S102		220.2	500	575	75	2.93	28.71	
S103		203.7	600	670	70	2.91	28.51	
S104		309.7	460	570	100	3.09	30.28	
S409	RSS2	213.7	565	650	85	2.51	24.59	24.83
S410		197.1	470	550	80	2.46	24.10	
S411		232.2	605	700	95	2.44	23.91	
S412		355.2	520	650	130	2.73	26.75	
S501	RSS5	307.6	585	685	100	3.07	30.08	28.78
S502		360.2	600	720	120	3.00	29.4	
S503		240.3	400	480	80	3.00	29.4	
S504		212.5	621	700	79	2.68	26.26	
S201	RSS2	227.1	600	680	80	2.48	24.34	26.14
S202		285	700	800	100	2.85	27.95	

Appendix K: Classification of UCS of rock according to Deere and Miller (1966).

Unconfined compressive strength (UCS) (MPa)	Description of strength
Over 224	Very High strength
116-224	High strength
56-112	Medium strength
28-56	Low strength
Less than 28	Very low strength

Appendix L : Geological strength index (GSI) Values estimated in the field based on the weathering condition of discontinuity surface, rock mass structure and interlocking of rock blocks in successive site visit as proposed by chart for GSI, Hoek and Marinos, 2000.

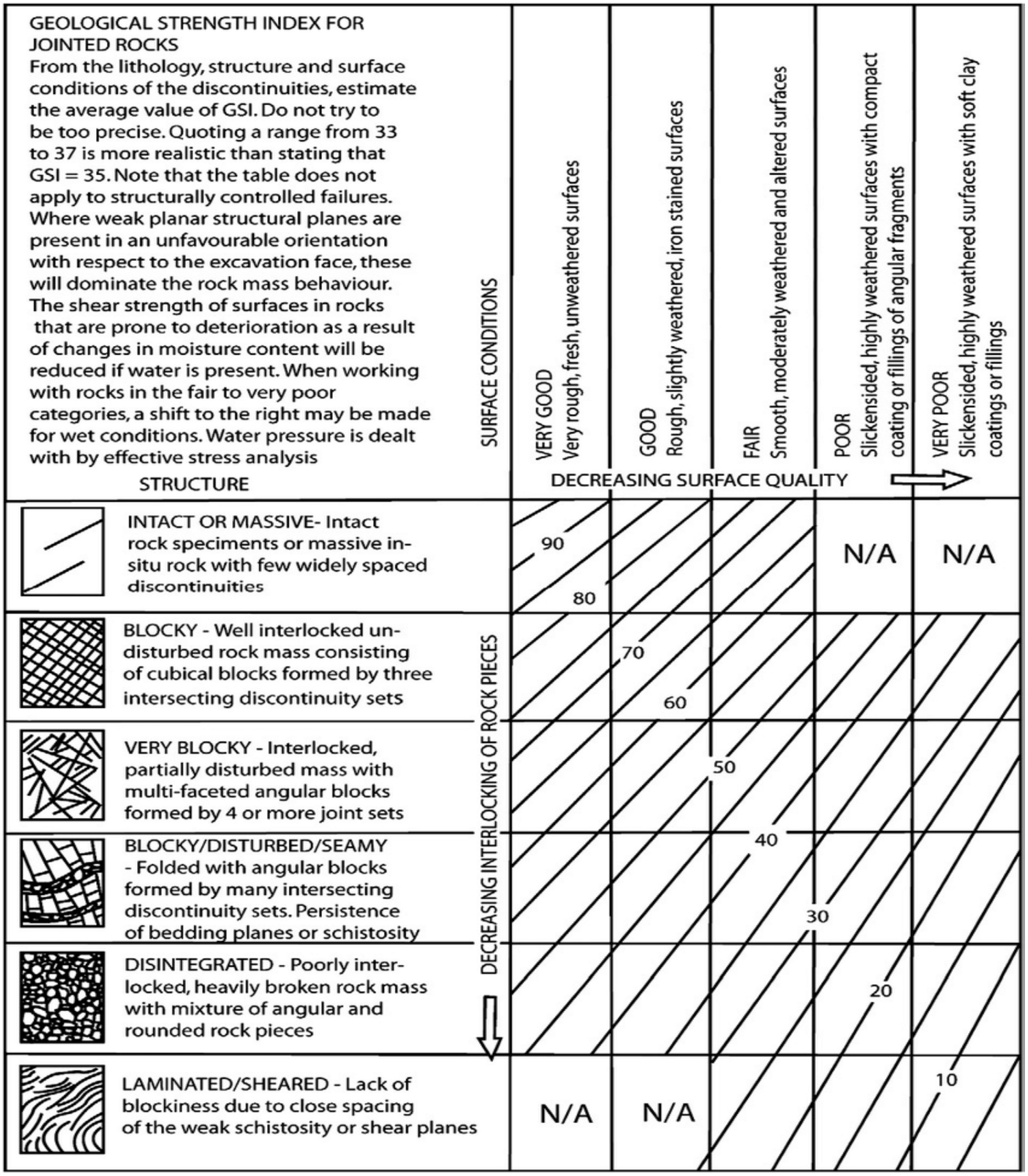

Appendix M: Plasticity Chart Das, (2002)

Plasticity index (PI)	Descriptions
0	Non plasticity
1-5	slightly plasticity
5-10	low plasticity
10-20	Medium plasticity
20-40	High plasticity
>40	Very high plasticity

Appendix N: Classification of UCS of rock according to Deere and Miller (1966).

Unconfined compressive strength (UCS) (MPa)	Descriptions
Over 224	Very High strength
112-224	High strength
56-112	Medium strength
28-56	Low strength
Less than 28	Very low strength

Appendix O: Estimated shear strength parameters of rock mass using RocData software for the critical slope sections of rocks

SS1

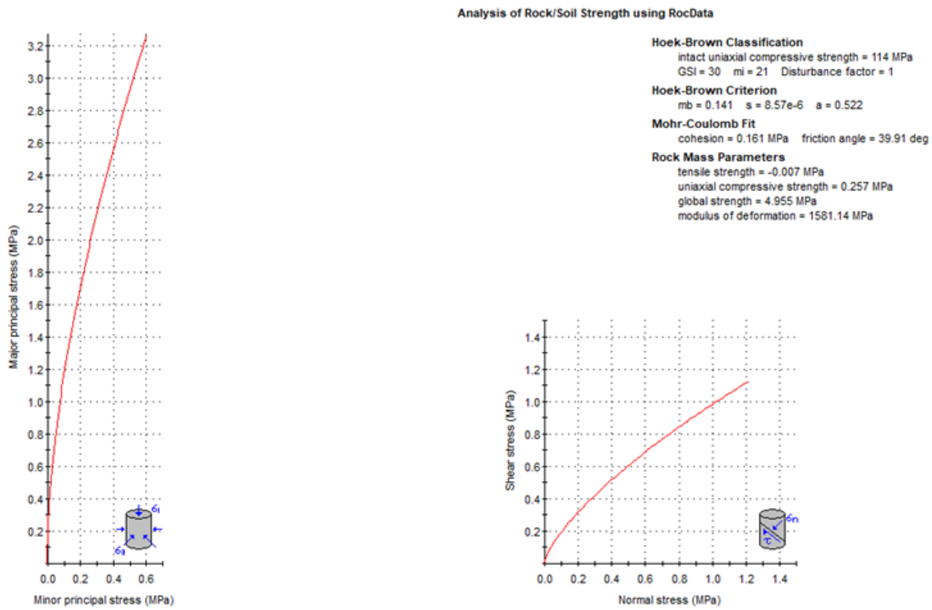

SS5

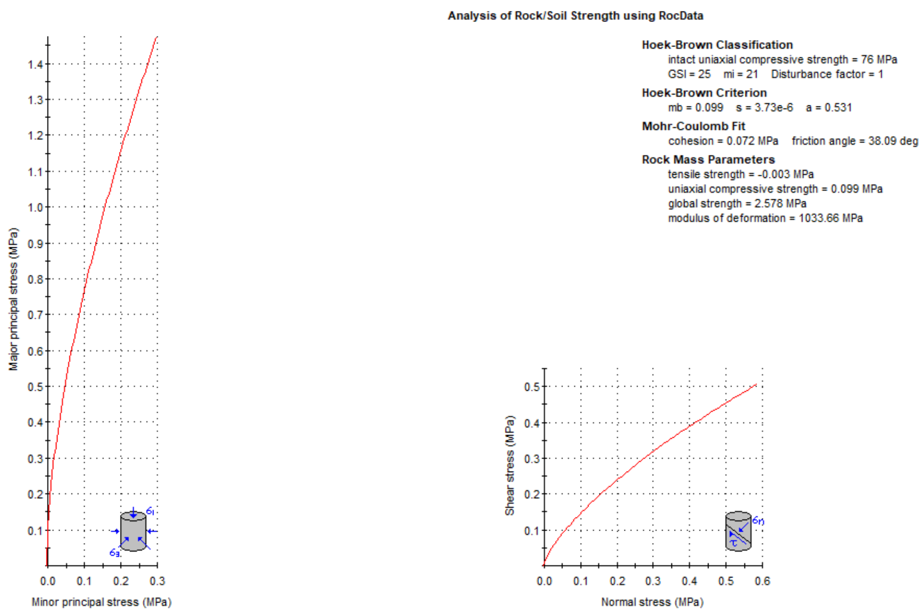

Appendix P: The evaluated shear strength parameters critical failure planes (joints) using Barton Bandis

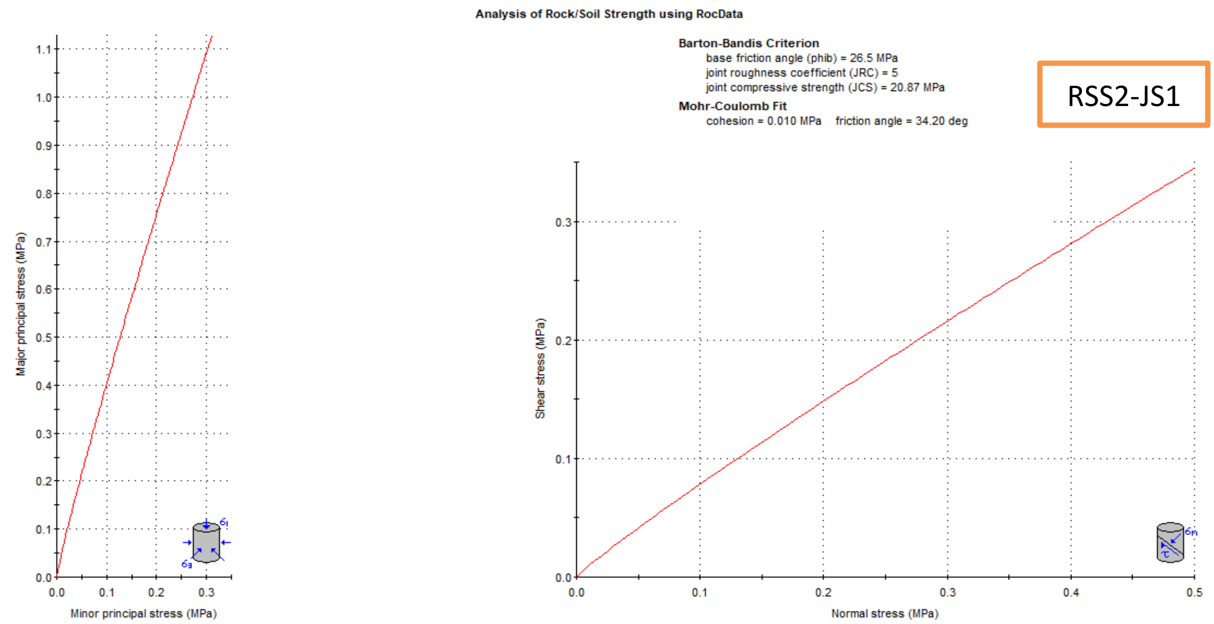

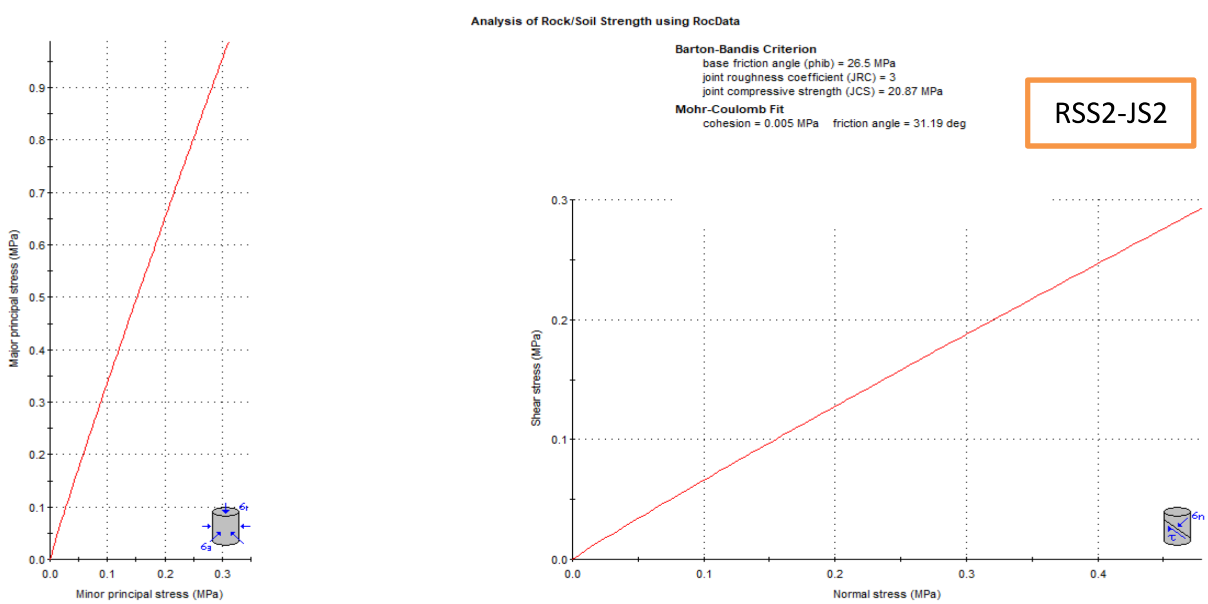

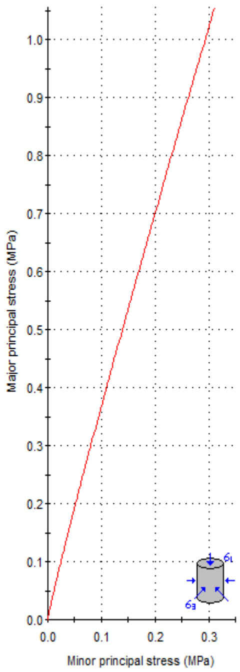
Major principal stress (MPa)
Minor principal stress (MPa)
0.0
0.1
0.2
0.3
0.4
0.5
0.6
0.7
0.8
0.9
1.0

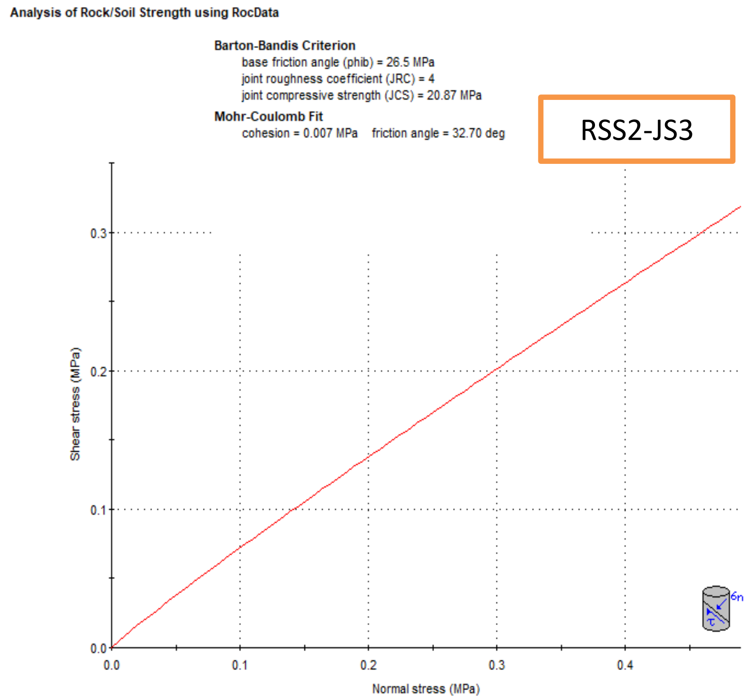
Analysis of Rock/Soil Strength using RocData
Barton-Bandis Criterion
base friction angle (phib) = 26.5 MPa
joint roughness coefficient (JRC) = 4
joint compressive strength (JCS) = 20.87 MPa
Mohr-Coulomb Fit
cohesion = 0.007 MPa friction angle = 32.70 deg
RSS2-JS3
Shear stress (MPa)
Normal stress (MPa)
0.0
0.1
0.2
0.3
0.4

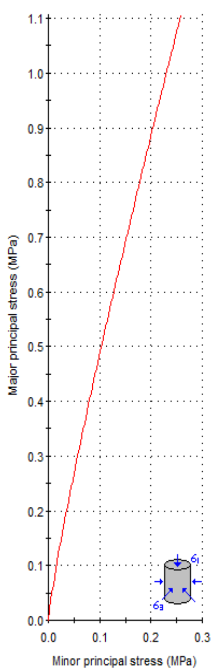
Major principal stress (MPa)
Minor principal stress (MPa)
0.0
0.1
0.2
0.3
0.4
0.5
0.6
0.7
0.8
0.9
1.0
1.1

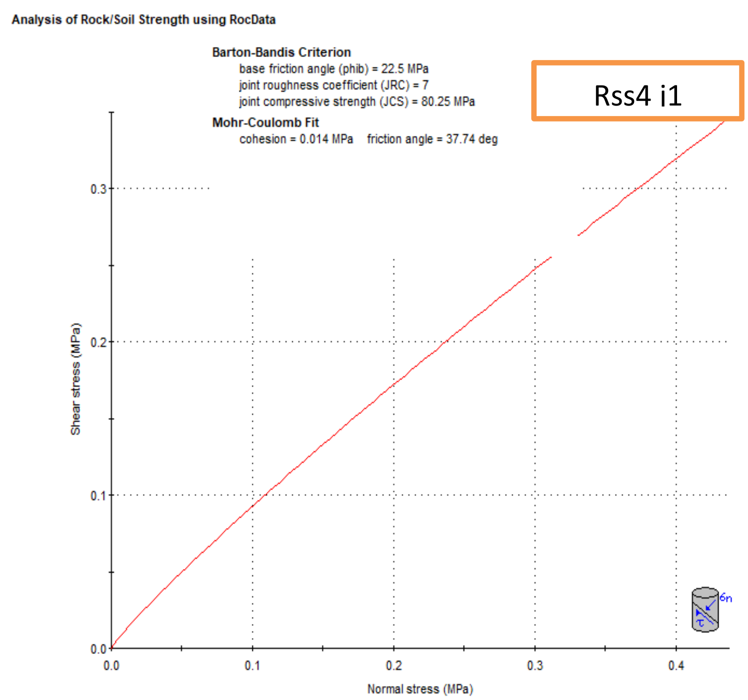
Analysis of Rock/Soil Strength using RocData
Barton-Bandis Criterion
base friction angle (phib) = 22.5 MPa
joint roughness coefficient (JRC) = 7
joint compressive strength (JCS) = 80.25 MPa
Mohr-Coulomb Fit
cohesion = 0.014 MPa friction angle = 37.74 deg
Rss4 j1
Shear stress (MPa)
Normal stress (MPa)
0.0
0.1
0.2
0.3
0.4

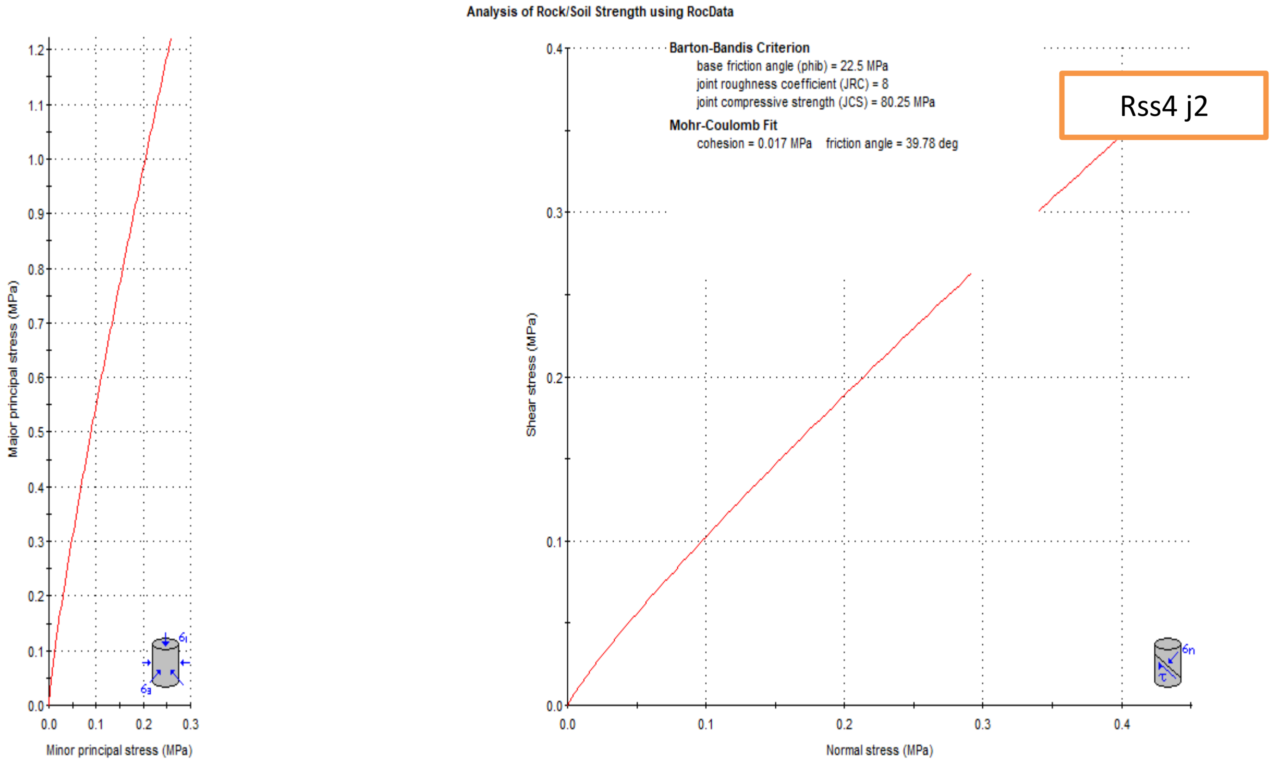
Analysis of Rock/Soil Strength using RocData
Barton-Bandis Criterion
base friction angle (phib) = 22.5 MPa
joint roughness coefficient (JRC) = 8
joint compressive strength (JCS) = 80.25 MPa
Mohr-Coulomb Fit
cohesion = 0.017 MPa friction angle = 39.78 deg
Rss4 j2
Major principal stress (MPa)
Minor principal stress (MPa)
Shear stress (MPa)
Normal stress (MPa)

Appendix Q: Precipitation data of Morka-Gircha-Chencha during 9 years (2012-2021)

NAME	ELEVATIO	Element	YEAR	Jan	Feb	Mar	Apr	May	Jun	Jul	Aug	Sep	Oct	Nov	Dec
Chencha	2632	PRECIP	2012	1.2	5	45									
Chencha	2631	TMPAVG	2016		15.1	15.2	15.2	15.4	15.1	15.2	15.1		15.6	14.9	14.8
Chencha	2631	TMPAVG	2014	15.3	15.4		15.6	15.4	15.4	15.9	16.1	15.6	15.7	15.7	15.8
Chencha	2631	TMPAVG	2015		16.9	15.6	15.1	14.9	14.6	14.5	14.1	14.2	15.1	15.3	14.8
Chencha	2631	TMPAVG	2012										14.7		
Chencha	2631	TMPAVG	2013								15.5	15.7	15.3	15.7	15.4
Chencha	2631	PRECIP	2021		8	16	42.2	78.8	3.2	74			18.2		
Chencha	2631	PRECIP	2012										114.4		
Chencha	2631	PRECIP	2013								88	97.4	252.6	97.4	0
Chencha	2631	PRECIP	2014	5.8	52.6		81.6	304.8	105.9	29.4	127.2	162.8	276.8	103	4
Chencha	2631	PRECIP	2015		3.4	54.8	151.6	247.2	88.2	72.2	12.6	42.2	112.8	138	55.6
Chencha	2631	PRECIP	2016		13.6	44.4	187.2	122.6	102.8	100.6	48	81.6	189.6	36.3	23.6
Chencha	2631	PRECIP	2017		44.4		97.6	242	24.8	47.4	150.4	79.4	74.4	29.2	0
Chencha	2631	PRECIP	2018	0	46.4	48.6		97	33.2	45.8	33.2	26.3	38	30.6	14.4
Chencha	2631	PRECIP	2019	0		7.2	48.8	126.8	202.1	118.2		50.8	59		44.4
Chencha	2631	PRECIP	2020	43	12.6	16.2	53.4	49	31.8	84.4	57.7	45.7	53.2	6	
Chencha	2631	TMPMAX	2012										20.3		
Chencha	2631	TMPMAX	2013								22.1	21.2	21.3	21.4	20.8
Chencha	2631	TMPMAX	2014	20.5	20.8		21.2	20.8	20.6	21.5	21.6	21	21.1	21	21.3
Chencha	2631	TMPMAX	2015		22.4	21	20.2	20.1	19.5	19.6	19	19.3	20.4	20.4	20.1
Chencha	2631	TMPMAX	2016		20.2	20.2	20.5	20.5	20.2	20.4	20.6	20.5	20.5	20.4	20.6
Chencha	2631	TMPMAX	2017		20.6		20.8	20.5	20.5	20.4	20.7	20.7	20.7	20.5	20.5
Chencha	2631	TMPMAX	2018	20.5	20.5	20.5		20.4	20.4	20.5	20.4	20.5	20.5	20.5	20.4
Chencha	2631	TMPMAX	2019	20.5		20.3	20.3	20.4	20.4	20.4		20.4	20.5		20.2
Chencha	2631	TMPMIN	2012										9.1		
Chencha	2631	TMPMIN	2013								8.8	10.1	9.4	10	10
Chencha	2631	TMPMIN	2014	10.1	10		10	10	10.2	10.3	10.6	10.3	10.3	10.4	10.3
Chencha	2631	TMPMIN	2015		11.3	10.2	10	9.8	9.6	9.3	9.1	9.1	9.8	10.1	9.5
Chencha	2631	TMPMIN	2016		10	10.2	9.9	10.2	9.8	10	9.7		10.6	9.4	9.1
Chencha	2631	TMPMIN	2017		10.1		10.3	9.9	10.1	10.1	10.3	10.4	10.3	10.1	10.1
Chencha	2631	TMPMIN	2018	10.3	10.3	10.3		10.2	10.1	10.3	10.3	10.3	10.3	9.7	10.5
Chencha	2631	TMPMIN	2019	10.2		10.2	10	10.1	10	10.1		10.1	10.4		9.8
Chencha	2631	TMPMIN	2020	9.9	10	10.5	10.1	10.1	9.8	10	9.7	9.8	10.1	10	
Chencha	2631	TMPAVG	2020	15	15.2	15.4	15.2	15.2	14.9	15.2	15.1	15	15.1	15.1	
Chencha	2631	TMPAVG	2017		15.3		15.6	15.2	15.3	15.2	15.5	15.6	15.5	15.3	15.3
Chencha	2631	TMPMAX	2020	20.1	20.3	20.2	20.3	20.2	20.1	20.3	20.2	20.1	20.2	20.2	
Chencha	2631	TMPMIN	2021		9.8	10.1	9.8	10.1	9.9	9.9			9.9		
Chencha	2631	TMPAVG	2021		15	15.3	14.9	15.2	15.1	15.1			15		
Chencha	2631	TMPMAX	2021		20.2	20.4	20	20.3	20.2	20.3			20.2		
Chencha	2631	TMPAVG	2018	15.4	15.4	15.4		15.3	15.3	15.4	15.4	15.4	15.4	15.1	15.5
	2631	TMPAVG	2019	15.4		15.3	15.1	15.3	15.2	15.3		15.3	15.5		15

RESEARCH FUND ACKNOWLEDGMENT

This research project is funded by Adama Science and Technology University under grant number ASTU/SM-R/701/23, Adama, Ethiopia